



저작자표시-비영리-변경금지 2.0 대한민국

이용자는 아래의 조건을 따르는 경우에 한하여 자유롭게

- 이 저작물을 복제, 배포, 전송, 전시, 공연 및 방송할 수 있습니다.

다음과 같은 조건을 따라야 합니다:



저작자표시. 귀하는 원저작자를 표시하여야 합니다.



비영리. 귀하는 이 저작물을 영리 목적으로 이용할 수 없습니다.



변경금지. 귀하는 이 저작물을 개작, 변형 또는 가공할 수 없습니다.

- 귀하는, 이 저작물의 재이용이나 배포의 경우, 이 저작물에 적용된 이용허락조건을 명확하게 나타내어야 합니다.
- 저작권자로부터 별도의 허가를 받으면 이러한 조건들은 적용되지 않습니다.

저작권법에 따른 이용자의 권리는 위의 내용에 의하여 영향을 받지 않습니다.

이것은 [이용허락규약\(Legal Code\)](#)을 이해하기 쉽게 요약한 것입니다.

[Disclaimer](#)

2023년 8월

박사학위 논문

The effects of overexpression of MUDENG on liver and skin of mice

조선대학교 대학원

의과학과

명 승 현

The effects of overexpression of MUDENG on liver and skin of mice

MUDENG의 과발현이 마우스의 간과 피부 조직에 미치는 영
향

2023년 8월 25일

조선대학교 대학원

의과학과

명 승현

The effects of overexpression of MUDENG on liver and skin of mice

지도교수 김 태 형

이 논문을 이학박사 학위신청 논문으로 제출함.

2023년 4월

조선대학교 대학원

의과학과

명 승현

명승현의 박사 학위논문을 인준함

위원장	조선대학교 교수	이 성행	(인)
위 원	조선대학교 교수	방 일수	(인)
위 원	조선대학교 교수	조 주연	(인)
위 원	KBSI 책임연구원	박 재일	(인)
위 원	조선대학교 교수	김 태형	(인)

2023년 6월

조선대학교 대학원

CONTENTS

LIST OF TABLES.....	III
LIST OF FIGURES.....	IV
국문 초록	Vii
영문 초록	iX
CHAPTER 1. INTRODUCTION	1
1.1 The novel protein, MUDENG (Mu-2-related death-inducing gene, MuD) .	2
1.2. The functions of MUDENG in cellular perspective.....	8
1.3 The roles of Adaptin Protein (AP) complex.....	11
1.4 Liver	15
1.5 Liver fibrosis	16
1.6 Liver fibrosis caused by toxin-induced liver injury	23
1.7 Liver fibrosis caused by Cholestatic liver damage	24
1.8 Mouse model of liver fibrosis	25
1.9 Treatment of liver fibrosis	28
1.10 Hair loss	30
CHAPTER 2. Materials and Methods	34
2.1 Reagents	35

2.2 Cell Culture	35
2.3 Lenti virus production.....	35
2.4 Animals	36
2.5 CCl ₄ -induced liver fibrosis model	36
2.6 RNA sequencing of liver tissue	36
2.7 PCR	39
2.8 Histological Analysis	41
2.9 Western blot analysis	41
2.10 Statistical Analysis	42
CHAPTER 3. Results and Discussion	43
3.1 The generation of human AP5M1 transgenic mice	44
3.2 Hair loss in hMUDENG Tg mice	47
3.3 Total RNA sequencing in liver	57
3.4 The Liver of hMUDENG Tg mice	67
3.5 The effect of hMUDENG on CCl ₄ -induced liver fibrosis	69
3.6 The effect of mIL11 and mIL11 mutein on CCl ₄ -induced liver fibrosis of C57BL/6	75
3.7 mIL11 mutein is not sufficient to block the liver fibrosis in hMUDENG Tg induced by CCl ₄	81
CHAPTER 4. Conclusion.....	84
Acknowledgements	89
Reference	91

LIST OF TABLES

Table 1-1. Stage of liver fibrosis	21
Table 1-2. The medications for NAFLD	29
Table 2-1. For identification of the transgenic mice, the PCR was performed using tail genomic DNA.....	40

LIST OF FIGURES

Figure 1-1. Schematic illustration of extrinsic and intrinsic cell death	4
Figure 1-2. DNA sequence of human MUDENG	5
Figure 1-3. Protein sequence of human MUDENG	6
Figure 1-4. Sequence alignment of MUDENG (197~417 residues) with AP2M1	7
Figure 1-5. Schematic diagram illustrating the effects of MUDENG overexpression and silencing in different cell types	10
Figure 1-6. The location of AP complex	14
Figure 1-7. Development of liver fibrosis and cirrhosis	19
Figure 1-8. Schematic illustration of the phenotypic changes of HSCs during the development and regression of liver fibrosis	22
Figure 1-9. Schematic illustration of the hair cycle of mice	33
Figure 2-1. Overview scheme of process of LAS company's RNA sequencing	38
Figure 3-1. Diagram illustrating the structure of the pDEST-hMUDENG-Flag vector	45
Figure 3-2. The location of hMUDENG-Flag ORF and each primers (P1~P5)	45
Figure 3-3. Identification of hMUDENG Tg mice	46
Figure 3-4. Identification of transcription of hMUDENG-Flag in various tissues of hMUDENG Tg mice	46
Figure 3-5. Photographs of hMUDENG Tg mice taken between 2 and 6 weeks of age	49
Figure 3-6. Histological examination of skin tissue from hMUDENG Tg mouse at postnatal day 12 (P12) to postnatal day 36 (P36)	50

Figure 3-7. Photographs of H&E staining of the skin of C57BL/6 mice and hMUDENG Tg mice at postnatal day 24 (P24) 52

Figure 3-8. H&E staining of Kidney, Lung, and Liver of hMUDENG Tg and WT mouse 53

Figure 3-9. H&E staining of liver of hMUDENG Tg and WT mouse at postnatal day 24 54

Figure 3-10. The Body weight of hMUDENG Tg and C57BL/6 mouse55

Figure 3-11. Liver weight (L.W) per body weight (B.W) of mice at 6-weeks 56

Figure 3-12. The result of total RNA sequencing in liver of C57BL/6 and hMUDENG Tg mice 59

Figure 3-13. Heat map of RNA transcripts levels related to lipid metabolism, detoxification, and oxidation and reduction in liver of hMUDENG Tg per C57BL/6 mice at postnatal day 18 (P18) and 30 (P30)..... 63

Figure 3-14. The changes of fetal liver markers in liver of MUDENG Tg mice 64

Figure 3-15. The changes of iron homeostasis related genes in liver of MUDENG Tg mice 64

Figure 3-16. The changes of inflammation related factors in liver of MUDENG Tg mice 65

Figure 3-17. The changes of immune cells markers in liver of MUDENG Tg mice 65

Figure 3-18. The heat map of RNA transcripts levels of representative genes in liver fibrosis in liver of hMUDENG Tg per C57BL/6 mice at postnatal day 18 (P18) and 30 (P30) 66

Figure 3-19. Masson’s trichrome staining of liver of hMUDENG Tg and C57BL/6 mouse 68

Figure 3-20. Designing a CCl₄-induced liver fibrosis model for the observation of susceptibility to CCl₄ in hMUDENG Tg mice 71
Figure 3-21. Survival rate of hMUDENG Tg after treatment of CCl₄ 71
Figure 3-22. Schematic diagram of CCl₄-induced liver fibrosis model 72
Figure 3-23. The effect of hMUDENG on CCl₄-induced liver fibrosis 73
Figure 3-24. Signal of IL11 wild type and IL11 mutein 76
Figure 3-25. Schematic diagram of Lenti mIL11 and Lenti mIL11 mutein vector construction 77
Figure 3-26. Schematic diagram of CCl₄-induced liver fibrosis model mice following injection of lenti mIL11 viruses and lenti mIL11 mutein for data shown in (Figure 3-21a, b) 79
Figure 3-27. The effect of Lenti:mIL11 and Lenti:mIL11 mutein on CCl₄-induced liver fibrosis in C57BL/6 mouse 80
Figure 3-28. . The effect of Lenti mIL11 and Lenti mIL11 mutein on CCl₄-induced liver fibrosis in hMUDENG Tg mouse 82
Figure 3-29. The proteins levels of collagen, α -SMA, and TGF- β in fibrotic liver induced by CCl₄ in hMUDENG Tg and C57BL/6 mouse 83
Figure 4-1. Summary figure depicting the physiological changes resulting from overexpression of hMUDENG 87

초록

MUDENG의 과발현이 마우스의 간과 피부 조직에 미치는 영향

저자: 명승현

지도 교수: 김태형 교수

조선대학교 대학원 의과학과

유전자의 기능을 연구하는 것은 인간의 생명 현상을 탐구하는 가장 기초적이고 근본적인 연구이면서, 나아가 관련된 질병들에 대해 이해하고 약물을 개발하는데 도움을 줄 수 있다. 많은 유전자의 기능이 밝혀져 왔지만, 아직까지 기능이 완전히 알려지지 않은 유전자가 상당히 존재한다. 그러한 유전자 중 하나가 MUDENG (Mu-2-related death-inducing gene, MuD, and called also as Adaptin Protein (AP) 5 mu subunit (AP5M1)) 이다. MUDENG은 Fas라고 하는 세포 사멸을 유도하는 인자에 의한 세포 사멸 시 관련된 유전자 발굴 작업을 통해 처음 발굴되었고, 김태형 교수 실험실에서 유전자 클로닝과 세포에서의 기능연구를 통해 처음으로 알려지게 되었다. 이후로 MUDENG과 세포 사멸과의 연관성에 대한 논문이 나왔지만, 정확한 기능에 대해서는 아직까지 완벽하게 이해하지 못하고 있다.

본 논문에서는 MUDENG 단백질을 과발현하는 형질전환 마우스를 이용하여 처음으로 동물 모델에서 MUDENG에 의한 생리학적인 변화를 관찰하였다. Human MUDENG을 발현하는 동물 모델 (hMUDENG Tg) 은 상동 유전자 재조합 시스템을 이용한 방법으로 생식 줄기세포에서 제작하여 마우스의 다양한 조직에서 발현할 수 있게 되었고, 이를 이용하여 피부와 간에서 hMUDENG의 과발현에 의한 표현형의

변화를 관찰 할 수 있었다. MUDENG Tg 마우스의 두드러진 표현형의 변화는 탈모와 느린 성장이다. 탈모와 느린 성장의 원인은 간 조직에서의 대사 문제로 확인되었다. MUDENG Tg 마우스는 생후 약 2주차에 미성숙한 간을 갖는 것으로 확인 되었다. 미성숙한 간은 지방 대사를 포함한 대사 문제와 산화 환원 반응에 관여하는 많은 유전자 발현이 감소하는 것으로 알려졌다. 또한 MUDENG Tg 마우스는 간 조직에 염증 반응이 일어나는 것을 관찰할 수 있었고, 이러한 결과는 간 섬유화와 밀접하게 관련되어 있다. 이러한 추측과 일치하게 MUDENG Tg 마우스의 간 조직에서는 많은 섬유성 단백질과 초기 염증 유발 인자인 transforming growth factor- β (TGF- β)의 발현이 증가한 것을 관찰하였다. 간 염증에 대해 추가적인 관찰 결과 hMUDENG의 과발현만으로 간 조직에 경미한 염증을 유발하고, 외부 자극 특히 사염화탄소에 민감하게 만드는 것을 관찰하였다. 사염화탄소에 의한 자극으로 간 섬유화가 정상 마우스보다 더욱 빠르고 강하게 악화되는 것을 관찰하였다. 그리고 기존에 간과 심혈관 섬유화에 중요하다고 알려진 Interleukin11 (IL11)도 hMUDENG Tg 마우스에서 상향 발현 되고 있었지만, 추가적인 IL11의 공급 혹은 IL11 mutein (길항제)의 공급에도 큰 영향을 받지 않는 것을 확인하였다.

MUDENG은 Adaptor protein (AP) 5 complex의 mu 소단위체로써 엔도솜, 후기 엔도솜, 골지체로 수송에 관여하는 것으로 알려졌으며, 이러한 수송은 특히 지방 대사에 중요하게 관련되어 있으며, NAFLD 발달에 밀접하게 관련되어 있다.

본 연구 결과 hMUDENG의 과발현이 피부 조직에서 탈모의 발달에 중요한 영향을 미치고, 간 조직에서 염증 반응을 유발하고 간 섬유화의 발달에 매우 중요한 역할을 할 수 있다. 또한 NAFLD를 포함한 여러 간 질환에서도 중요한 영향을 미칠 것이라 생각한다. 앞으로 추가적인 연구에서 MUDENG과 여러 간 질환과의 연관성 연구가 간 조직에서 유발될 수 있는 많은 질환들을 이해하는데 도움을 줄 수 있을 것이라 생각한다.

ABSTRACT

The effects of overexpression of MUDENG on liver and skin of mice

By: Seung Hyun Myung

Advisor: Prof. Tae Hyoung Kim

Department of biomedical science,

Graduate School of Chosun University

Studying gene function is fundamental and essential research that explores human biological phenomena, and it can provide insights into related diseases and aid in drug development. While the functions of many genes have been elucidated, there still exist genes whose functions are not fully understood. One such gene is MUDENG (Mu-2-related death-inducing gene, MuD), also known as Adaptin Protein (AP) 5 mu subunit (AP5M1). MUDENG was initially discovered using a ribozyme library related to cell death induced by Fas. Professor Tae-Hyung Kim's laboratory conducted gene cloning and functional studies in cells, leading to its initial characterization. Subsequently, papers have been published on the association between MUDENG and cell death, but the precise function remains incompletely understood.

In this study, physiological changes induced by MUDENG were observed for the first time in an animal model using transgenic mice overexpressing the MUDENG protein. The animal model overexpressing human MUDENG (hMUDENG Tg) was generated through germline production using a homologous recombination system, allowing for its expression in various tissues of mice. Using this model, phenotypic changes caused by overexpression of hMUDENG were observed in the skin and liver. The prominent phenotypic changes in MUDENG Tg mice are hair loss and slow growth. The underlying cause of hair loss and slow growth was identified as metabolic issues in liver

tissue. At approximately 2 weeks of age, MUDENG Tg mice exhibited immature livers, and it is known to involve a decreased expression of many genes related to metabolism, including lipid metabolism and oxidative-reduction reactions. Additionally, inflammation was observed in the liver tissue of MUDENG Tg mice, which is closely associated with liver fibrosis. Consistent with this hypothesis, increased expression of fibrous proteins and the initial inflammatory inducer TGF- β were observed in the liver tissue of MUDENG Tg mice. Additional observations regarding liver inflammation revealed that overexpression of hMUDENG alone induces mild inflammation in liver tissue and renders it particularly susceptible to external stimuli, especially Carbon tetrachloride (CCl₄). The stimulation by CCl₄ resulted in faster and more severe liver fibrosis in MUDENG Tg mice compared to normal mice. Furthermore, IL11, known to be important for liver and vascular fibrosis, was upregulated in hMUDENG Tg mice. However, its expression was not significantly affected by additional IL11 supply or the administration of IL11 mutein (an antagonist) in MUDENG Tg mice.

MUDENG is known as the mu subunit of the AP5 complex involved in trafficking to endosomes, late endosomes, and the Golgi apparatus. Such trafficking is particularly relevant to lipid metabolism and is closely associated with developing non-alcoholic fatty liver disease (NAFLD).

The results of this study suggest that overexpression of hMUDENG exerts a significant influence on the onset of hair loss in skin tissue and induces inflammation in liver tissue, playing a crucial role in liver fibrosis development. Moreover, it is anticipated to have important implications in various liver diseases, including NAFLD. Further investigations into the relationship between MUDENG and diverse liver diseases can enhance understanding of the broad spectrum of disorders caused by liver dysfunction.

CHAPTER1

INTRODUCTION

1.1 The novel protein, MUDENG (Mu-2-related death-inducing gene, MuD)

MUDENG (Mu-2-related death-inducing gene, MuD) was first named by Tae-Hyoung Kim (1). For the first time, Kawasaki and Taira found 43 unknown genes that are thought to be involved in the Fas-mediated death signaling pathway using randomized hammerhead-structure hybrid ribozyme libraries. The ribozyme is a type of RNA sequence that has the ability to cleave RNA. The ribozyme library is a comprehensive collection of ribozymes fused with random sequences, each approximately 20 nucleotides in length. This library facilitates the identification of genes associated with cell death by cleaving RNA molecules of target genes when the cells are induced to undergo cell death under specific circumstances such as exposure to cell death ligands like FasL TRAIL and TNF-alpha (Figure 1-1). Kawasaki and Taira provided sequences of about 20 nucleotides of 7 known genes and 43 unknown genes related to Fas-induced cell death (2). Tae-Hyoung Kim's lab investigated the ORF of the 43 unknown genes using the blast search program in Genbank and successfully amplified 7 unknown genes using RT-PCR from total RNAs isolated from HeLa cells. For the investigation of functions of 7 unknown genes, 7 unknown genes were co-transfected with GFP. One of these 7 unknown genes was MUDENG. MUDENG significantly induced cell death in HCT116 (human colon cancer cells), HeLa (human cervical carcinoma cells), and Jurkat (human T lymphocytes) when it was overexpressed in their cell lines (1).

The MUDENG is encoded on human chromosome 14q22.3, and the Genbank accession number is AK001675. MUDENG consists of 1473 nucleotide base pairs (Figure 1-2) and 490 amino acids (Figure 1-3). It contains a domain (residues 197-417) that exhibits similarity to the mu2 subunit of the AP1 (adaptor protein) complex (Figure1-4) (1). That's why AK001675 was named the mu2-related death-inducing gene, MUDENG. The MUDENG has a significantly conserved sequence from mammals to amphibians. It could be thought MUDENG could have conserved and important roles in cells. But the functions of MUDENG are not revealed well so far. In cell experiments, MUDENG seems to be involved in apoptosis in both ligand-induced cell death and cell survival (1, 3-8). This conflicted result in cell death could be thought to depend on cell type. The functions of MUDENG

in cell death will be discussed in more detail following sections.

MUDENG is also known as AP5 complex mu1 subunit (AP5M1). The AP5 complex was identified relatively later than other AP complexes (9). The AP complexes are involved in transporting substances, and the Mu subunit plays a role in recognizing the cargo. The substrates transported by AP5 have not yet been discovered. Recently, one of the roles of the AP5 complex was discovered that is involved in late endosome to Golgi retrieval (10). The retrieval plays a crucial role in maturation, signaling, and membrane trafficking (11, 12). Pathological diseases such as hereditary spastic paraplegia and other neurodegenerative disorders caused by endosome/lysosome dysfunction show the importance of AP5 and retrieval (10). In addition, it is observed that overexpression of AP5M1 in mouse tissues, especially the liver, induced liver fibrosis more quickly and strongly. The liver is also vital in transporting lipids and proteins and retrieving late endosomes to the Golgi apparatus. These results emphasize the importance and necessity of the continuous study of AP5M1, namely MUDENG.

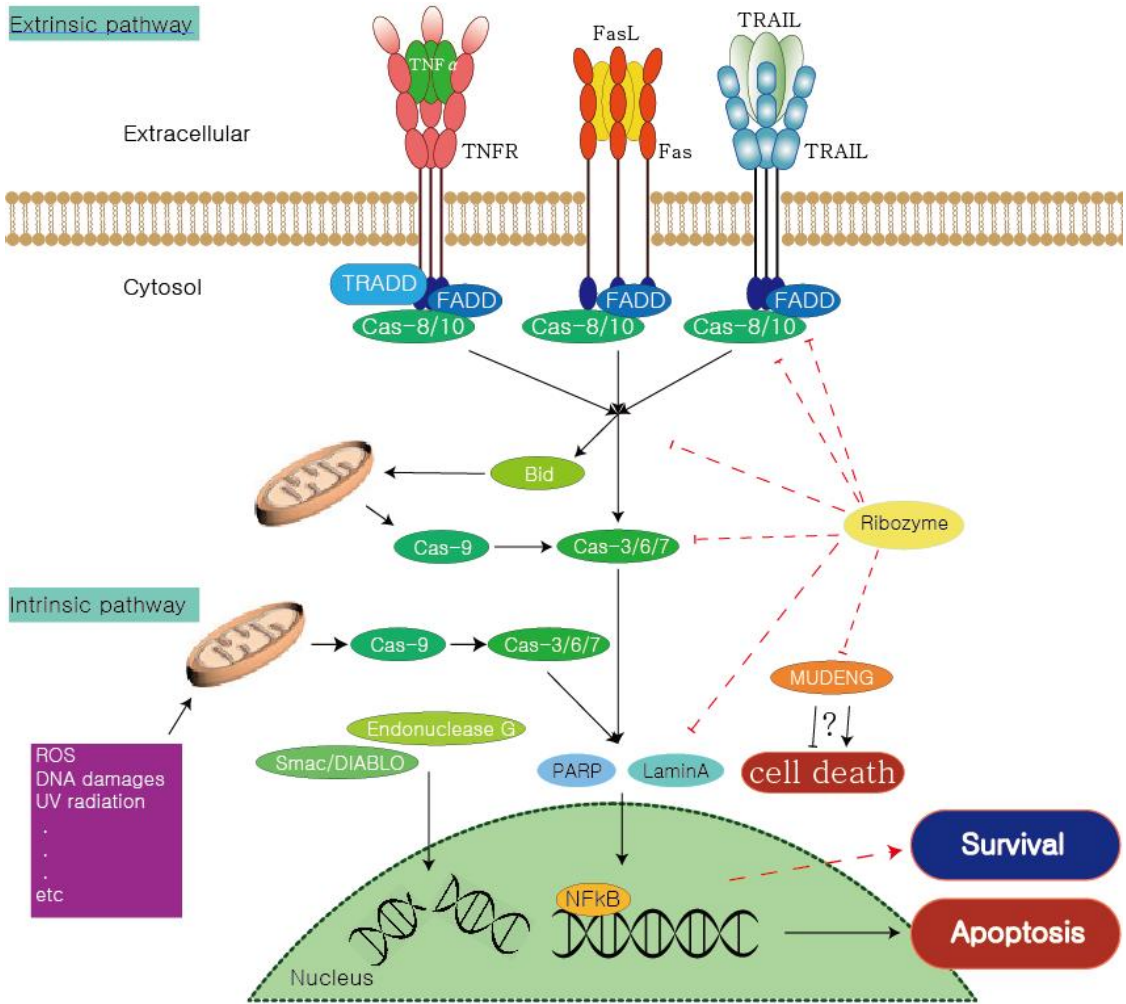


Figure 1-1. Schematic illustration of extrinsic and intrinsic cell death. Cells can undergo death due to intracellular damage or external stimuli, such as TNF α , FasL, and TRAIL. Ribozymes have the ability to cleave RNA molecules, and cleaving mRNA associated with cell death signals may lead to cell survival although cell death signals are sent by death ligands. Black arrow represent cell death signal pathway. Red dotted arrow represent blocking of cell death and cell survival.

5'-ATGGCGCAGCGGGCAGTGTGGCTCATAAGCCACGAACCGGAACTCCACTTTGTGGCACCGTGA
 GATTCTCCAGACGGTATCCAACCTGTTGAAAAACGAGCCAGAGTCTTCAATGGAGCAAGTTATGTGCTT
 GTTCCTGAAGATGGTCCCTTTCTTAAAGCACTGCTCTTTGAACTTAGATTATTGGATGATGATAAAGACT
 TCGTTGAGAGTCGTGATAGCTGTTACGCATCAATAAAACATCCATTTATGGACTCCTGATAGGAGGTG
 AAGAACTCTGGCCAGTTGTTGCTTTTCTGAAGAATGACATGATATATGCTTGTGTTCCACTAGTTGAAC
 AAACCTCTGTCCCCTCGTCCGCACTAATTAGTGTGAGTGGAGTTTCACAAGGCTTTGAATTTCTTTTTG
 GGATACAGGATTTTCTTTATTCAGGTCAAAAAATGACTCTGAGCTGAATACAAAATTGAGCCAGTTG
 CCTGACTTGCTTCTGCAGGCTTGTCCATTTGGTACTTTATTAGATGCCAACTTACAGAATTCATTAGATA
 ATACCAATTTTGCATCTGTGACTCAGCCACAGAAACAGCCAGCTTGGAAAACCTGGGACGTACAAAGG
 AAAACCACAAGTTTCTATTTCTACTGAAAAGGTAAAATCCATGCAATATGATAAACAGGGTATAGC
 AGATACATGGCAAGTTGTTGGAACAGTGACTTGCAAGTGTGATTTGGAAGGAATCATGCCAAATGTTA
 CCATCAGCTTGAGTCTCCCCACCAATGGATCTCCACTTCAGGATATTCTAGTTCACCCCTTGTTAACTTC
 TCTTGACTCTGCAATTCTGACTTCTAGTAGTATTGATGCAATGGATGACTCTGCATTTAGTGGGCCTTAC
 AAATTTCCATTCACTCCACCTTTAGAGTCATTCAACTTATGCTTCTACACTTCCCAGGTCCCTGTCCCAC
 CAATTTGGGTTTTTATCAAATGAAGGAGGAAGAAGTACAACCTAAGAATAACCATTAATTTAAAACCTT
 CATGAAAGTGTGAAAAATAATTTTGAATTCTGTGAAGCCCATATACCTTTTTTACAATAGAGGTCCAATTA
 CACATTTGGAATACAAAACCTAGTTTTGGCCAGCTTGAAGTATTTGAGAGAAAAGCTTATTGATCTGG
 ATTATTGGCCAGAAGTTCCCAAAATCAATGGAAATTAGTCTTTCTGGAACCTGTAACCTTTGGAGCCAAG
 AGCCATGAGAAGCAGCCATTTGACCCAATTTGTACTGGAGAAACAGCATATTTAAAGCTTCATTTTAG
 GATCTTAGATTACACACTTACTGGATGTTATGCAGATCAGCATTCAAGTTTTTGCATCAGGAAA
 ACCAAAAATAAGTGCACACCGGAAACTAATTTCTTCTGATTATTACATCTGGAATTCTAAAGCCCCTGC
 TCCAGTAACATATGGATCATTATTATTGTAA-3'

Figure 1-2. DNA sequence of human MUDENG. Human MUDENG has 1473 nucleotide base pair.

MAQRAVWLISHEPGTPLCGTVRFSRRYPTVEKRARVFNNGASYVVPVDPEDGPFLLKALLFELR · · 60

 LLDDDKDFVESRDSCSRINKTSIYGLLIGGEELWPVVAFLKNDMIYACVPLVEQTLSPRP · · 120

 PLISVSGVSQGFELFGIQDFLYSGQKNDSELNTKLSQLPDLLLQACPFGLLDANLQNS · · 180

 LDNTNFASVTQPQKQPAWKTGTYKGKQPVSISITEKVKSMQYDKQGIADTWQVVGTVTCK · · 240

Adaptin domain

CDLEGIMPNVTISLSLPTNGSPLQDILVHPCVTSLDSAILTSSSIDAMDDSAFSGPYKFP · · 300

FTPPLESFNLCFYTSQVPVPPILGFYQMKEEEVQLRITINLKLHESVKNNFEFCEAHIPF · · 360

YNRGPITHLEYKTSFGQLEVFREKSLLIWIIGQKFPKSMEISLSGTVTFGAKSHEKQPF · · 420

 PICTGETAYLKLHFRILDYTLTGCIADQHSVQVFASGKPKISAHRKLISSDYIWNKAP · · 480

 A P V T Y G S L L L *

Figure 1-3. Protein sequence of human MUDENG. Human MUDENG has 490 amino acids. The underlined region (197 to 417 amino acids) represents the adaptin domain region.

1.2. The functions of MUDENG in cellular perspective

When initially discovered, MUDENG was observed to trigger apoptosis upon overexpression in HeLa and Jurkat cell lines. However, during TRAIL-induced cell death, it was observed that MUDENG protein was partially cleaved by caspase 3, resulting in the loss of its cell-killing function (3). The caspase cleavage site was identified to be located on the adaptin domain, D276 and D290, of MUDENG, which is considered to be a crucial region for cell killing. It is not yet fully understood how the loss of MUDENG's cell-killing ability by caspase-mediated cleavage affects TRAIL-induced cell death in BJAB and Jurkat cell lines. In contrast to the results observed in Jurkat, HeLa, and BJAB cells, it has been noted that MUDENG overexpression inhibits TRAIL-induced cell death in astrogloma cell lines, specifically U251MG and T98G cells (5). Moreover, during TRAIL-induced cell death in astrogloma cell lines, MUDENG appears to undergo cleavage. This cleaved form of MUDENG appears to lose its inhibitory function on TRAIL-induced cell death (Characterization of MUDENG, a novel anti-apoptotic protein) (Figure1.5). These two contradictory results have yet to be fully interpreted.

In cervical carcinoma cell lines, it was found that BAX plays a significant role in the cell death mechanism caused by MUDENG overexpression. Knocking out BAX was observed to significantly inhibit cell death caused by MUDENG overexpression (7). Furthermore, low mRNA levels of MUDENG, BAX, and BAK were observed in patient cervical carcinoma tissues (13). However, in astrocytes, a major glial cell line, MUDENG was found to inhibit TRAIL-induced and Bid-mediated cell death, which conflicts with its cell-killing ability in HeLa, BJAB, and Jurkat cell lines (1, 3, 14). Thus, it appears that MUDENG's role in cell death can differ depending on the cell type (Figure1.5).

MUDENG expression is thought related to survival of cancer patients. Although survival curves is little different depends on cancer types, Patients with kidney renal clear cell carcinoma (KIRC) have a poor prognosis when MUDENG expression is low. Confidence in breast invasive carcinoma (BRIA) (A) and lung adenocarcinoma (LUAD) was slightly less reliable, but unlike KIRC patients, high MUDENG expression seemed to have a poor prognosis (13). This result suggest that MUDENG

could be used for diagnostic marker and therapeutic target for cancer.

In addition, MUDENG may have a significant impact on cellular homeostasis in terms of the AP5 complex mu subunit, AP5M1. AP complex is crucial protein complex in several process in cell such as signal transduction and transports of vesicles and cargoes through vesicle formation and trafficking (9, 15). Almost all cells express AP complex proteins and deficiency of one of this proteins could lead to severe and various diseases such as neurodegenerative disorders by defect of AP3, developmental disorder by defect of AP1, immune disorder, and cancer (15). It is still unknown whether cell death activity of MUDENG is caused by a problem with the subunit of the AP5 complex or whether it is an independent function of MUDENG apart from the AP5 complex.

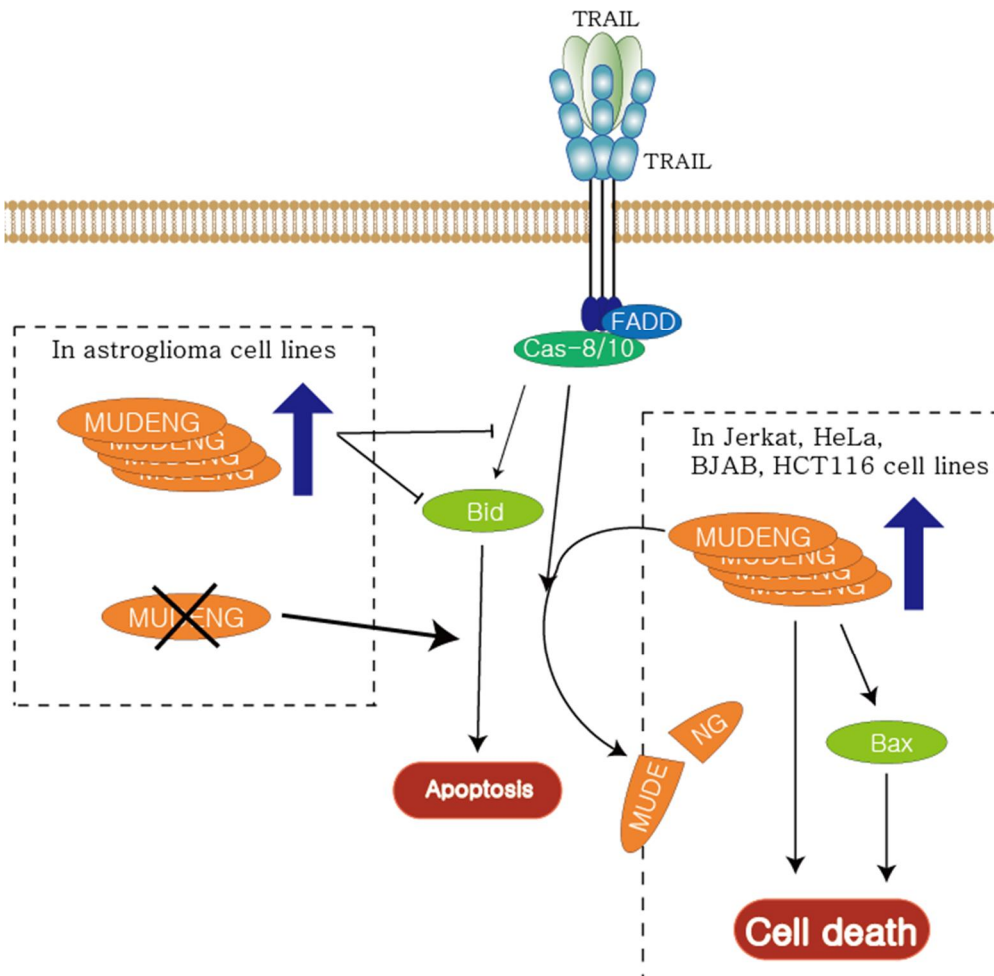


Figure 1-5. Schematic diagram illustrating the effects of MUDENG overexpression and silencing in different cell types. In the Jurkat, BJAB, HeLa, and HCT116 cell lines, overexpression of MUDENG can induce cell death. These cell death can be blocked by silencing Bax expression in HeLa cells. In addition MUDENG could be cleaved by caspase 8 (in BJAB cells) and caspase 3 (in HeLa, Jurkat, and BJAB cells) during TRAIL signal transduction. These cleaved MUDENG lose cell killing activity in HeLa, Jurkat cells. However, MUDENG overexpression can inhibit TRAIL-induced cell death in astroglioma cell lines, and MUDENG silence can significantly induce TRAIL-induced cell death in astroglioma cell lines, U251MG and T98G cells (3, 5, 7).

1.3 The roles of Adaptin Protein (AP) complex

The Adaptin Protein (AP) complexes have significantly important role in various process of cell such as metabolism, developments and cell survival. The major functions of the AP complex are known to sort substrates such as proteins and lipids into vesicles and to transfer cargo to their specific locations. Among AP complex family, the AP5 complex including AP5M1 was discovered relatively recently. All AP complexes are known to consist of a heterotetramer, two large subunits, a medium subunit, and a small subunit. As well as AP complex, some protein complex that is related to AP complex and acts to similar functions was known. One of them is the F subcomplex of the coat protein complex I (F-COPI), which consists of heterotetramers and is involved in retrograde trafficking from the Golgi apparatus to the ER (16). The AP1-3 complex is known to play a classical role that is binding to clathrin and transporting intracellular proteins (15). However, there is a slight difference in the location where the substance is transported, and recently, it has been reported that clathrin is not necessarily required for AP2 to transport the substance (17-19). AP4 has been discovered, and subsequently AP5 has also been identified. To understand their functions, further research is still needed. The functional studies of the AP1 to AP5 complexes have been elucidated by observing changes in phenotype due to mutations or deletion of their subunits.

Adaptor Protein 1 (AP1) is a crucial protein complex involved in clathrin-dependent protein transportation from the trans-golgi network (TGN) to endosomes (Figure 1.6), as well as in basolateral transport from the TGN in epithelial cells. Knockout of the AP1 complex is embryonically lethal, and mutations in the complex cause severe developmental deficiencies (15, 20-22). In addition, deficiency and mutation of one of AP1 could lead to severe disorders such as neurological defects, cancer, and cardiac arrest (22-26). Furthermore, AP1 also appears to contribute an important role in the immune system against viral infections (27, 28).

AP2 is known to be involved in clathrin-dependent endocytosis from the plasma membrane to the cytoplasm (Figure 1.6). However, some studies have suggested that the AP2 complex may not be necessary for this process (17-19). AP2 is still considered to be very important for development and

endocytosis. Deficiency of AP2 leads to embryonic lethal, and mutations or deficiency of certain isoforms of AP2 subunit proteins are associated with various diseases, such as cancer, Alzheimer's disease, obesity, coronary disease, chronic bronchitis, and nicotine withdrawal (29-36). Additionally, due to its ability to transport substances into the cell through endocytosis, AP2 may contribute to infection and drug resistance (37-42).

It is known that AP3 is involved in the trafficking of endosomes, lysosomes, lysosome-related organelles, and synaptic vesicles (43) (Figure 1.6). Unlike AP1 and AP2, the deficiency of AP3 did not result in embryonic lethality but instead led to the formation of abnormal lysosome-associated organelles (44). AP3 plays a crucial role in various biological processes such as development especially Notch signaling (45), melanocyte trafficking (46), neural development disorders (47), Alzheimer's disease (48), immune defense (49-52), and cancer (53-55).

AP4 is expressed ubiquitously in human tissues and performs important functions despite being expressed in smaller amounts than AP1-3 (56-58). Mutations or deficiencies in AP4 are associated with many diseases, especially intellectual disabilities and neurological symptoms (59-61). Through various studies, AP4 has been shown to be involved in sorting and transporting substances in the trans-Golgi network (TGN), particularly from the basolateral surface to endosomes, and in some cases directly to the plasma membrane (62-64) (Figure 1.6). Boehm and colleagues demonstrated that AP-4 is recruited to the TGN primarily by ARF1 and circulates between the membrane-bound and cytoplasmic states (65). Proteomic analysis of AP-4-enriched vesicle fractions revealed the presence of a protein called Tepsin, in addition to ARF1 (66).

AP5 was identified later than other AP complexes, and its functions are only partially understood. Therefore, further studies are needed to fully understand the roles of AP5 in cell and biophysics. The localization of AP5 has been observed in late endosomes and lysosomes, suggesting that it may be involved in late endosome retrieval (9) and recycling lysosomal proteins to the Golgi complex (67) (Figure 1.6). AP5 is known to be related to SPG11 and SPG48, and mutations in AP5Z1 have been reported in patients with hereditary spastic paraplegia (68-70), which have been suggested to partly

contribute to axonal mitochondrial defects (71). It has been observed that patients with sporadic spastic paraplegia have low levels of AP5M1 (70), and patients with allergic diseases have AP5B1 variants (72-75). AP5M1 has also been reported to be significantly related to cell death (1, 3, 5, 7, 8, 14). The trafficking at late endosome and endo-lysosome could affect to NALFD in liver (76). In addition, the liver is involved in various metabolic processes, regulates the recycling of various proteins and minerals, including iron in RBCs, and is crucial for the removal of toxins and microorganisms. Many of its functions require processing in the late endosome, lysosome, and Golgi, making the liver one of the most important organs for these tasks. This paper suggests that AP5M1 is also involved in liver fibrosis and may be involved in hair loss. Taken together, defects in AP5 could lead to other diseases related to lysosomal recycling (70), and lysosomal recycling may have far-reaching effects throughout the body.

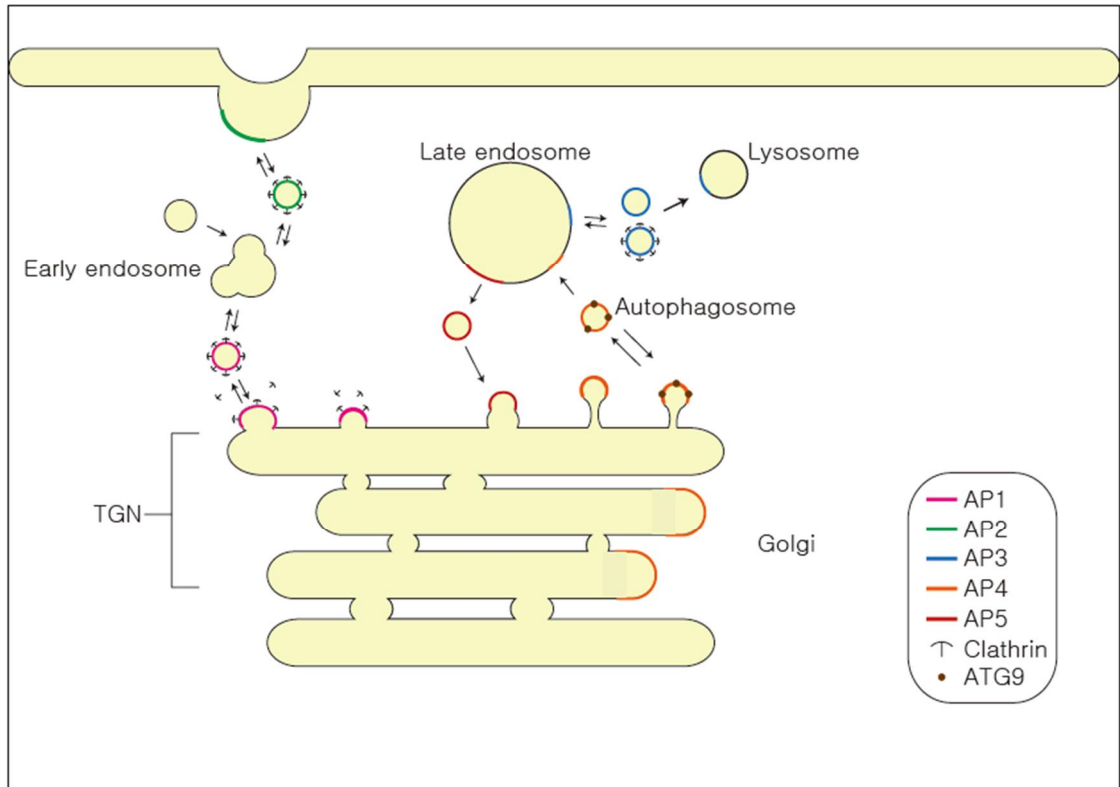


Figure 1-6. The location of AP complex (15). AP1~5 complexes are known until now. Transport between trans-golgi network (TGN) and endosome is mediated by AP1 complex. Transporting cargo by AP2 complex is involved in between plasma membrane and cytoplasm. AP3 is known to mediate trafficking of endosomes, lysosomes, lysosome-related organelles, and synaptic vesicles. Transport by the AP1~3 complex is known as clathrin-mediated transport. AP4 complex has been known to play a role in the sorting and transportation of substances within the TGN, and from the basolateral surface to endosomes. AP5 complex initially observed in endosome and recently observed that AP5 complex play a role in late endosome-to-golgi retrieval (9, 10, 15).

1.4 Liver

The liver is the largest organ and gland in the mammalian body and has many vital functions in mammals. These functions include bile production, the synthesis of serum proteins like albumin, regulation of blood clotting, neutralization and removal of toxins and bacteria from the blood, as well as the metabolism and storage of lipids, carbohydrates, vitamins, and minerals, and the regulation and removal of bilirubin (77). Liver damage can be fatal for mammals due to the many essential functions that the liver performs in their bodies. Despite various efforts to develop artificial liver replacements, none have been successful. Fortunately, unlike other tissues, the liver has a remarkable regenerative capacity and can partially recover even if up to 70% of its tissue is removed (78, 79). This is why liver diseases often reach an advanced stage before symptoms appear, c. Researchers are making significant efforts to discover indicators of liver damage to detect it at an early stage (80-82). Among them, ALT/AST is the most commonly used index to predict liver damage. However, The levels of ALT/AST don't always reflect the extent of liver damage (83). There are various other factors that can cause an increase in ALT/AST levels, such as muscle damage or stress. Therefore, further testing is usually required when the ALT/AST level increases by about 5 times or more than the reference level (84). In addition to ALT/AST, liver function is also assessed by measuring ALP, bilirubin, albumin, and prothrombin levels (83, 84).

The liver can be damaged by various factors such as infections, toxins, obesity, alcohol, inherited genetic disorders, and cancer. These dangerous factors could lead to cell death especially hepatocyte that is parenchymal cell of liver. Once liver tissue was damaged, liver tissue effort to repair the damage and eliminate the cause of the damage. In this process, the inflammation reaction is accompanied, and hepatic stellate cells and immune cells such as kupffer cell could be activated and involved in liver repair process (85, 86). During the liver repair process, hepatic stellate cells (HSCs) produce fibrous proteins (87). The accumulation of fibrous proteins in liver tissue during repetitive damage and repair processes is known as liver fibrosis. If liver damage continues to progress, it can lead to liver cirrhosis, liver failure, and even liver cancer (88). This study revealed

that in mice with overexpression of the MUDENG protein in liver tissue, there was an accelerated accumulation of fibrotic proteins induced by the hepatotoxin CCl₄ compared to normal mice. Furthermore, liver fibrosis progressed even in the absence of any stimuli. These findings suggest that MUDENG may play a significant role in the progression of liver fibrosis.

1.5 Liver fibrosis

Liver fibrosis results from scarring during the recovery process from chronic liver damage. It is a condition where extracellular matrix proteins accumulate and collagen proteins typically accumulate in the tissue, causing the liver to harden. Chronic liver damage can be classified into two major categories: hepatotoxic injuries and cholestatic injuries (89, 90). Hepatotoxic injuries include damage caused by bacterial or viral infections such as HBV and HCV, damage caused by toxic substances and alcohol, while cholestatic injury can be caused by defects in bile flow or fat accumulation in liver tissue due to genetic factors (89, 91). In the stage of liver fibrosis, if the underlying cause of liver damage is not removed and continuous liver injury persists, it can develop to cirrhosis. Liver cirrhosis is characterized by the excessive accumulation of fibrous proteins in liver tissue, resulting in liver stiffness. This condition can obstruct the flow of blood and bile, leading to portal hypertension. Moreover, these circulatory disturbances and ongoing liver damage can cause excessive cell death, leading to liver failure. Consequently, the loss of liver function, which is responsible for detoxification, various metabolic activities, can lead to metabolic disorders. Additionally, toxins may infiltrate other tissues and accumulate, causing damage to other organs such as hepatic encephalopathy and potentially leading to intra-abdominal infections. Furthermore, it is well-known that the progression of liver cirrhosis is strongly associated with the development of hepatocellular carcinoma (Figure1.7).

There are several methods for diagnosing liver fibrosis. Initially, additional tests can be performed when liver damage indicators are out of the normal range through blood tests (83, 84, 92).

More precise methods for confirming liver fibrosis include liver tissue biopsy, liver stiffness measurement using sound waves, and MRI (93-95). Various systems such as Knodell, Ishak, METAVIR, and Scheuer are utilized to determine the stages of liver fibrosis (96, 97). In Korea, the Korean Society of Gastrointestinal Pathology has established a grading system that quantifies liver fibrosis (Table 1.1). The Korean classification system ranges from stage 0 to stage 4. Stage 0 indicates no fibrosis, stage 1 indicates fibrosis expansion from the portal vein but not spreading to the septa, stage 2 indicates brief spreading of fibrosis to the septa and around the portal, stage 3 indicates spreading of fibrosis to the surrounding portal tracts and hepatic venule, and stage 4, also known as cirrhosis, is the stage in which fibrosis progresses from the portal vein to the central hepatic vein, and fibrous crystals are observed.

Liver fibrosis can occur due to various causes, but it is defined by the accumulation of fibrous proteins. Excessive accumulation of these fibrous proteins can eventually lead to the development of cirrhosis. Fibrotic proteins accumulate in the liver tissue, especially in the sinusoid, during hepatic fibrosis, and the main source of these proteins is myofibroblasts. Although myofibroblasts are rarely found in healthy livers, they could be increased when liver damage occurs (98). Myofibroblasts have a spindle or stellate shape and express abundant fibrous proteins. They originate from various cells, mainly hepatic stellate cells (HSCs) and portal fibroblasts, as well as some transformed cells from bone marrow-derived cells (99). In cases of liver damage caused by toxins, HSCs dominate the myofibroblast population and contribute to the fibrotic response in the centrilobular and perisinusoidal regions (100). However, in cholestatic liver fibrosis, both HSCs and portal fibroblasts are involved. In experimental cholestatic liver fibrosis induced by bile duct ligation (BDL), portal fibroblasts initially account for more than 70% of myofibroblasts, and activated HSCs gradually increase after approximately 17 days (98, 100).

HSCs, the main cells contributing to liver fibrosis, are normally located in the space of Disse in a dormant state. HSCs in a quiescent state store retinoid lipid droplets and are a major store of vitamin A, which is required to maintain their quiescent state (87, 98). During liver damage, cytokines and

other factors convert HSCs from a resting state to an activated state. TGF- β is the main cytokine responsible for this conversion (101, 102). Activated HSCs express ECM proteins such as Colla1, Colla2, Activin, and Pail in response to TGF β . ECM proteins such as Colla1 are also produced through the JAK-STAT3 pathway by Leptin, IL-6, and IL-17 (102, 103). Additionally, connective tissue growth factor (CTGF) and IL-13 can induce the expression of Colla1 independently of TGF β (104). A recent study showed that IL11 activates HSCs through an ERK-dependent pathway in the NASH model and can directly affect liver fibrosis (Figure1.8) (105). The current study on MUDENG suggests that it enhances the expression of TGF β and IL11, which may be related to diseases such as liver fibrosis.

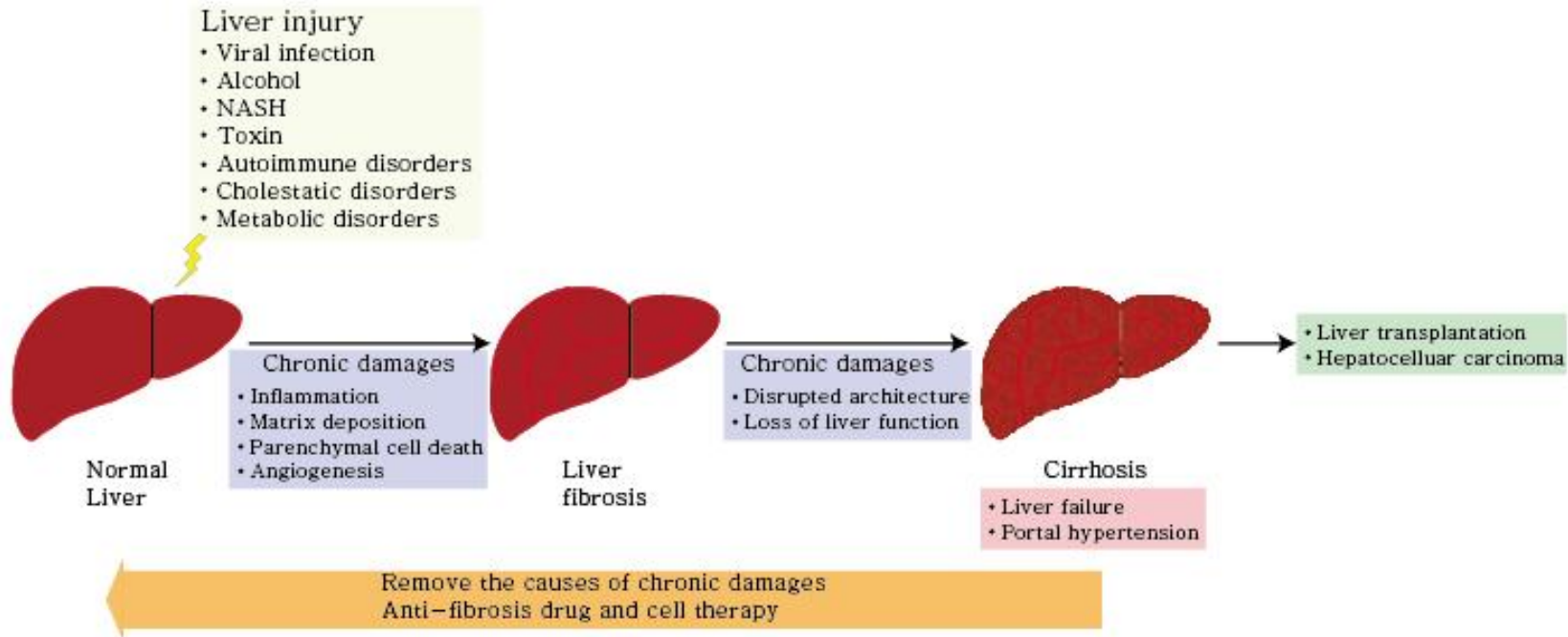


Figure 1-7. Development of liver fibrosis and cirrhosis. Normal liver can progress to fibrosis due to chronic injuries caused by factors such as viruses, alcohol, toxins, NASH (nonalcoholic steatohepatitis), and other inflammatory disorders. During the process of fibrosis, the liver tissue undergoes the deposition of extracellular matrix. Numerous fibrous proteins, particularly Collagen type 1 protein, are accumulated in the liver tissue. Unless the underlying causes of liver damage are removed, liver fibrosis can develop to cirrhosis. Cirrhosis is characterized by the excessive accumulation of fibrous proteins, which impede the flow of blood and bile acids. It could lead to portal hypertension. The portal hypertension could

result in varicose veins, ascites that increase risk of infection, hepatic encephalopathy, Splenomegaly that could decreased platelet count and increased risk of bleeding. In addition, the excessive death of hepatocytes by chronic damages, hypoxic condition due to impaired blood stream, and toxins such as bile acid also lead to liver failure. It can be cured only by liver transplantation so far. Cirrhosis can also developed hepatocellular carcinoma. The progression to cirrhosis has a very poor prognosis for the patient. It can lead to various complications that can result in death, and it can also progress to hepatocellular carcinoma (HCC) (106).

Descriptive diagnosis	Score	Definition
No fibrosis	0	Normal connective tissue
Portal fibrosis	1	Fibrous portal expansion without septa
Periportal fibrosis	2	Periportal fibrosis with short septa extending into lobules or rare porto-portal septa(intact architecture)
Septal fibrosis	3	Fibrous septa reaching adjacent portal tracts and terminal hepatic venule (architectural distortion but no obvious cirrhosis)
Cirrhosis	4	Diffused nodular formation

Table 1-1. Stage of liver fibrosis (adapted from Joon Mee kim, Pathologic Dianosis of Hepatic Fibrosis).

Score 1 corresponds to portal fibrosis, characterized by the deposition of fibrous proteins limited to the portal vein without extending into the septa. Score 2 corresponds to periportal fibrosis, characterized by periportal fibrosis with short septa extending into lobules or rare porto-portal septa, while maintaining an intact liver structure up to the present. Score 3 corresponds to septal fibrosis, characterized by fibrous septa reaching adjacent portal tracts and terminal hepatic venules, indicating architectural distortion without obvious cirrhosis. Score 4 corresponds to cirrhosis, characterized by diffuse nodular formation.

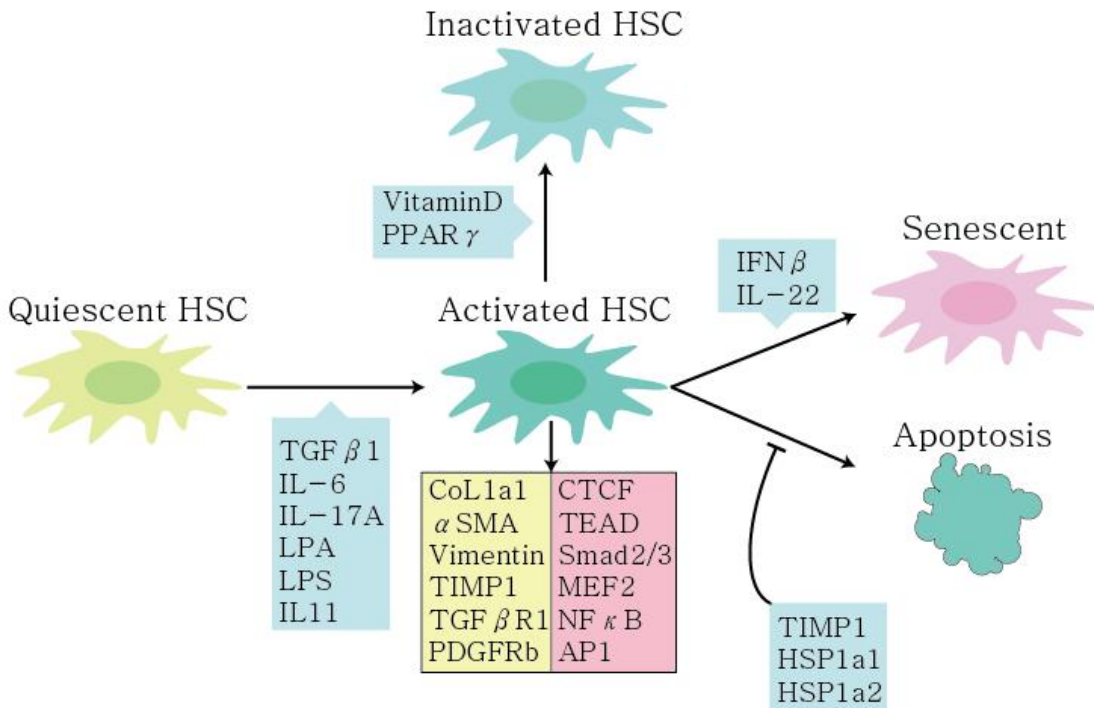


Figure 1-8. Schematic illustration of the phenotypic changes of HSCs during the development and regression of liver fibrosis. In normal physiological conditions, hepatic stellate cells (HSCs) exist in a quiescent state within the liver's microvasculature called sinusoids. Quiescent HSCs can be activated by cytokines like TGF β 1, IL11, IL6, and external stimuli such as LPS. Activated HSCs secrete numerous fibrotic proteins for repair scar in liver tissue. When the inflammatory response subsides, approximately half of the activated HSCs undergo apoptosis and are eliminated. IFN β 1 and IL22 promote the senescence of activated HSCs. Additionally, HSCs that do not undergo apoptosis enter an inactivation with a similar phenotype to the quiescent state. Vitamin D and PPAR γ can induce the transition of activated HSCs to an inactive state. The yellow boxes represent genes expressed by activated HSCs, while the red boxes represent the transcription factors that are expressed in activated HSC (90).

1.6 Liver fibrosis caused by toxin-induced liver injury

Liver damage caused by viruses, specifically HBV and HCV, has been recognized as the primary cause of chronic liver damage for several decades. These viruses can be transmitted through blood and body fluids and constantly replicate within liver cells, leading to the destruction of infected cells and subsequent damage to liver tissue. HBV has a surface antigen (HBsAg), while HCV utilizes E1 and E2 envelope glycoproteins to enter cells and contains the minimal information required for gene replication and expression. These HBsAg, E1, and E2 proteins become inflammatory mediators and can continuously cause an inflammatory response in liver tissue, and also cause damage to liver tissue through cell death of hepatocytes infected with the virus (107, 108). A large number of patients with liver cirrhosis caused by HBV and HCV infections are at risk for developing hepatocellular carcinoma, since approximately 70% of HCC patients are HBV and HCV patients (109). In viral hepatitis, excessive hepatic fibrosis occurs within the portal vein and extends into the liver parenchyma, causing persistent portal inflammation (110).

Alcohol liver disease (ALD) is one of the main causes of liver cirrhosis, liver failure, and liver cancer. Liver damage can occur due to the metabolites of alcohol, such as acetaldehyde and ROS, as well as the accumulation of fat resulting from alcohol metabolism. This damage can lead to the development of steatohepatitis and fibrosis, which in turn can progress into hepatocellular carcinoma (HCC). Alcohol enters the liver through the digestive system and is broken down by alcohol dehydrogenase and CYP450 2E1 enzymes into acetaldehyde, a toxin that damages the liver (111, 112). Alcohol-induced damage to liver cells is related to the secretion of cytokines such as IL-8, IL-17, and CXCL1, which activate immune cells in liver tissue and bone marrow-derived immune cells, leading to an inflammatory response (113). Alcohol intake also can cause the accumulation of fatty droplets in the liver tissue through the synthesis of SREBP1 and SREBP2, which are involved in cholesterol expression in the liver (114, 115). During the inflammatory response, TGF β , an important regulator of fibrosis, is secreted, which can activate hepatic stellate cells (HSCs) and can more exacerbate liver fibrosis.

1.7 Liver fibrosis caused by Cholestatic liver damage

Cholestatic liver damage is primarily caused by problems with bile secretion. Bile is produced by liver cells and stored in the gallbladder through bile ducts before being secreted into the small intestine. Problems with bile secretion can result from genetic defects, such as Alagille syndrome (116), or dysregulation of the immune response, such as primary biliary cholangitis or primary sclerosing cholangitis, which can lead to liver damage (117). Normally, bile flows along the bile ducts without harming liver tissue. However, if there is a problem with bile secretion, such as obstruction or rupture of the bile duct, bile may leak into the liver tissue and the hepatic vein. Bile that leaks into liver tissue can cause liver damage and progress to liver fibrosis (118). Moreover, bile that leaks through the hepatic vein can spread throughout the body and cause symptoms such as jaundice (168).

The incidence of non-alcoholic fatty liver disease (NAFLD) in the United States is approximately 25%, equivalent to more than 84 million people (119). In Korea, according to the announcement of the Korean Association for the Study of the Liver in 2018, one out of every three adults has NAFLD (120). Of these patients, approximately 20% can develop non-alcoholic steatohepatitis (NASH) (90), which is associated with metabolic disorders, obesity, and diabetes. The pathological features of NASH include hepatocyte inflammatory response, hepatocyte ballooning degeneration, peri-sinosoidal fibrosis, and cirrhosis (121). There are two main causes of NASH. The first is due to diet-induced obesity, where excessive accumulation of triglycerides, fatty acids, or cholesterol disrupts the balance of resistin or leptin, leading to adipose tissue accumulation in the liver and mediating inflammatory response, resulting in liver fibrosis (122). The second cause has not yet been precisely identified but is thought to be related to bacteria, toxins, and reactive oxygen species (ROS) originating from the large intestine (123, 124). NASH patients are rapidly increasing in recent years, and research is actively being conducted to develop treatments for this condition.

1.8 Mouse model of liver fibrosis

To study liver fibrosis, both in vitro cell models and in vivo animal experiments can be used. Animal models are particularly useful for histological and physiological observations, and various animal models have been developed and utilized for studying liver fibrosis and liver cirrhosis, with rats and mice being the most commonly used. Different methods are used in animal experiments, including chemical methods using drugs, diet control methods, surgical methods such as bile duct ligation, methods using genetically mutated mice, and methods using viruses (89, 125).

The chemical method is reproducible, relatively short in duration, and easy to perform, making it a popular choice. Representative chemical agents used include ethanol, carbon tetrachloride (CCl₄), thioacetamide, dimethylnitrosamine (DMN), and diethylnitrosamine (DEN).

To observe liver fibrosis in rodents caused by alcohol consumption, various methods have been used, such as feeding alcohol in water or directly into the stomach (126). However, these methods have limitations in reaching liver fibrosis and do not reflect human ALD caused by alcohol consumption. To overcome this, methods using a combination of alcohol intake with diet or drugs have been introduced, but these methods have the disadvantage of complicating the cause of liver fibrosis and making it difficult to analyze the results.

Carbon tetrachloride, an old and widely used liver toxin, is effective in inducing liver fibrosis in rodents. It has high reproducibility and shows characteristics close to human liver fibrosis (125). Carbon tetrachloride is metabolized by cytochrome p450 2E1 to generate trichloromethyl radical (CCl₃-), which induces lipid peroxidation, necrosis of liver cells, and the inflammatory response in liver tissue (125, 127, 128). It is widely used in mice and rats, and the sensitivity of mice to CCl₄ depends on the strain. The liver fibrosis induction model using C57BL/6 mice has been standardized by intraperitoneal injection twice a week for 6 weeks or 3 times a week for 4 weeks at a dose of about 0.5 to 0.7 μl/g. Other methods of administration, such as oral administration, subcutaneous injection, and inhalation, have limitations such as granuloma formation or requiring specialized equipment and skills (125).

Thioacetamide (TAA) is metabolized by CYP450 in the liver and becomes cytotoxic. The precise mechanism by which TAA's sulfur dioxide, produced via CYP450 in liver cells, leads to liver fibrosis is not yet fully understood. However, a proteomic analysis of thioacetamide-induced hepatotoxicity and cirrhosis in rat livers revealed changes in enzymes involved in β -oxidation of fatty acids, degradation of amino acids and methionine, and factors related to lipid peroxidation and oxidative stress (129). TAA can be used to induce liver fibrosis in both rat and mouse models, and TAA is more commonly used in rats. The standard dose in rats is 100-200 mg/kg body weight, administered intraperitoneally three times a week for 6-12 weeks to induce liver fibrosis. Additionally, an oral administration method is available, which takes about 2-4 months to induce liver fibrosis in C57BL/6 mice (125).

Dimethylnitrosamine (DMN) and diethylnitrosamine (DEN) are carcinogenic substances that induce HCC via liver fibrosis. Like the other chemicals described above, they generate ROS and oxidize nucleic acids, proteins, and lipids, leading to liver cell death and inflammation of liver tissue. Rat and mouse models can be generated, and sensitivity varies according to the strain, with the R16 strain being more susceptible to carcinogenic chemicals. DMN can be injected intraperitoneally at a dose of 10 μ g/g body weight, three times a week for 3 weeks, to generate a liver fibrosis model, while DEN can be injected once a week at a dose of 40-100 mg/kg body weight for 2 weeks to generate a liver fibrosis model. Oral administration and oral gavage administration are also possible (125, 130, 131).

Various methods are used to create a NASH model that does not involve chemical intervention, including the use of a methionine-deficient and choline-deficient (MCD) diet, a choline-deficient L-amino acid deficient diet, and a high-fat diet. The MCD diet induces liver stress and steatosis, resulting in increased triglyceride in the liver tissue of mice and promotes liver fibrosis and lipotoxicity (132). However, this model does not entirely represent human NASH, as it does not exhibit human-like characteristics such as obesity and insulin resistance. The choline-deficient L-amino acid deficient diet has a similar phenotype to the MCD diet, with added benefits of weight

gain and insulin resistance, which can progress to HCC with continuous feeding. The high-fat diet overcomes the drawbacks of the MCD diet, but it takes about 50 weeks to create NASH model in mice (133), and NASH cannot be induced in rats using only a high-fat diet. A NASH model in rats can be created by using a high-cholesterol diet, which takes about 9 weeks, but this model does not exhibit obesity or insulin resistance (134).

The surgical procedure is bile duct ligation, which is an effective animal model for biliary fibrosis. This method is applicable to both rats and mice and involves inducing hepatic fibrosis by tying the bile duct leading to the small intestine, resulting in the accumulation and concentration of bile in the liver tissue. The occlusion of the bile duct increases pressure in the biliary tract, causing stasis and regurgitation. This, in turn, causes portal fibrosis to develop first, which then progresses to perisinusoidal fibrosis. Bile contains toxic substances, such as bile acids and bilirubin, which can cause inflammation when they escape the bile duct and accumulate in the liver tissue. Eventually, the number of B cells and T cells increases in the portal tract, and activated HSCs secrete fibrous proteins significantly. In the bile duct ligation model in mice, portal fibrosis can be observed after about 1 week, perisinusoidal fibrosis after 10 days, and the mortality rate reaches about 20% after 5 to 6 weeks (125, 135-137).

Other methods for making animal models of liver fibrosis include genetic mutation models and virus infection. Genetic mutation models utilize mice that have been genetically engineered to overexpress genes associated with liver fibrosis, such as TGF- β , PDGF, TIMP-1, Mdr2, and Alms1 (138, 139). Virus infection models, on the other hand, require transgenic mice with immune system deficiencies, as hepatitis viruses do not induce liver fibrosis in mice (140)

1.9 Treatment of liver fibrosis

Liver fibrosis, if not progressed to cirrhosis, has the possibility of recovery to some extent through the removal and management of substances that cause liver damage. However, in cases where fibrosis has significantly progressed, treatment is difficult as there is no approved drug available for treating liver fibrosis even after removing the cause of liver damage. An effective drug has been developed to suppress the replication of HBV and HCV viruses, allowing for the maintenance of a relatively healthy liver through consistent management along with the medication. However, since there is currently no drug that can completely eliminate HBC and HCV viruses, continuous management is still necessary. Acetyl-CoA carboxylase inhibitors can reduce triglycerides in patients with NASH-related syndrome and improve liver fibrosis (141). Additionally, IL-11 has been suggested as an important mediator of the fibrosis process, including in recent NASH models, with the possibility of development as a therapeutic agent (105). The FGF21 receptor A antagonist has shown the ability to improve insulin resistance and obesity, cause weight loss, and improve liver fibrosis (142). Several drugs are currently being studied to relieve symptoms in people with NAFLD before they develop NASH. Most of these drugs aim to inhibit the absorption and secretion of cholesterol and fat, suppressing the accumulation of fat in liver tissue. However, to date, there are no FDA-approved drugs for treating NAFLD (Table 1-2).

Drug class	Drug name	FDA approved	Effectivity
Gallstone solubilizing agents	Ursodiol	Not approved	7.7
	Actigall	Not approved	9.0
	Urso	Not approved	-
	Urso Forte	Not approved	-
Nutraceutical products	Betaine	Not approved	-
	Cystadane	Not approved	-
Thiazolidinediones	Pioglitazone	Not approved	-
	Actos	Not approved	-
	Avandia	Not approved	-
	rosiglitazone	Not approved	-
Peripherally acting antiobesity agent	Orlistat	Not approved	5.5

Table 1-2. The medications for NAFLD (This table was created by referring to information from <https://www.drugs.com/>.) Although there are currently no FDA-approved drugs specifically for the direct treatment of liver fibrosis, ongoing research and medical-grade studies are investigating potential drugs aimed at alleviating symptoms associated with liver conditions.

1.10 Hair loss

Hair plays a crucial role in the survival of animals, as it regulates body temperature, shields the skin from the sun, and acts as the primary defense against external physical damage (143-145). Additionally, depending on the species, hair can aid in camouflage and enhance the senses through touch. Hair color in skin is determined by the quantity, quality, and distribution of eumelanin and pheomelanin within the hair follicle, with eumelanin producing black or brown hues and pheomelanin yielding reddish or yellow tones. Therefore, hair color can vary depending on the type and distribution of melanin in each individual. When hair is formed due to aging or stress, gray hair grows due to a lack of melanin pigment.

The process of hair growth and loss can be divided into three stages: anagen, catagen, and telogen. Anagen is the hair growth phase, catagen is the hair loss phase, and telogen is the resting phase (Figure 1-9). The duration of each phase varies depending on species and age, and may be influenced by internal or external factors (146-148). To study hair regrowth and loss, researchers have established a standardized hair cycle, which was summarized by studying C57BL/6 stain mice (147). However, in humans, the hair regrowth cycle is generally unsynchronized, with hair follicles of anagen, catagen, and telogen phases existing in a mosaic arrangement, with the anagen phase accounting for about 90% and 1-2% of catagen phase, and 8-9% of the telogen phase (146, 149).

Although the phenotype of hair loss is similar, hair loss can occur due to various factors, and it is common for the hair growth phase, known as the anagen phase, to not resume and instead remain in the resting phase, called the telogen phase. Furthermore, damage to the hair follicle, where the stem cells necessary for hair formation are located, can impair further hair growth. The causes of hair loss contain nutrient deficiencies, scalp heat, stress, hormones, infections, immune diseases, or genetic mutations. Therefore, although the hair loss phenotype is similar, the treatment may also be different depending on various causes. For this reason, research on hair loss is important, and it is still an active research field.

A recent study has reported on the relationship between immature liver and hair loss. It found

that immature livers in mice exhibited hair loss during the initial hair cycle in the early stages of growth. At the age of four weeks, the anagen phase started, triggering hair growth, and there were no further occurrences of hair loss observed. Iron homeostasis (150). These immature livers show a significant increase in the expression of fetal liver markers and are characterized by poor lipid metabolism and oxyreductase activity (151). Other cases of hair loss are impaired iron homeostasis in liver (152, 153), vitamins and minerals (154). In this paper, it was observed that overexpression of hMUDENG can induce temporary hair loss similar with result of immaturred liver.

Since there are various causes of hair loss, different treatments are required depending on the cause. Although many folk remedies exist, most of them have not been proven, and it is not recommended to try them recklessly due to the potential risks.

Currently, there are some of FDA-approved hair loss treatments: Rogaine (minoxidil), Propecia (finasteride), Olumiant (baricitinib). Minoxidil can be purchased without a prescription, and its effect may vary depending on the individual. It is thought that minoxidil has a hair loss prevention effect by activating ERK and Akt, signal transduction factors related to cell survival, and preventing cell death in human dermal papilla cells (DPC). Additionally, when used as a vasodilator, minoxidil opens potassium channels sensitive to adenosine triphosphate in smooth muscle cells, causing vasodilation. Vascular contraction, one of the causes of male pattern baldness, is thought to have been affected by minoxidil through its vasodilatory effect. It is also thought that minoxidil has a hair loss relief effect by inducing the production of prostaglandin endoperoxide synthase-2 (PGHS-2) observed in the hair follicles during the growth phase. Although the clear mechanism of action of minoxidil is still unknown, it has been shown to shorten the telogen phase and prolong the anagen phase in animal studies, and it is believed that a similar result may be observed in humans (155-158).

Finasteride is an antiandrogenic compound used only in men and is not prescribed for women due to the risk of infertility or birth defects. Its mechanism of action involves inhibiting steroid type II 5 α -reductase, an enzyme that converts testosterone to 5 α -dihydrotestosterone (DHT).

Finasteride is more effective for early to moderate hair loss than in cases where hair loss has progressed significantly. It can be used in combination with hair transplant surgery to enhance its effect (159, 160)

Baricitinib was approved as a systemic treatment for severe alopecia areata in adults on June 13th, 2022. It has previously been approved as a safe treatment for rheumatoid arthritis and COVID-19. Baricitinib competitively blocks signals by Janus kinase (JAK) 1, 2, and 3, thereby preventing various cytokines that transmit signals through JAK from delivering their signals. In the pathophysiology of alopecia areata (AA), various cytokines, such as IL2, IL7, IL15, and IL21, are involved, and effective inhibition of these cytokines has shown improvement in hair loss (161-163).

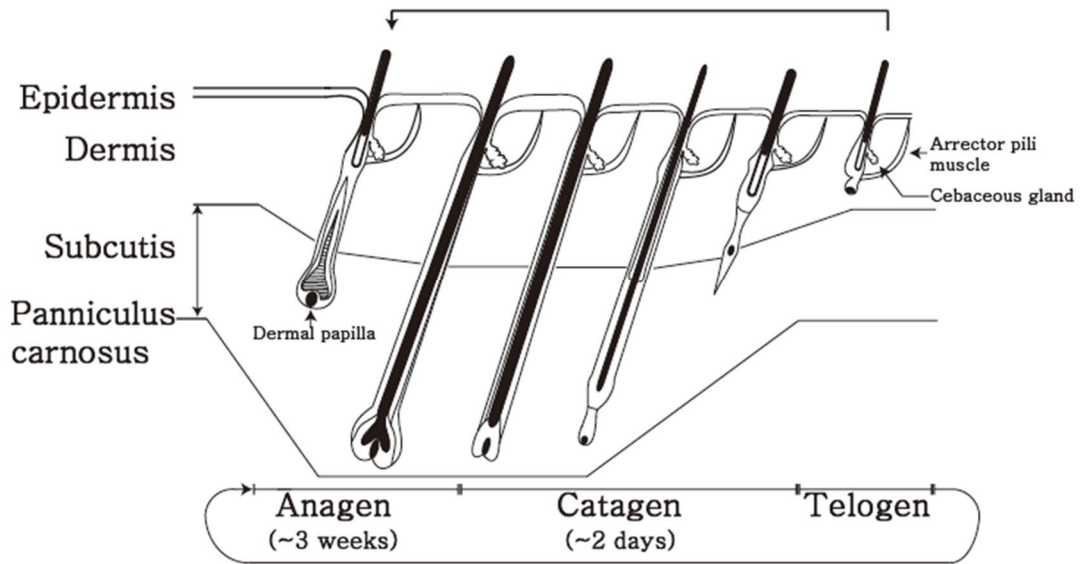


Figure 1-9. Schematic illustration of the hair cycle of mice. In the hair cycle, which consists of repeated stages of anagen, catagen, and telogen, the catagen phase is the shortest while the anagen phase is the longest. The duration of each stage may vary among different species and individuals. In mice, the average duration of the anagen phase is approximately 3 weeks. Mice exhibit mostly synchronized hair cycles, whereas humans have unsynchronized cycles, mosaic arrangement of hair follicles. The majority of the hair cycle (about 90%) is spent in the anagen phase, with catagen accounting for 1-2% and telogen accounting for 8-9% in human. During the catagen and telogen phases, the epidermis becomes progressively thinner, with telogen being the thinnest phase (147).

CHAPTER2

Materials and Methods

2.1. Reagents

Dulbecco's Modified Eagle Medium (DMEM) and fetal bovine serum (FBS) were purchased from GenDEPOT (Barker, USA). Hematoxylin (MA0101010MIRA01) and Eosin (MA0101015MIRA01) was purchased from Mirax (Suwon-si, Korea). Picrosirius red staining kit (24901) was purchased from Polysciences (Warrington, USA). Olive oil (o1514) was purchased from Sigma-Aldrich (St. Louis, MO, USA)

2.2, Cell Culture

Lenti x 293T cells were purchased from Takara Bio (Kusatsu, Japan). Lenti x 293T cells were cultured in DMEM contained 10% FBS, 100 units/ml penicillin, and 100 mg/ml streptomycin at 37 °C in a humidified 5% CO₂atm.

2.3. Lenti virus production

To produce lentivirus, the HEK293T cell line, known for its efficient virus packaging capability, was cultured in DMEM medium supplemented with FBS and antibiotics. The cell culture procedures followed previous protocols. When the cells reached approximately 80-90% confluency, they were co-transfected with the desired gene-containing vector (plenti-x-puro-IL11(WT) and plenti-x-puro-IL11 mutein) along with vectors containing viral envelope proteins and packaging proteins (psPAX2 and pMD2.G). After 12 hours of transfection, to eliminate potential interference from FBS during virus purification, the medium was replaced with EGF-containing DMEM medium without FBS. Following a 2-3 day incubation period, the supernatant was collected from the cell culture, and debris was removed by centrifugation at 10000 xg for 10 minutes. The collected supernatant was then filtered through a 0.45 µm filter to remove any remaining cell fragments. To precipitate the virus, the culture supernatant containing the virus was mixed with 5% PEG6,000 and 0.5M NaCl, and centrifuged at 20,000 xg for 20 minutes. The virus

pellet was resuspended in saline, and stored in an ultra-low temperature freezer until needed. The virus was subsequently utilized according to the desired quantity.

2.4. Animals

Specific pathogen-free C57BL/6 mice (male, 6 weeks old) were purchased from ORIENT BIO Inc. (Seongnam, Korea). Animals were housed under normal laboratory conditions (21–24 C, 40–60% RH) under a 12-h light/dark cycle with free access to standard rodent food and water.

2.5. CCl₄-induced liver fibrosis model

Animal experiments were performed according to our institutional guidelines. For observation of survival rate of hMUDENG Tg mouse against carbon tetrachloride (CCl₄)-induced liver damage, the CCl₄ was mixed with Olive oil in a ratio of 1:7. And 6 µl/g of CCl₄-olive oil mixture was injected intraperitoneally to mouse twice a week for 10 weeks. For histologic and molecular biologic observation of CCl₄-induced liver fibrosis, the CCl₄ was mixed with Olive oil in a ratio of 1:7. 2 µl/g of CCl₄-olive oil mixture was injected intraperitoneally to mouse twice a week for indicated period (0, 2, 4, 6 weeks). To infect the Lenti virus (the Lenti-mIL11 and Lenti-mIL11 mutein virus) were injected intraperitoneally into 6-week-old mice, and injected intranasally into the mouse after a week. Injection of CCl₄ began at 8-week-old mice for 6 weeks.

2.6. RNA sequencing of liver tissue

To investigate the transcriptome changes in the liver tissue of hMUDENG Tg mice, liver tissues of hMUDENG Tg mice and C57BL/6 mice were harvested at postnatal day 18 and 30, respectively, and immediately snap-frozen to prevent degradation. To perform RNA sequencing, I sent the liver samples to the LAS company and requested their analysis services. A summary of the RNA sequencing analysis process performed by LAS company is as follows (Figure 2-1) : “To ensure the strand-specificity of the sequencing libraries prepared using Illumina’s strand-specific

library preparation kit, the mapping process applied the strand-specific library option, --library-type=fr-firststrand. Cuffquant in Cufflinks ver 2.2.1 was used to quantify the mapped reads on the reference genome into gene expression values, using the same strand-specific library option and other default options. Gene annotation of the reference genome mm10 from UCSC genome (<https://genome.ucsc.edu>) in GTF format was used as gene models and expression values were calculated in Fragments Per Kilobase of transcript per Million fragments mapped (FPKM) unit. Differentially expressed genes between the two biological conditions were identified by Cuffdiff in Cufflinks package, using the same strand-specific library option and other default options. Scatter plots for the gene expression values and volcano plots for the expression-fold changes and p-values between the two selected samples were generated using in-house R scripts. To gain insight into the biological functional role of the differentially expressed genes, a gene set overlapping test was performed between the analyzed differentially expressed genes and functional categorized genes, including biological processes of Gene Ontology, KEGG pathways, and other functional gene sets, using g:Profiler2 ver 0.2.0.” (referenced from data and instruction given by LAS bioinformatics company)

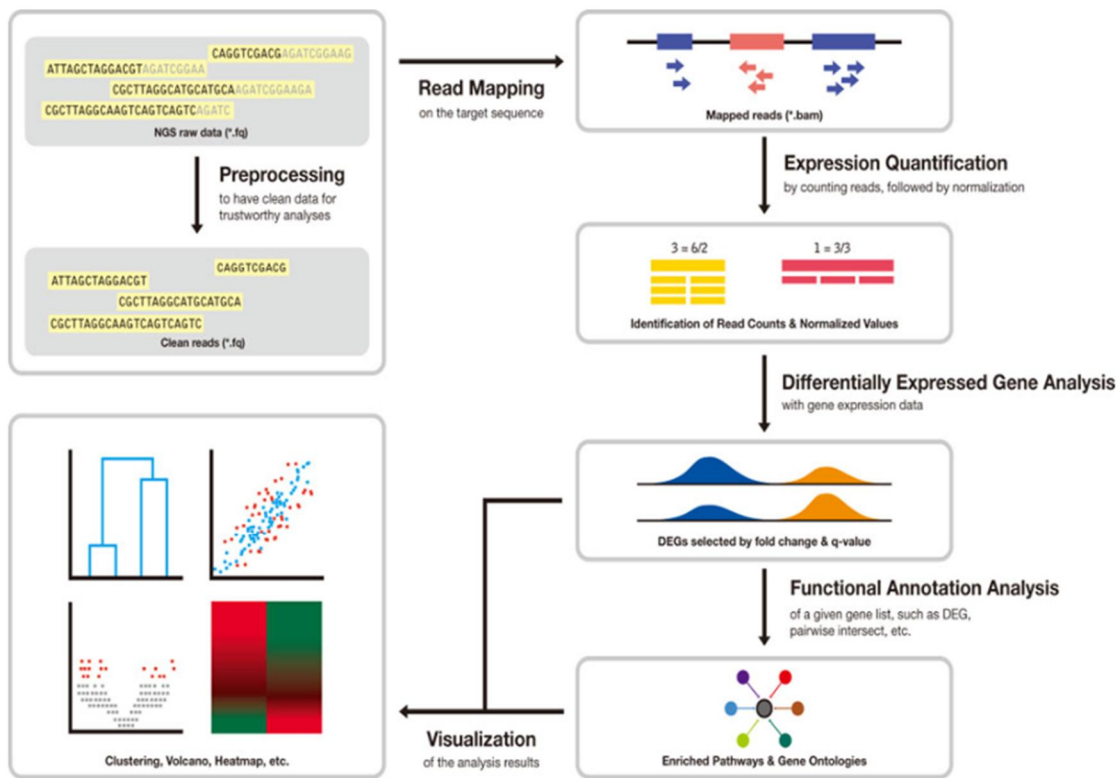


Figure 2-1. Overview scheme of process of LAS company's RNA sequencing (Adapted from figure given by LAS bioinformatics company)

2.7. PCR

The primer sequence is summarized in table1. To identify transcription of AM5M1 in various tissues, reverse transcription (RT) PCR was executed. Total RNA was extracted from various tissues using TRIZOL (#12183555, Invitrogen, Waltham, Massachusetts, USA). The concentration of RNA was measured using TECAN Infinite M200 nanoquant.

Primer name	Primer sequence
P1	5' AGTTACAGCCTTTCCCATCCGAG 3'
P2	5' GCTTTTGTCTGTGCATGATAGG 3'
P3	5' GCCATTTACCGTAAGTTATGTAACG 3'
P4 (For RT PCR)	5' GCAGTGTGGCTCATAAGC 3'
P5 (For RT PCR)	5' CACCTCCTATCAGGAGTC 3'
GAPDH Forward	5' ACCACAGTCCATGCCATCAC 3'
GAPDH Reverse	5' CACCACCCTGTTGCTGTAGCC 3'

Table 2-1. For identification of the transgenic mice, the PCR was performed using tail genomic DNA. The primers P1 and P2, derived from mouse chromosome 3, are located in the 5' and 3' regions outside the MUDENG open reading frame (ORF), respectively. The primer P3 is designed to target the promoter region within the MUDENG ORF. By utilizing these primers, MUDENG Tg mice can be identified through selective amplification of their genomic DNA via PCR. Specifically, the combination of P1 and P3 primers is used to amplify DNA from MUDENG Tg mice, while the combination of P1 and P2 primers is used for amplification from C57BL/6 mice. Primers P4 and P5 were designed for RT-PCR analysis to assess the expression of MUDENG using the internal sequence of the CMV promoter within the MUDENG ORF. The combination of GAPDH primers serves as a reference primer set for quantification in RT-PCR.

2.8. Histological Analysis

For the paraffin section, tissues from skin, kidney, lung, liver, and fibrosis-induced liver were fixed for 48 hours at 4 °C in 4% formalin (JUNSEI, Tokyo, Japan), dehydrated and embedded in the paraffin (Leica, Wetzlar, Germany). The paraffin-embedded tissues were cut to 4 μm thickness. The sections were stained with Hematoxylin and Eosin, Masson's trichrome, and Picrosirius red according to the manufacturer's manual. And images of collagen stained by Sirius red were isolated same color using adobe photoshop program. The graph of % collagen area was indicated using the prism7 program.

2.9. Western blot analysis

For immunoblot analysis, the liver tissues were harvested from fibrosis induced mice at indicated time point. The liver tissue in RIPA buffer were homogenized with homogenizer. Protein concentration were quantified with the bicinchoninic acid (BCA) assay method (ThermoFisher Scientific, Waltham, MA, USA). The equal amount of protein samples was separated by SDS-PAGE and transferred onto polyvinylidene fluoride (PVDF) membranes (GE Healthcare Life Science, Marlborough, MA, USA). The membrane blocked with 4% skim milk (BD; Becton, Dickinson and Company, Franklin Lakes, NJ, USA) for 1 hour and incubated with primary antibodies; IL11 (sc-133063, SantaCruz, Dallas, Texas, USA), α-SMA (14-9760-82, Invitrogen, Waltham, Massachusetts, USA), TGF-β (ab92486, abcam, Cambridge, UK), GAPDH (2118, Cell Signaling, Danvers, Massachusetts, USA), Collagen type1 (PA1-26204, Invitrogen, Waltham, Massachusetts, USA). To visualize the protein level, the chemiluminescent horseradish peroxidase substrates (Millipore, Burlington, Massachusetts, USA) were used.

2.10. Statistical Analysis

All data values were indicated as mean \pm standard deviations. And statistical differences between groups were analyzed by Student's *t*-test; p value less than 0.5 were considered statistically significant.

CHAPTER3

Results and Discussion

3.1 The generation of human AP5M1 transgenic mice

To investigate MUDENG function in mice, vectors containing the MUDENG ORF were constructed called as pDEST-MUDENG-Flag vector (Figure 3-1). First Human MUDENG (hMUDENG) gene was fused with Flag tag at 3' of hMUDENG gene to verify expression using Flag tag. And the hMUDENG fused with Flag tag has CMV promoter to transcribe independently using hMUDENG ORF. The hMUDENG ORF fragment (approximately 2.3 kb) was obtained from the pDEST-MUDENG-Flag vector using Pci and Ssp1 restriction enzymes (Figure 3-1). The fragment was then inserted into the germ cells of mice using electroporation, and the resulting mice were bred with female mice to obtain transgenic mice. Some mice may have multiple copies of the gene, while others may not have the hMUDENG ORF at all. Through continuous breeding with C57BL/6 mice as the control group, a single transgenic strain was selected until only one copy of the hMUDENG ORF remained.

To check insertion site and copy number of hMUDENG ORF, we performed whole genomic DNA sequencing. We found that two copies of the hMUDENG ORF were inserted into chromosome 3 in opposite direction (Figure 3-2). hMUDENG Tg mice can be screened by PCR using two primer pairs, two primers (P1 and P2) on chromosome 3 and an internal primer (P3) on the 5' position of the hMUDENG ORF (Figure 3-3). hMUDENG Tg mouse (Tg-a1, Tg-a2, and Tg-a3) were identified by PCR using primer 1 and primer 3 that could amplify 328 bp of PCR product between chromosome 3 and 5' region of the hMUDENG ORF, but not amplified in C57BL/6 mouse (WT-a1 and WT-a2). And, hMUDENG Tg mouse were not amplified 318 bp of internal sequence on chromosome 3 using primer 1 and primer 2 but C57BL/6 mouse were amplified (Figure 3-3). To determine whether the hMUDENG is transcribed in tissues of hMUDENG Tg mice, we performed RT-PCR using mRNA extracted from various tissues using primers (P4 and P5), which prime the CMV promoter site (P4) and the hMUDENG site (P5). The hMUDENG was transcribed in various tissues such as brain, lung, liver, skin, testis, and blood cells (Figure 3-4).

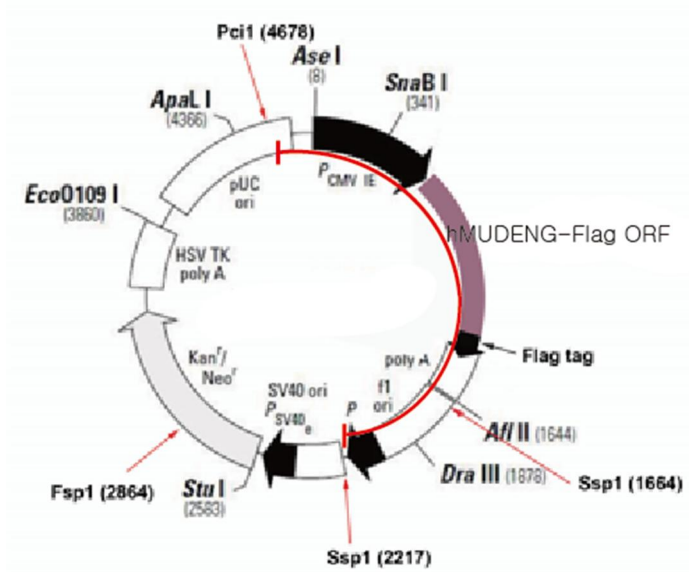


Figure 3-1. Diagram illustrating the structure of the pDEST-hMUDENG-Flag vector. hMUDENG-Flag ORF was obtained by cut with PciI and SspI restriction enzyme, and that size is 2.3 kilobase pair. The hMUDENG-Flag ORF was inserted into germ stem cells to generate MUDENG Tg mice.

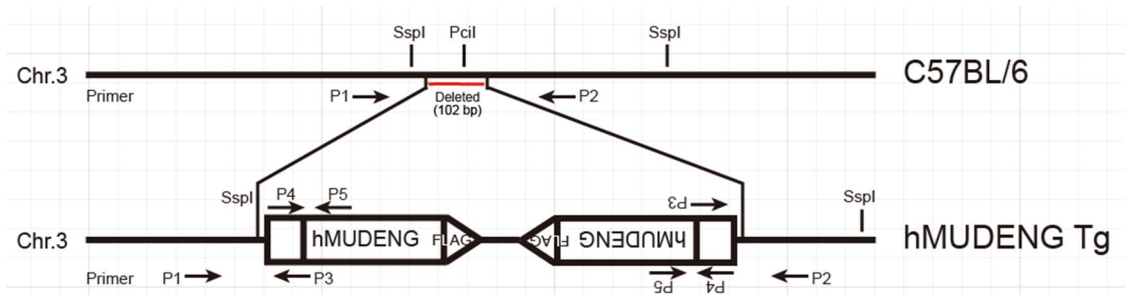


Figure 3-2. The location of hMUDENG-Flag ORF and each primers (P1~P5). Approximately 100 base pairs of the sequence on chromosome 3 were substituted with two copies of the hMUDENG ORF inserted in opposite directions.

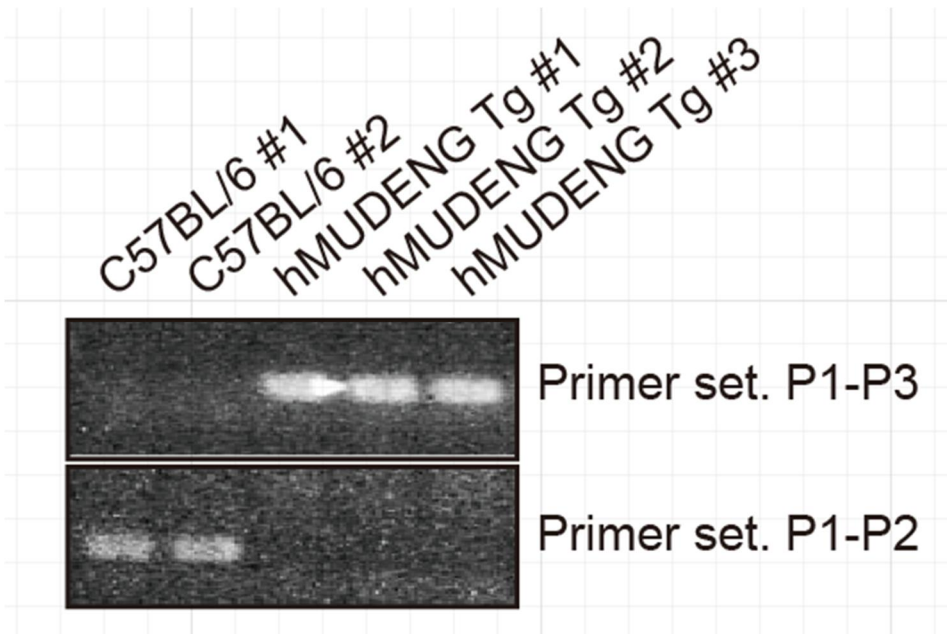


Figure 3-3. Identification of hMUDENG Tg mice. C57BL/6 and hMUDENG Tg were identified by PCR using different primer set, WT; primer1 (P1) and primer2 (P2), and AP5M1 Tg; primer1 (P1) and primer3 (P3), respectively.

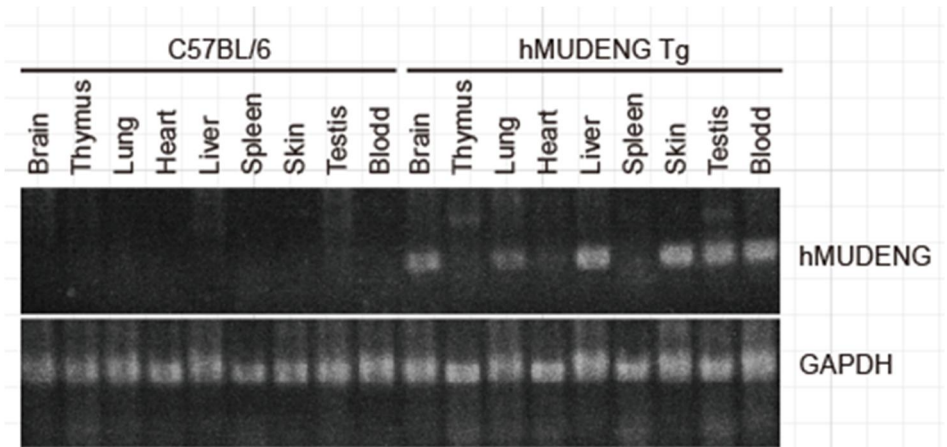


Figure 3-4. Identification of transcription of hMUDENG-Flag in various tissues of hMUDENG Tg mice. Transcribe mRNA was verified by reverse transcription (RT) – PCR using primer4 (P4) and primer5 (P5).

3.2 Hair loss in hMUDENG Tg mice

After selecting hMUDENG Tg mice until one copy of the hMUDENG-Flag ORF remains in the genome of the hMUDENG Tg mouse, I observed that most of the hairs fell out around 2 weeks of age in mice, except for a part at the tip of the head and tail (Figure 3-5). The catagen phase of C57BL/6 mice is about 2 weeks of age, and they enter the anagen phase from about 4 weeks of age, and hair growth can be observed in about 4.5 weeks (Figure 3-5). Although the hair cycle was in the catagen phase at 2 weeks of C57BL/6 mouse, they mouse was not undergo total skin hair loss. However, hMUDENG Tg mouse undergo total hair loss at about 2 weeks except for a part at the tip of the head and tail for about 4 weeks unlike C57BL/6 mouse. Hair starts to grow at about 4.5 weeks and grows to full growth at about 6 weeks in hMUDENG Tg mouse. Although hair follicles return to the catagen phase, after that hair loss is no longer observed in hMUDENG Tg. I thought that hMUDENG could affect hair loss from hair follicle at 2 weeks. I observed the skin tissue of hMUDENG-Tg during the hair loss process using the Hematoxylin and Eosin staining method (Figure 3-6). I observed that hMUDENG-Tg mice entered the catagen phase slightly earlier than the control C57BL/6 mice. Moreover, the length of the telogen phase in hMUDENG-Tg mice was longer than that of C57BL/6 mice, and they entered the anagen phase more slowly (Figure 3-6). In addition, the skin of C57BL/6 mice gradually becomes thinner after catagen phase IV, and has the thinnest skin just before the anagen phase starts again (147). However, the skin of hMUDENG-Tg mice did not become relatively thin even in the catagen and telogen phases (Figure 3-7). In addition, although the C57BL/6 mouse is in the catagen phase, traces of the hair root and the appearance of the follicle remain, but in the hMUDENG Tg mouse, almost all hair follicles are damaged, so the hair follicle is almost invisible, and the hair root is also swollen and all hairs are lost. (Figure 3-7). It could be hypothesized that there were two major causes of hair loss in hMUDENG Tg mice. One cause was an inflammatory reaction caused by hMUDENG overexpressed in skin tissue, and the second cause could be a problem with nutrient supply in liver tissue (164, 165).

I checked whether there were problems such as inflammation in other tissues as in the skin

tissue (Figure 3-8). In the Lung and kidney tissue, no detectable difference between C57BL/6. But, I observed that in the liver tissue of hMUDENG Tg mice, the liver cells were less dense than normal liver cells on day 15, and on day 24, there were more blood cells in the liver tissue of hMUDENG Tg mice than in normal liver tissue (Figure 3-8, 9). In addition, it was observed that hMUDENG Tg mice had a slower growth rate than C57BL/6 mice (Figure 3-10). In general, slow growth is also closely related to poor supply of nutrients. In addition, liver per body weight of hMUDENG Tg mouse were heavier than that of C57BL/6 mice (Figure 3-11). It strongly indicates that MUDENG Tg mice may have issues in their liver tissue around the age of two weeks after birth.

Taken together, these findings suggest that overexpression of hMUDENG may have an impact on the liver, leading to immune cell infiltration into liver tissue, and which could potentially contribute to the slow growth observed in hMUDENG Tg mice. To investigate the changes in transcripts between the liver tissue of hMUDENG Tg mice and C57BL/6 mice, total RNA sequencing was performed on the liver tissue of hMUDENG Tg mice.





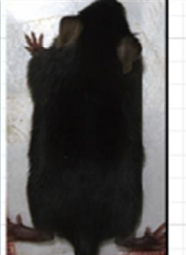







		2 weeks	4 weeks	4.5 weeks	6 weeks
C57BL/6	normal phenotype				
	Depilation of dorsal hair				
hMUDENG Tg	Dorsal				
	ventral				

Figure 3-5. Photographs of hMUDENG Tg mice taken between 2 and 6 weeks of age. These are dorsal and ventral photographs of hMUDENG Tg mice exhibiting progressive hair loss at various time points. Hair loss is a notable phenotypic alteration that initiates around 2 weeks of age and persists until approximately 4 weeks, after which hair regrowth ensues. Subsequently, no additional instances of hair loss were observed.

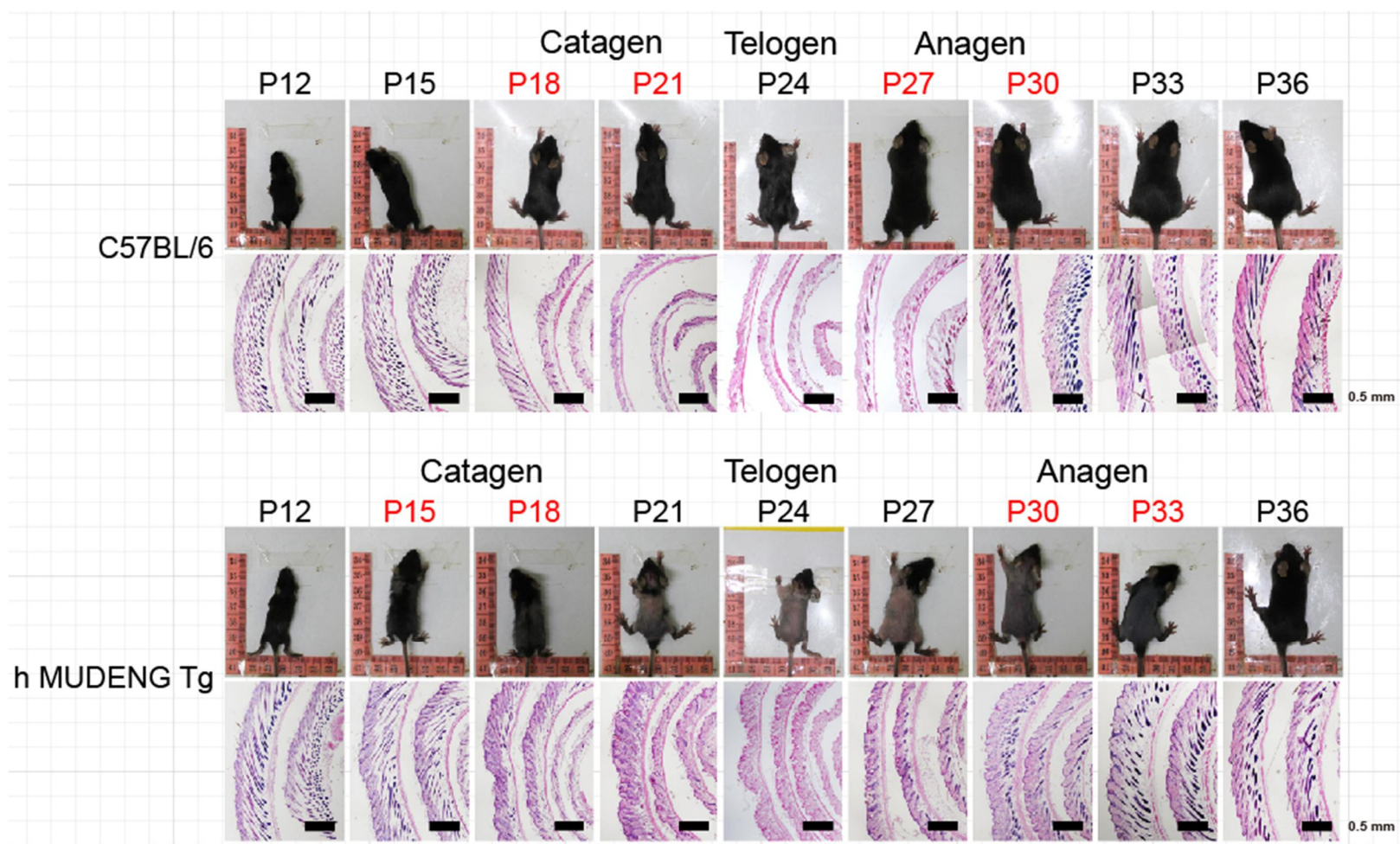


Figure 3-6. Histological examination of skin tissue from hMUDENG Tg mouse at postnatal day 12 (P12) to postnatal day 36 (P36). These are photographs of the dorsal side of C57BL/6 mice and hMUDENG Tg mice taken at different ages ranging from 12 days to 36 days postnatal. Additionally, histological examination of the skin tissue was performed using H&E staining. The skin samples were rolled from the head to the tail, fixed horizontally with paraffin, sectioned at a thickness of 5 micrometers, and stained with hematoxylin and eosin. The hair cycle of hMUDENG Tg mice progressed differently from that of C57BL/6 mice. It was observed that the catagen phase progressed early and the anagen phase started late in skin of hMUDENG Tg mice than that of C57BL/6 mice.

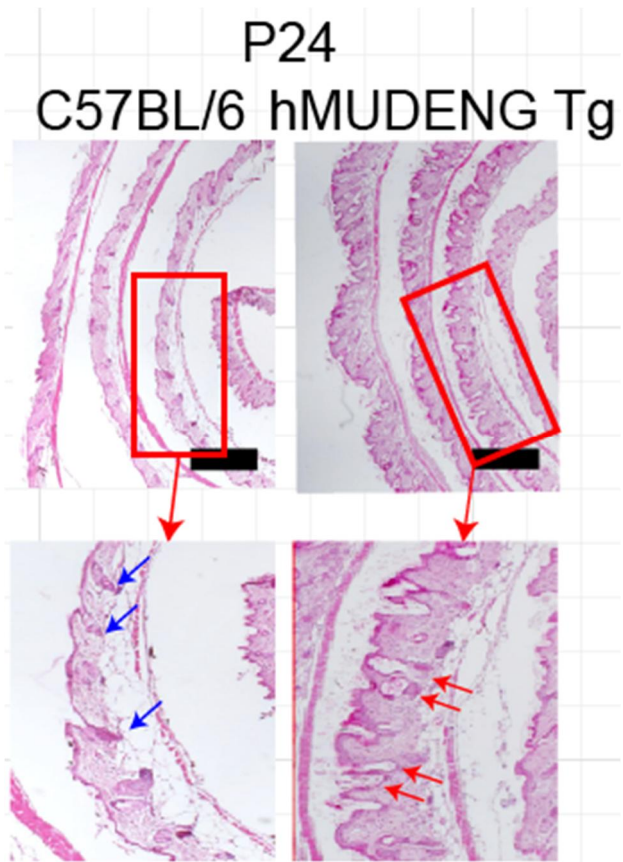


Figure 3-7. Photographs of H&E staining of the skin of C57BL/6 mice and hMUDENG Tg mice at postnatal day 24 (P24). The blue arrows point to hair root sites and presumed follicles. The red arrow points to where the hair root may have been. In contrast to C57BL/6 mice, hMUDENG Tg mice exhibit thick dermis during the telogen phase.

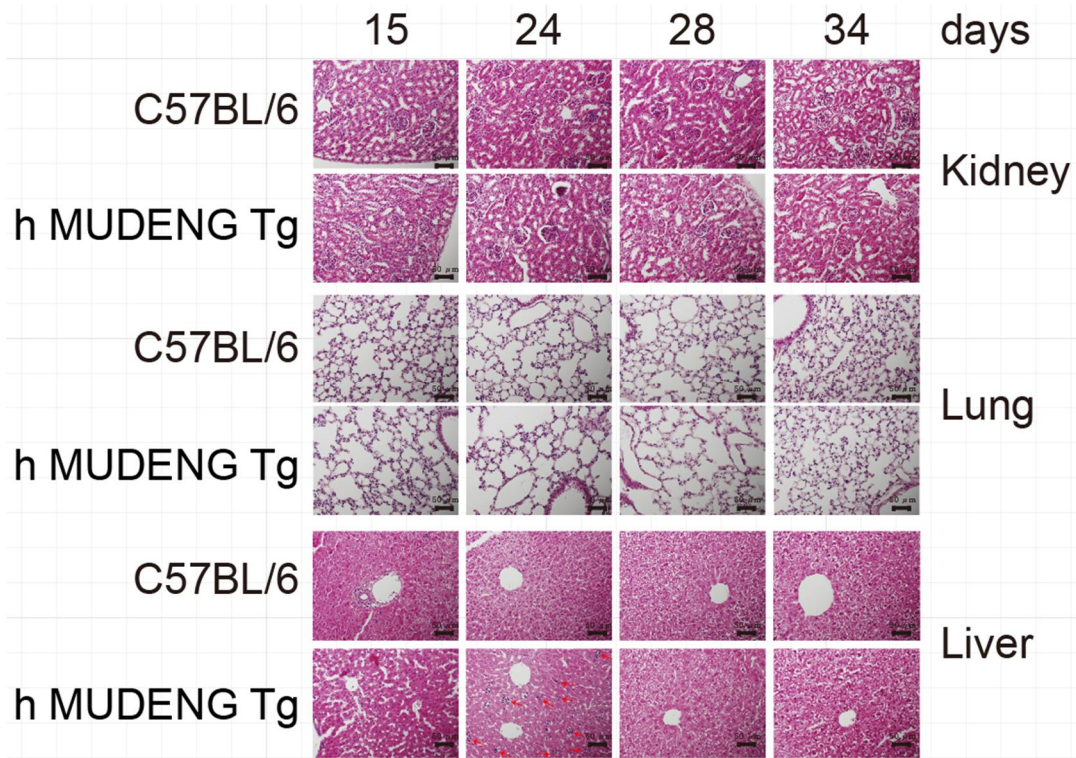


Figure 3-8. H&E staining of Kidney, Lung, and Liver of hMUDENG Tg and WT mouse. H&E staining was performed in the kidney, lung, and liver tissues for each period and comparative observations were made. No differences were found in the kidneys and lungs between MUDENG Tg mice and C57BL/6 mice. However liver tissue of MUDENG Tg has difference with that of C57BL.6 mice. Liver cells of MUDENG Tg mice were less dense than normal liver cells on day 15, and it can be seen that immune cells are infiltrated into the liver tissue of 24-day-old MUDENG Tg mice. Immune cells are indicated by red arrows.

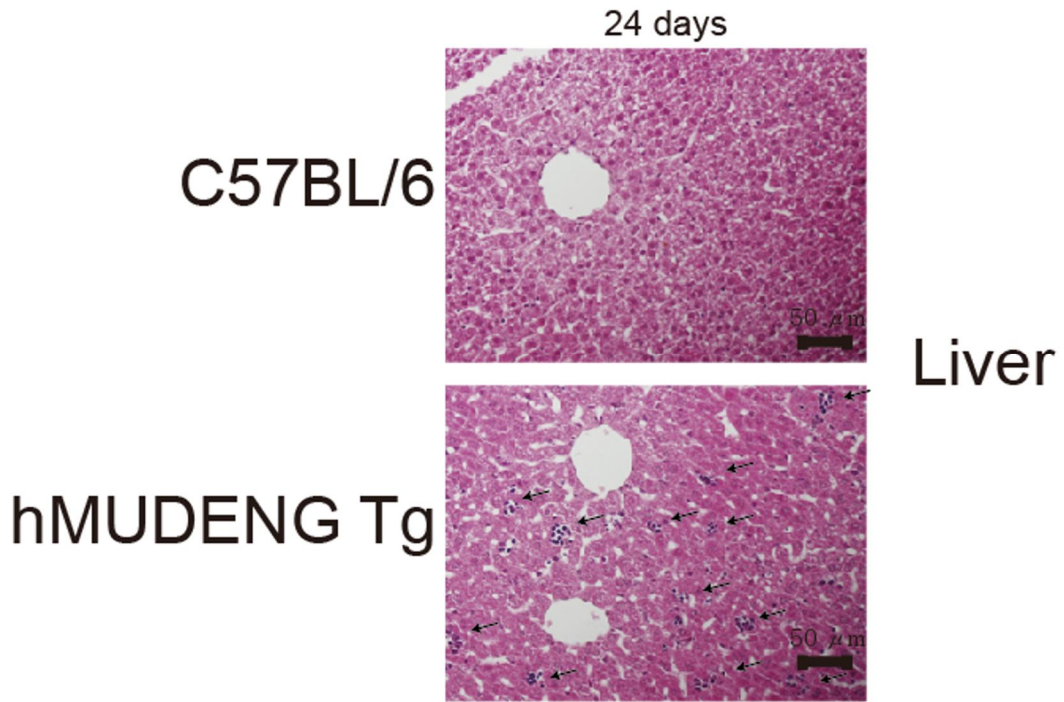


Figure 3-9. H&E staining of liver of hMUDENG Tg and WT mouse at postnatal day 24. The black arrow points to immune cells infiltrated in liver tissue.

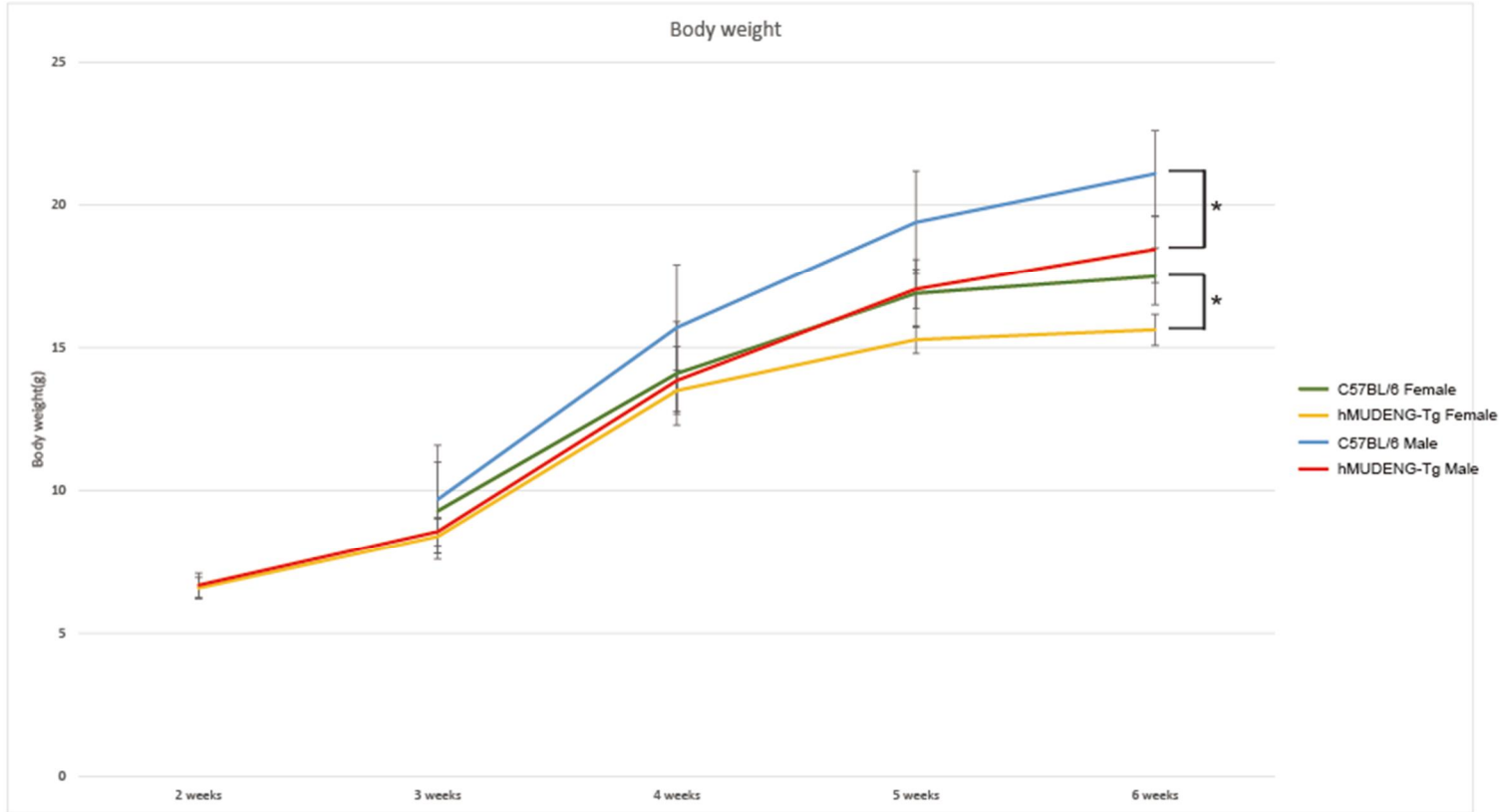


Figure 3-10. The Body weight of hMUDENG Tg and C57BL/6 mouse. The p-value was lower than 0.5 (represented by asterisk, *). Body weight measurements were conducted on MUDENG Tg mice starting from 2 weeks after birth, and on C57BL/6 mice starting from 3 weeks after birth. Both males and females of MUDENG Tg mice grow slower than males and females of normal mice.

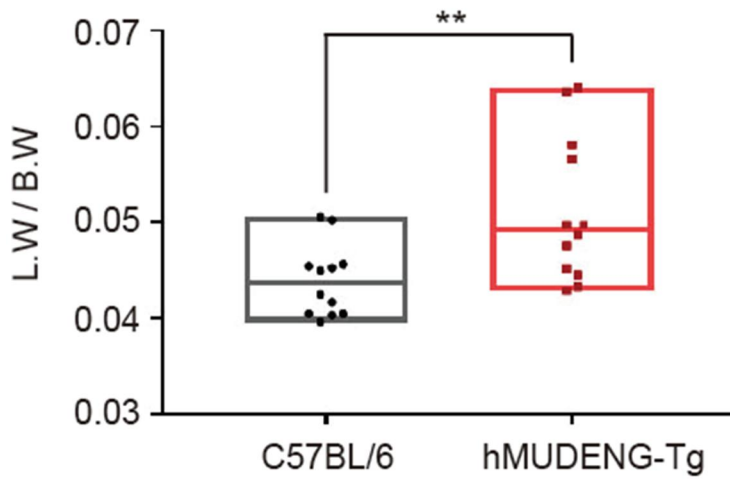


Figure 3-11. Liver weight (L.W) per body weight (B.W) of mice at 6-weeks. It was observed that MUDENG Tg mice weighed less than C57BL/6 mice, but had similar or heavier liver weights. The p-value was lower than 0.01 (represented by asterisk, **).

3.3 Total RNA sequencing in liver

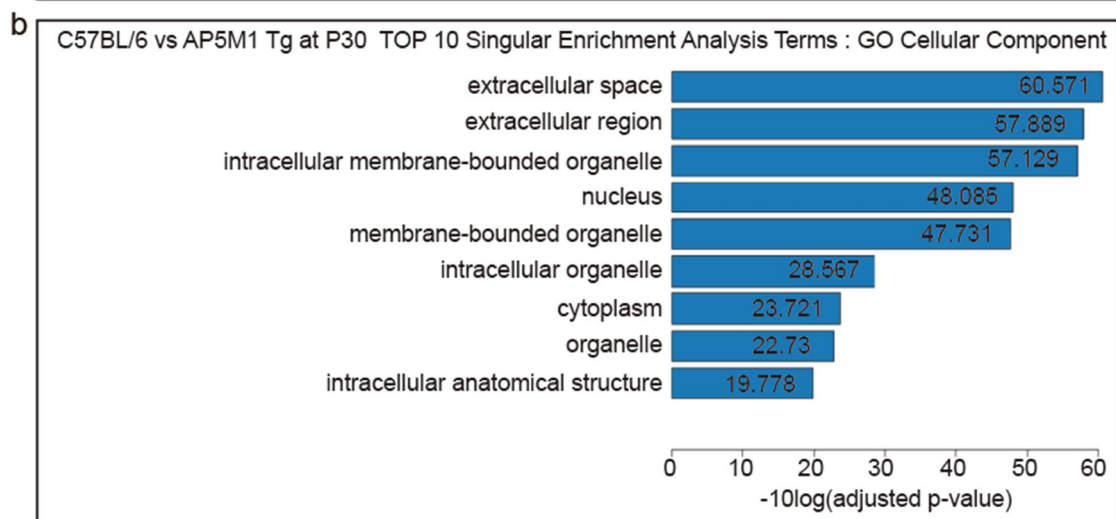
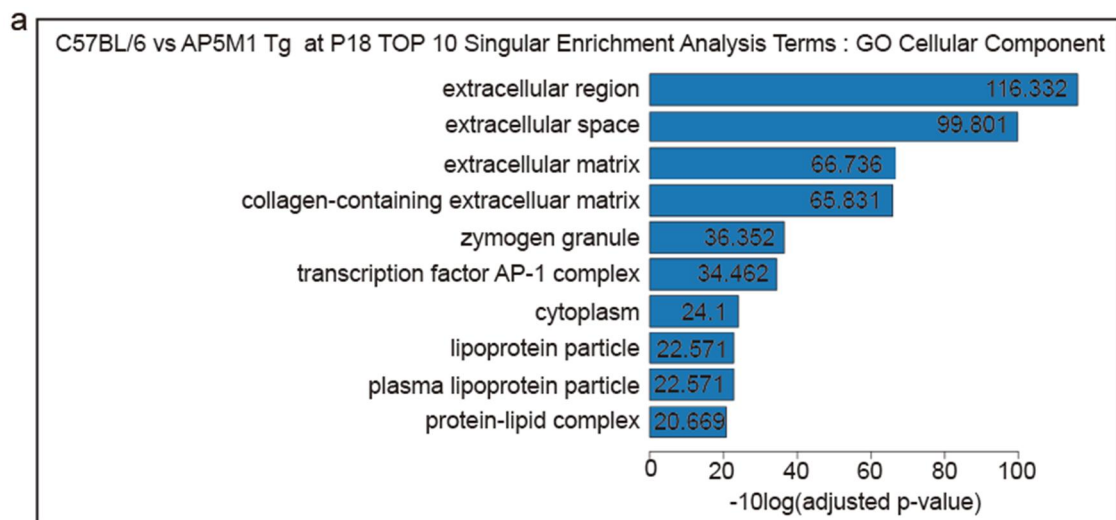
To investigate the mRNA expression profiles in livers of hMUDENG Tg and C57BL/6 normal mice, transcriptome analysis in liver tissues were performed (Figure 3-12a~g). Transcriptome data showed many changes in the livers of hMUDENG Tg compared to C57BL/6 mice. The changes in gene expression in the liver tissue of MUDENG Tg mice were prominently observed from the perspective of cellular components, specifically in the alterations of gene expression related to extracellular factors (Figure 3-12a, b). From a cellular physiological standpoint, significant changes were observed in genes associated with lipid and fatty acid metabolism, iron homeostasis, as well as oxidation and reduction processes (Figure 3-12c~g). It suggest that overexpression of hMUDENG could affect significantly to mouse liver functions. And the transcripts levels changed in liver of hMUDENG Tg include many metabolic proteins especially lipid and fatty acid metabolism at postnatal day 18 (Figure 3-12e). This could affect the hair loss phenotype of hMUDENG Tg mice. The vitamin D receptor (VDR) is one of the transcripts related to lipid metabolism. And there is a research report suggesting that hair loss may be related to a problem with VDR (262-264). In addition, in 2020, Suzuki and his colleagues reported that immaturity of the liver affects the hair cycle in early life in mice (150). The immature liver showed decreased expression of genes related to oxyreductase and lipid metabolism, and significantly increased expression of genes mainly expressed in the early fetal liver such as Alpha-fetoprotein (Afp), H19, Insulin like growth factor 2 (Igf2) (151). At postnatal day 18, the liver tissue of MUDENG Tg mice showed an increase in the expression of fetal liver gene markers (Figure 3-14) and a notable decrease in the expression of genes associated with lipid metabolism, oxidation, and reduction (Figure 3-13). These findings strongly suggest that the hair loss observed in MUDENG Tg mice is a result of immature liver function. Additionally, changes were observed in the expression of genes *Hamp1* and *Hamp2*, known to be associated with iron homeostasis and previously linked to hair loss (Figure 2-15) (166).

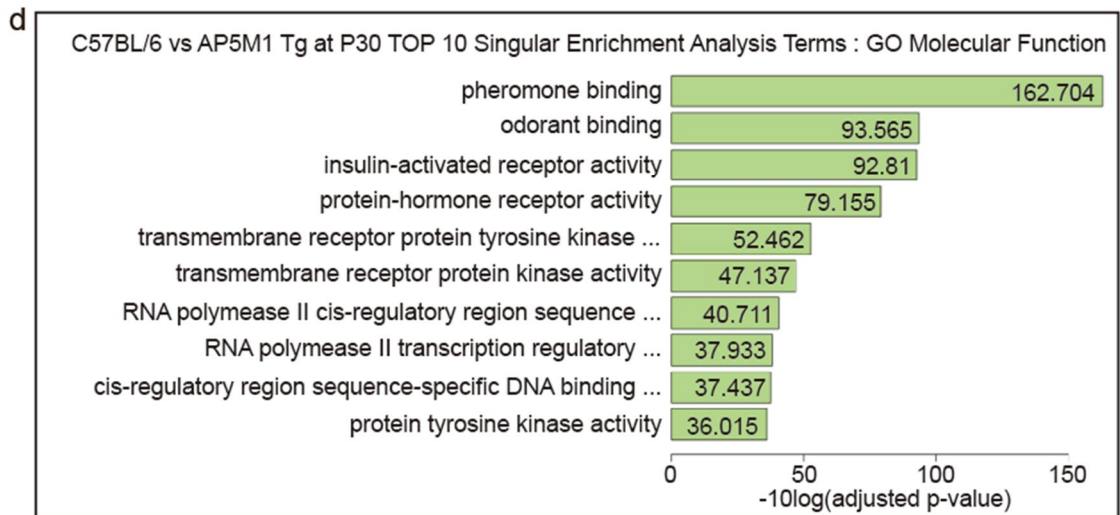
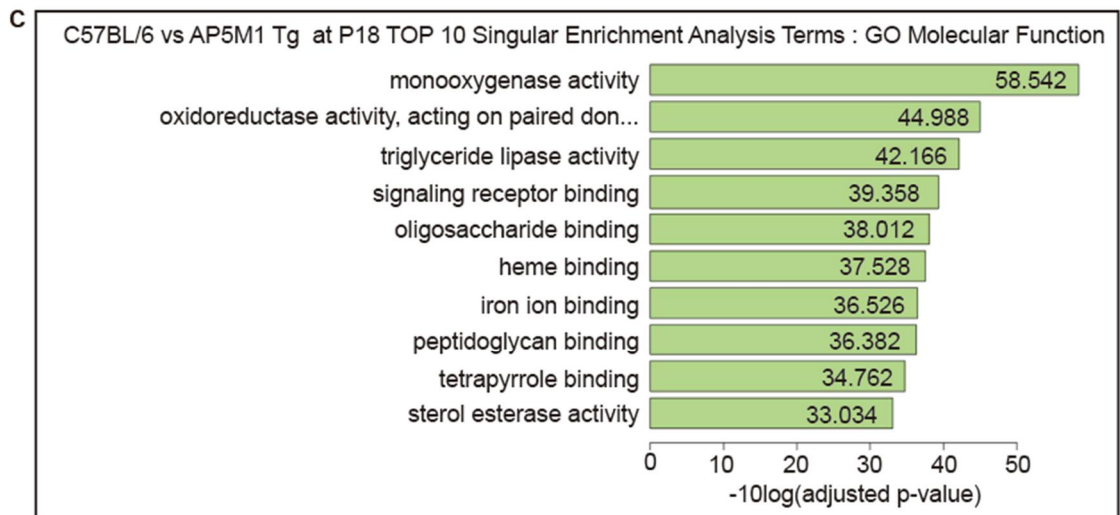
Taken together, it is difficult to pinpoint a single underlying cause for the hair loss observed in MUDENG Tg mice. The overexpression of MUDENG is thought to impair various liver

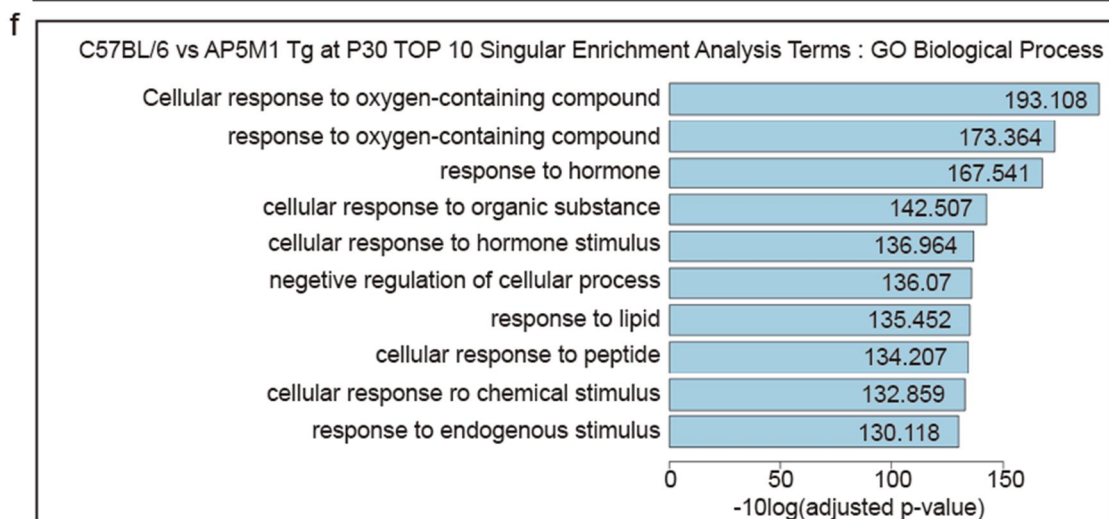
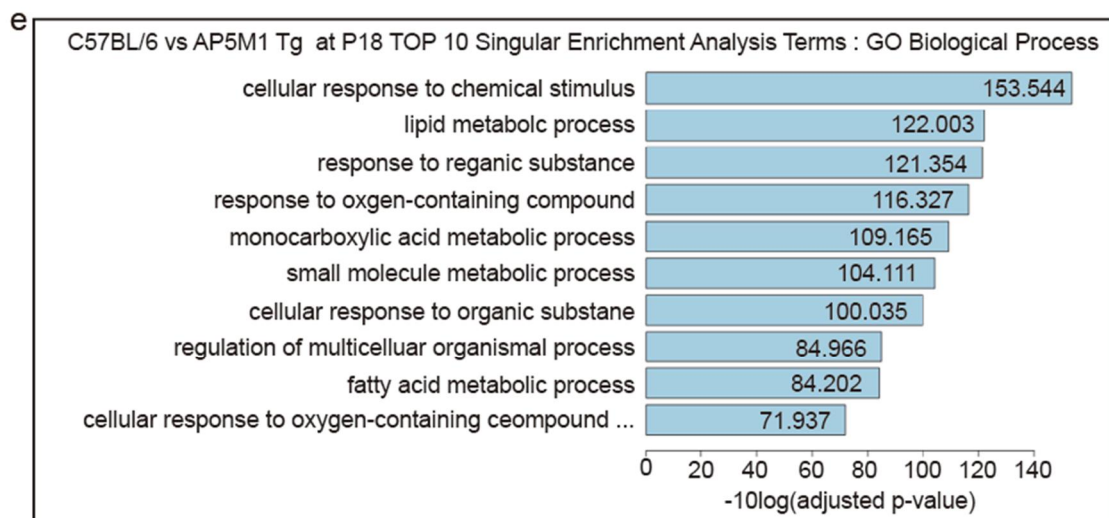
functions such as metabolisms, iron homeostasis, and detoxification, ultimately leading to hair loss.

In Figure 3-9, infiltration of immune cells within the liver tissue was observed at postnatal day 24. Interestingly, similar results were obtained from the transcriptome analysis conducted on the liver of MUDENG Tg mice. Increased expression of factors associated with liver inflammation was observed (Figure 3-16), along with the presence of various immune cell markers (Figure 3-17). In Figure 3-9, infiltration of immune cells within the liver tissue was observed at postnatal day 24. Interestingly, similar results were obtained from the transcriptome analysis conducted on the liver of MUDENG Tg mice. Increased expression of factors associated with liver inflammation was observed (Figure 3-16), along with the presence of various immune cell markers (Figure 3-17). These findings indicate the occurrence of an inflammatory response within the liver tissue, which is closely associated with liver fibrosis. Interestingly, the expression levels of genes involved in liver fibrosis (265-267) such as transforming growth factor (TGF)- β and fibrous proteins such as collagen type1, collagen type3, and α -Smooth muscle actin (α -SMA) were increased in liver of hMUDENG Tg than C57BL/6 mice (Figure 3-18). These alterations could potentially lead to liver damage and subsequent fibrosis (Figure 3-18).

Taken together, these results suggest that overexpression of hMUDENG can induce a mild inflammatory response and promote fibrosis in liver tissue. Although the direct cause of hair loss in hMUDENG Tg mice was not identified, changes of expression levels of lipid metabolism, oxidation and reduction-related factors, iron homeostasis factors, and fetal liver markers could be a contributing factor to hair loss. Moreover, inflammatory reaction in liver could be closely involved in liver fibrosis.







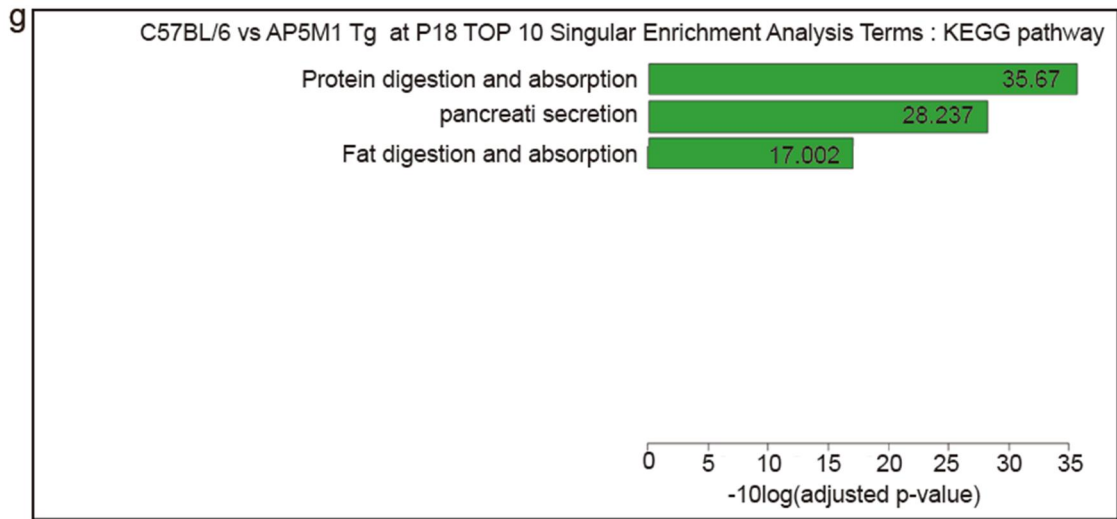


Figure 3-12. The result of total RNA sequencing in liver of C57BL/6 and hMUDENG Tg mice. The enriched biological terms from the 402 Differential Expression Genes (DEGs) of ($|\text{Fold-Change}| \geq 2$) \cap ($P\text{-value} \leq 0.05$) in liver of hMUDENG Tg per C57BL/6 mice at postnatal day 18(P18) and 30 (P30).

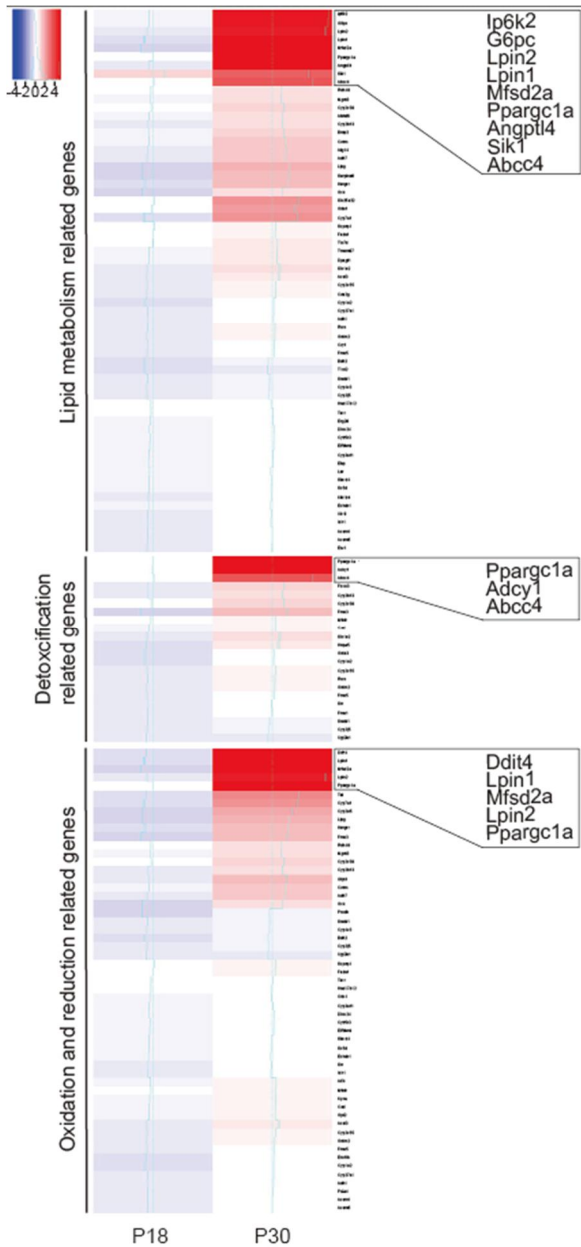


Figure 3-13. Heat map of RNA transcripts levels related to lipid metabolism, detoxification, and oxidation and reduction in liver of hMUDENG Tg per C57BL/6 mice at postnatal day 18 (P18) and 30 (P30). At day 18 postnatal, the liver tissue of hMUDENG Tg mice showed lower expression of multiple genes associated with fat metabolism, detoxification, oxidation, and reduction compared to C57BL/6 mice.

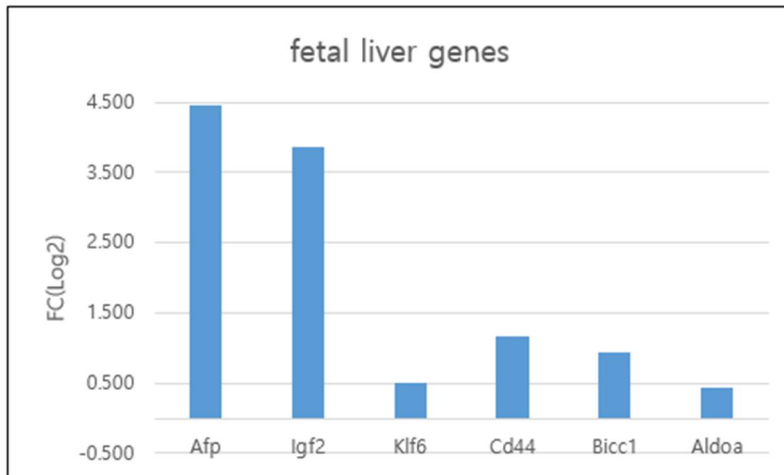


Figure 3-14. The changes of fetal liver markers in liver of MUDENG Tg mice. These genes such as alpha fetoprotein (Afp), insulin growth factor2 (Igf2), Krüppel-like factor 6 (Klf6), CD44, Bicaudal C homolog 1 (Bicc1), Aldoa genes are known expressed during fetal liver development. The FL(Log2) typically refers to the Fold Change (Log2) value.

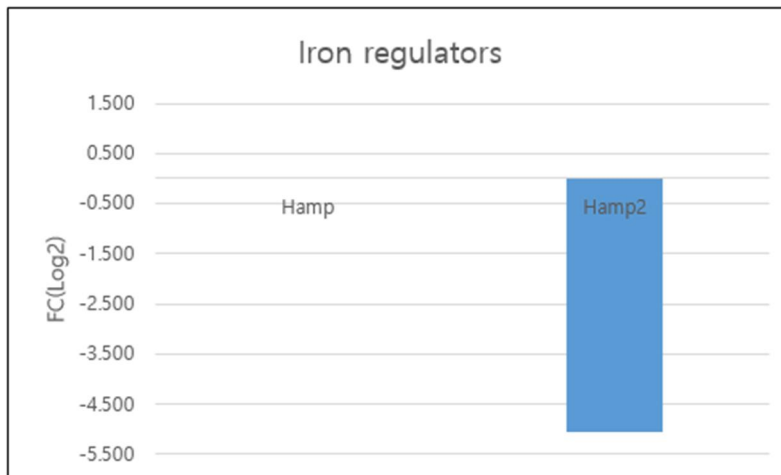


Figure 3-15. The changes of iron homeostasis related genes in liver of MUDENG Tg mice. The FL(Log2) typically refers to the Fold Change (Log2) value. There is no significant difference in the expression level of Hamp between hMUDENG Tg mice and C57BL/6 mice, but Hamp2 showed an FC(Log2) approximately 5-fold lower in hMUDENG Tg mice compared to C57BL/6 mice. This value indicates that the actual expression level can decrease by up to 33-fold.

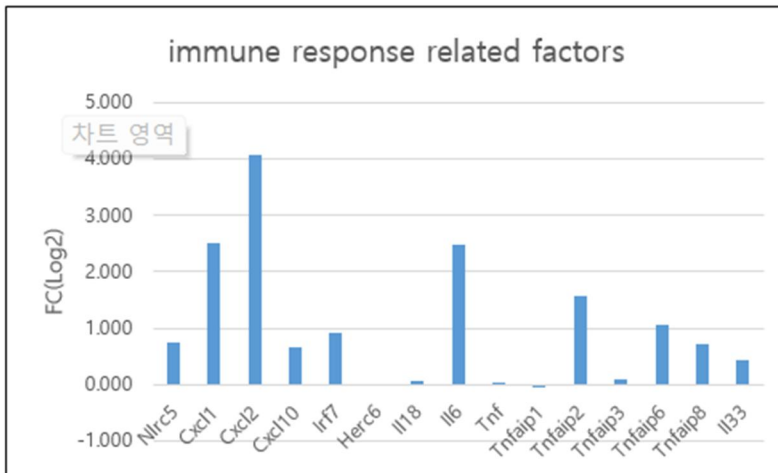


Figure 3-16. The changes of inflammation related factors in liver of MUDENG Tg mice. Some immune response-related cytokines exhibit increased expression in hMUDENG Tg mice. The FL(Log2) typically refers to the Fold Change (Log2) value.

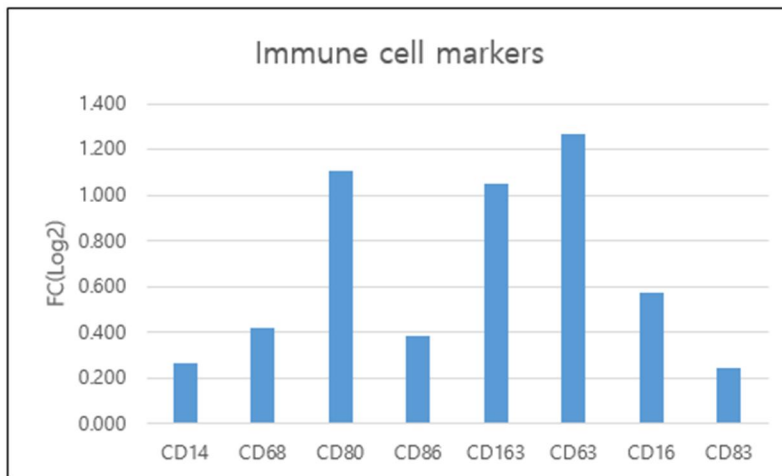


Figure 3-17. The changes of immune cells markers in liver of MUDENG Tg mice. CD14 is a marker of monocytes, and CD68 is a marker of macrophages. CD80 and CD86 are markers of type 1 macrophages, while CD163 is a marker of type 2 macrophages. CD63 is a marker gene expressed in activated natural killer (NK) cells and basophils, and CD16 is a marker gene expressed in NK cells and neutrophils. CD83 is a marker of activated dendritic cells (DCs). The FL(Log2) typically refers to the Fold Change (Log2) value.

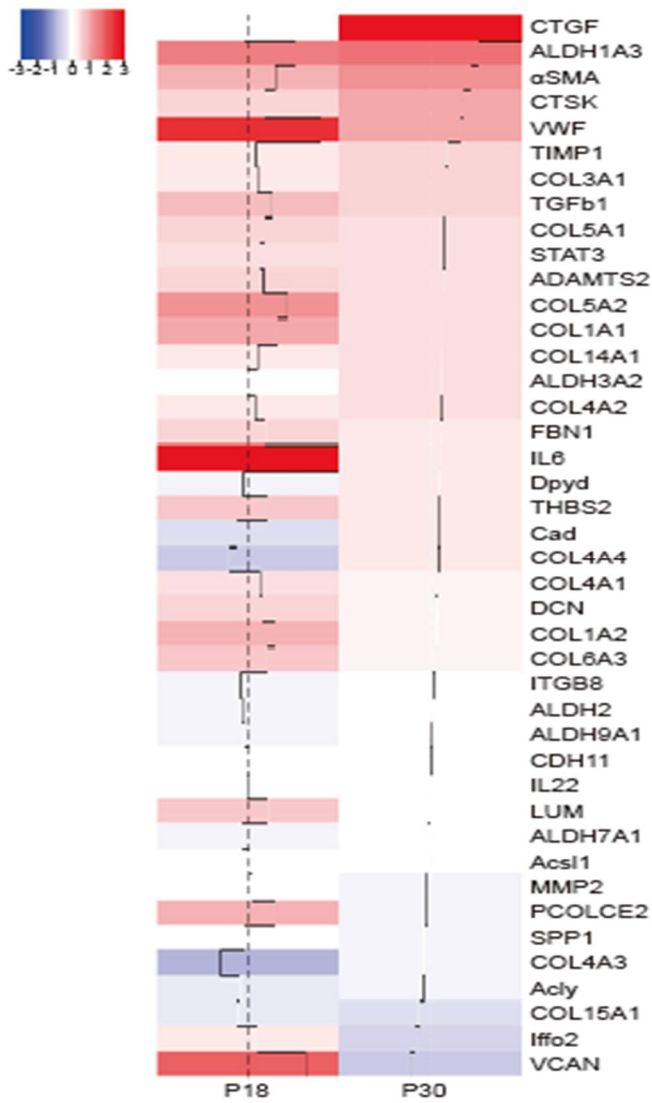


Figure 3-18. The heat map of RNA transcripts levels of representative genes in liver fibrosis in liver of hMUDENG Tg per C57BL/6 mice at postnatal day 18 (P18) and 30 (P30). At 18 and 30 days postnatal, the liver tissues of hMUDENG Tg mice exhibited significantly increased expression of numerous genes known to be involved in liver fibrosis compared to those of C57BL/6 mice.

3.4 The Liver of hMUDENG Tg mice

In the liver tissue of hMUDENG Tg mice, the expression of immune cell markers and pro-inflammatory factors such as TGF- β , IL-6, and IL-11 was increased without any stimulation, and it was observed that factors related to fibrosis such as CTGF, collagen proteins, alpha smooth muscle actin, STAT3, and CYP family were also increased (Figure 3-16~18). This strongly supports the close association between overexpression of hMUDENG and liver fibrosis in mice. To investigate whether there are changes in the liver tissue of hMUDENG Tg mice as the results of RNA sequencing, I observed the degree of fibrosis in the liver tissues of hMUDENG Tg and C57BL/6 mice by Masson's trichrome staining method (Figure 3-19). The Masson's trichrome stain method is used to stain collagen protein, which is responsible for fibrosis, in blue or green color. Keratin and muscle fibers are stained in red, cytoplasm in bright red or pink, and cell nuclei in dark brown or black. It was observed that hMUDENG overexpression could induce mild sinusoidal fibrosis in the liver tissue even without any additional stimulation.

In summary, the transcriptome analysis of liver tissue in MUDENG Tg mice revealed a close association between the overexpression of MUDENG and liver fibrosis, and the results of Masson's trichrome staining strongly support the speculation of a link between MUDENG and liver fibrosis.

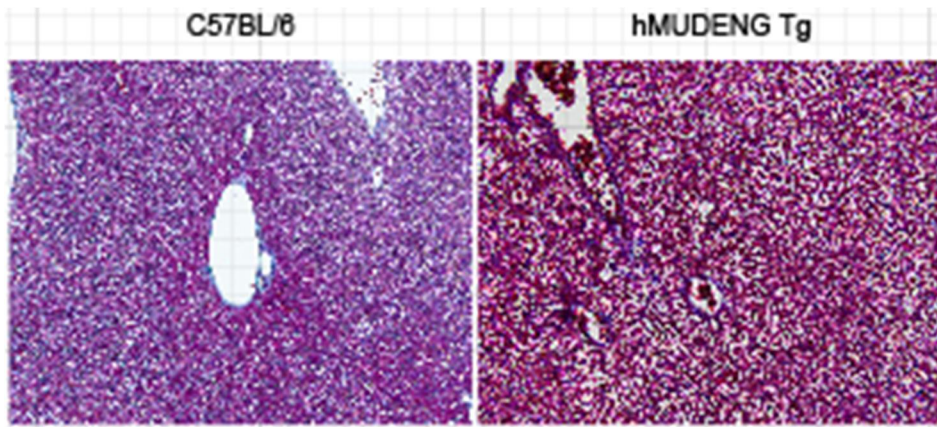


Figure 3-19. Masson's trichrome staining of liver of hMUDENG Tg and C57BL/6 mouse. In hMUDENG-Tg mice, accumulation of weak fibrous proteins in the sinoid was observed, and some necrotic cell death was observed.

3.5 The effect of hMUDENG on CCl₄-induced liver fibrosis

Since transcriptome data suggested that overexpression of hMUDENG in hMUDENG Tg may lead to liver damage, the liver fibrosis in hMUDENG Tg was further examined. To investigate whether hMUDENG Tg is more susceptible to the liver damage or not, I induced liver damage by injecting carbon tetrachloride (CCl₄) mixed with olive oil into hMUDENG Tg and C57BL/6 mice for 10 weeks to induce liver fibrosis (Figure 3-20). While all C57BL/6 mice survived the CCl₄ treatment, hMUDENG Tg mice exhibited 90% mortality between 7 and 10 weeks after the treatment. This finding may support the hypothesis that hMUDENG Tg mice are susceptible to liver damage such as CCl₄ toxin (Figure 3-21). For histologic and molecular biologic observation, I decreased CCl₄ concentration from 0.7 μ l/g body weight to 0.25 μ l/g body weight. I injected CCl₄ mixed with olive oil intraperitoneally (I.P.) twice a week for 2, 4, and 6 weeks to hMUDENG Tg and C57BL/6 mouse (Figure 3-22). The collagen accumulation shown by Sirius red staining was monitored in the liver tissues of hMUDENG Tg and C57BL/6 mice upon CCl₄ injection twice a week, and I found that the collagen in the liver of hMUDENG Tg mice was more rapidly accumulated than that in the liver of C57BL/6 mice (Figure 3-23). The collagen panels in Figure 3-23a are a color-isolated region from an area stained with Sirius red using the Adobe Photoshop program (Figure 3-23a). The collagen accumulation area quantitatively measured by NIH image J analysis tools from the collagen panels in Figure 3-23a clearly showed that hMUDENG Tg mice are more susceptible to CCl₄-induced liver fibrosis compared to normal C57BL/6 mice (Figure 3-23b). Furthermore, the liver in hMUDENG Tg mice contained accumulated collagen area even without CCl₄ injection, indicating that overexpression of hMUDENG in liver causes liver to be susceptible to the liver damage. It is worth to note that the expression levels of TGF- β and IL11 were higher in the liver of hMUDENG Tg mice, even, without the treatment of CCl₄ (Figure 3-23c). Western blot analysis further proved that the level of TGF- β in hMUDENG Tg mice without the treatment of CCl₄ were increased in consistent to transcriptome data shown in Figure 3-18 (Figure 3-23c). In addition, α -SMA, one of the major fibrous proteins absorbed in fibrotic liver, was also rapidly accumulated in the liver of hMUDENG Tg mice upon on the treatment of CCl₄

(Figure 3-18c). The activated form of TGF- β , the key protein in liver fibrosis, also showed the increased level in hMUDENG Tg than in C57BL/B mice. Moreover, the expression level of IL11 showed the similar pattern to that of TGF- β , suggesting that rapid increase of TGF- β and IL11 in response to CCl₄-induced liver damage may play a role in susceptibility of liver fibrosis (Figure 3-18c). Taken together, overexpression of hMUDENG in mouse liver may cause the increased background gene expression of TGF- β and IL11, resulting in rapid increase of collagen, α -SMA, TGF- β and IL11 in response to CCl₄.

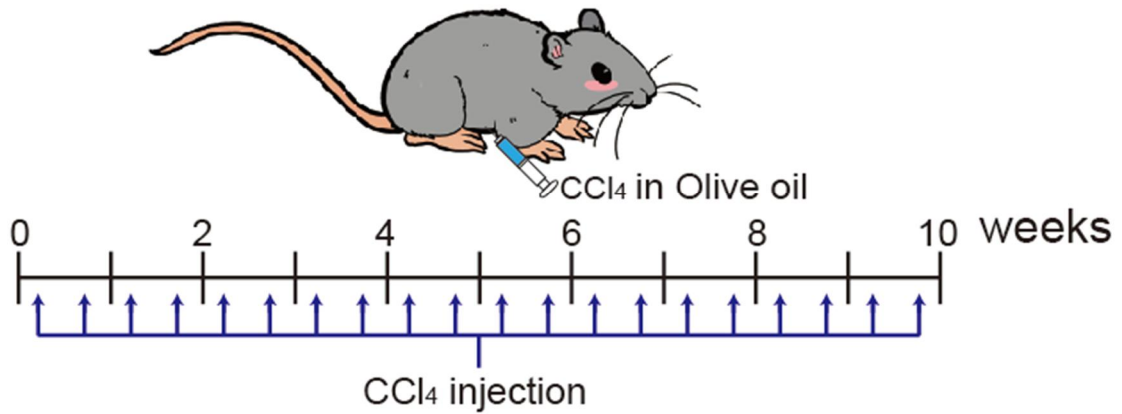


Figure 3-20. Designing a CCl₄-induced liver fibrosis model for the observation of susceptibility to CCl₄ in hMUDENG Tg mice. hMUDENG Tg and C57BL/6 mouse were injected with 0.7 μ l/g body weight of CCl₄ mixed with olive oil in 1:7 (CCl₄:1, olive oil:7) ratio for 10 weeks.

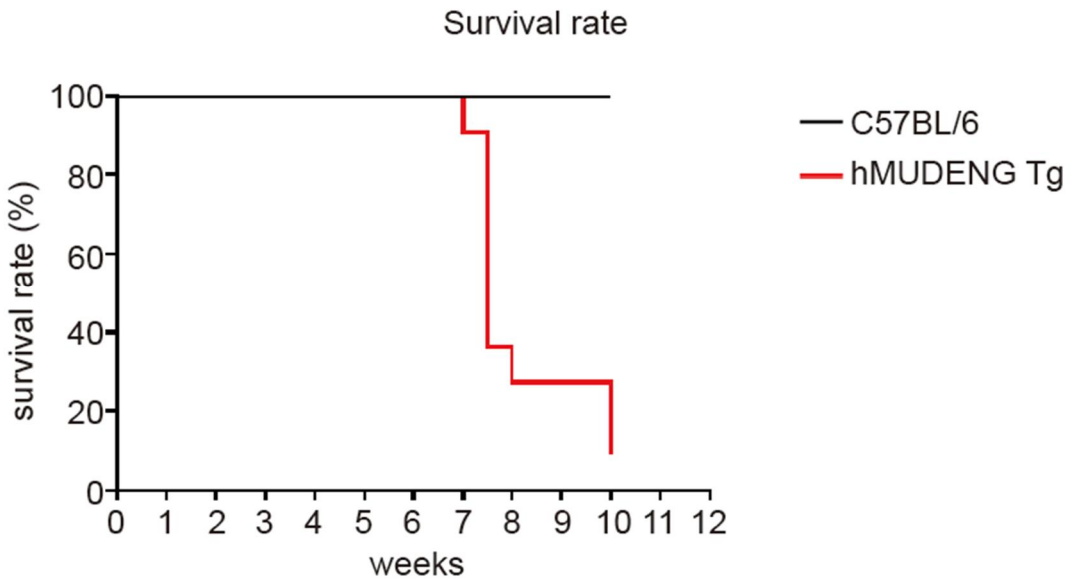


Figure 3-21. Survival rate of hMUDENG Tg after treatment of CCl₄. When hMUDENG Tg and C57BL/6 mice were injected with CCl₄ at a concentration of 6 μ l/g twice a week for 10 weeks, no mortality was observed in C57BL/6 mice, whereas hMUDENG Tg mice exhibited rapid lethality starting from week 7.

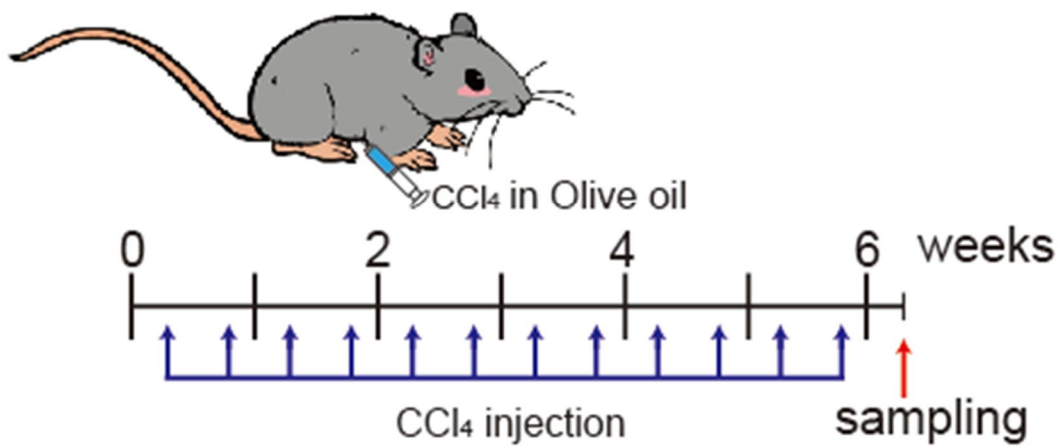
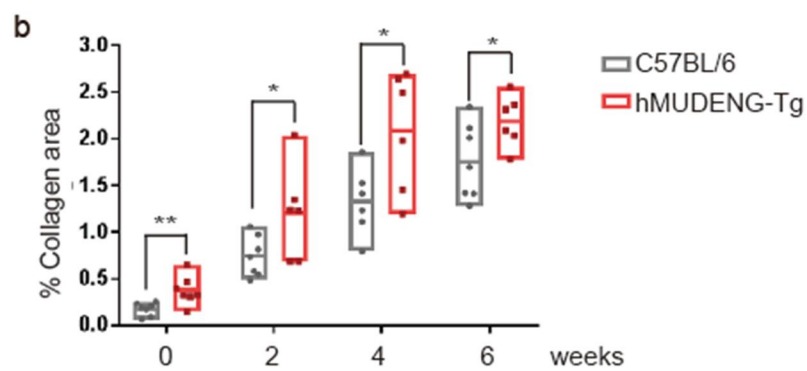
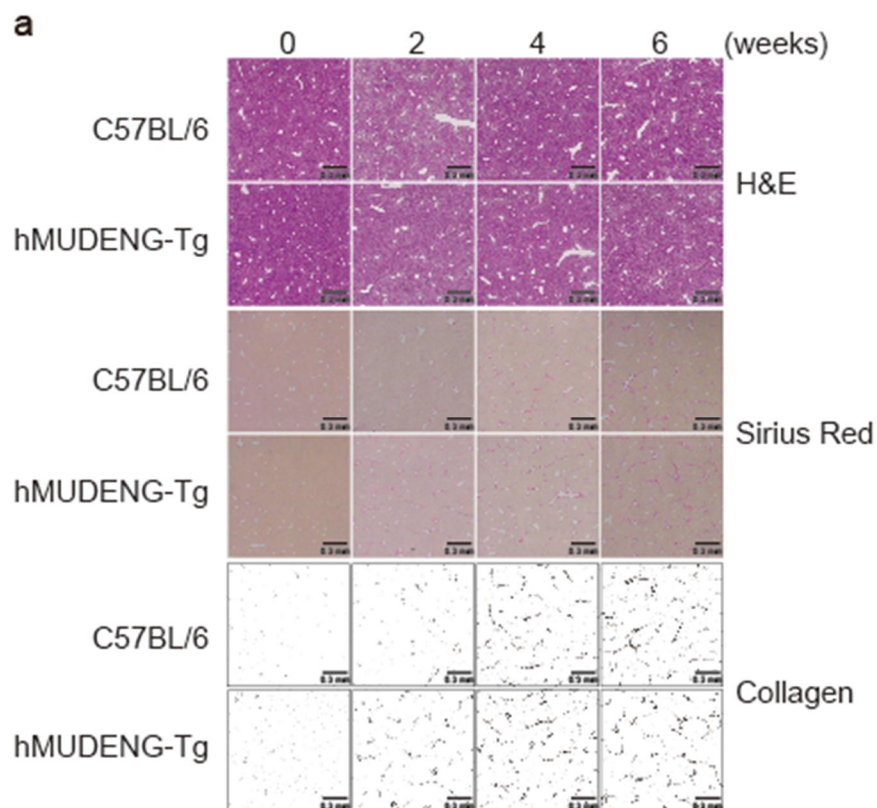


Figure 3-22. Schematic diagram of CCl₄-induced liver fibrosis model. hMUDENG Tg and C57BL/6 mouse were injected with 2 μ l/g body weight of CCl₄ mixed with olive oil in 1:7 (CCl₄:1, olive oil:7) ratio for 2, 4, and 6 weeks.



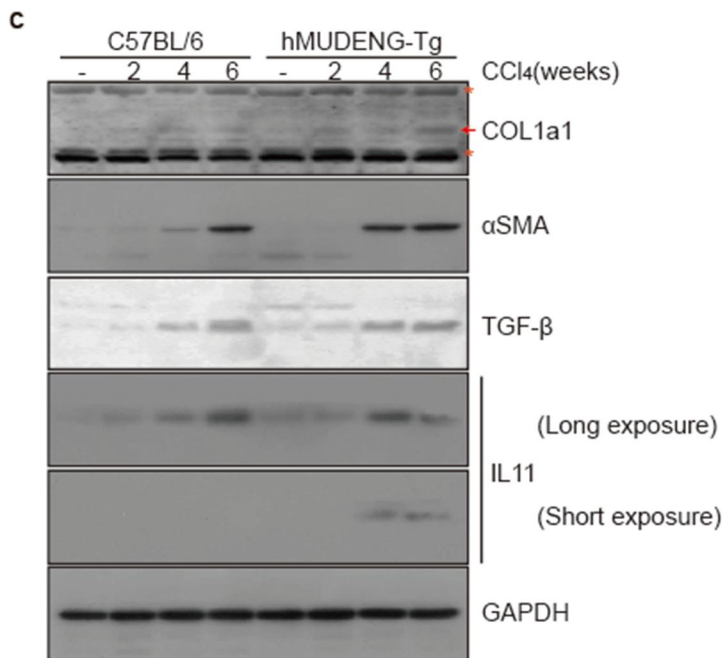


Figure 3-23. The effect of hMUDENG on CCl₄-induced liver fibrosis. (a) Comparison of histological staining (hematoxylin and eosin (H&E) and picrosirius red (sirius red)) of CCl₄-induced fibrotic liver of C57BL/6 and hAP5M1-Tg mice. For the collagen panel, only the collagen stained from the Sirius Red panels were isolated. (b) Percentage area of collagen in picrosirius red-stained tissue sections of CCl₄-induced fibrotic liver. (c) The fibrous proteins (collagen type1 and α-Smooth muscle actin (α-SMA)), IL11, and TGF-β was determined by western blot. The bottom panel of IL11 was short exposed, and upper panel was long exposed. Scale bars: 0.3 mm, * <0.05 , ** <0.01 .

3.6 The effect of mIL11 and mIL11 mutein on CCl₄-induced liver fibrosis of C57BL/6

Based on the results shown in Figure 3-17, mIL11 was thought to be a key player in CCl₄-induced liver fibrosis in both hMUDENG Tg and C57BL/6 mice. I assumed that mIL11 blocking could mitigate progression of liver fibrosis in hMUDENG Tg as well as C57BL/6 mice damaged by CCl₄. The mIL11 mutein, mIL11 antagonist that is first generated by Heath's group, has high affinity to their receptor, mIL11R; however, it could not bind to gp130, resulting in no signal transduction of mIL11 into intracellular downstream signaling pathway (Figure 3-24) (167). I designed lentivirus expression system that expresses mouse wild type IL11 (lenti mIL11) and mouse IL11 mutein (lenti mIL11 mutein) construct (Figure 3-25a,b). The mIL11 and mIL11 mutein genes were fused with human growth hormone signal sequence for secretion and furin cleavage site at the N-terminal region of mIL11 gene for elimination of unnecessary sequence (Figure 3-25a, b). To verify that both lenti mIL11 and lenti mIL11 mutein have infectivity, I infected 293 cells with lenti mIL11 and lenti mIL11 mutein. I expected that both mIL11 and mIL11 mutein were secreted to the medium from 293 cells; indeed, both mIL11 and mIL11 mutein were detected from conditioned media by western blot analysis (Figure 3-25c). These results indicate that lenti mIL11 and lenti mIL11 mutein can infect 293 cells and secrete mIL11 and mIL11 mutein.

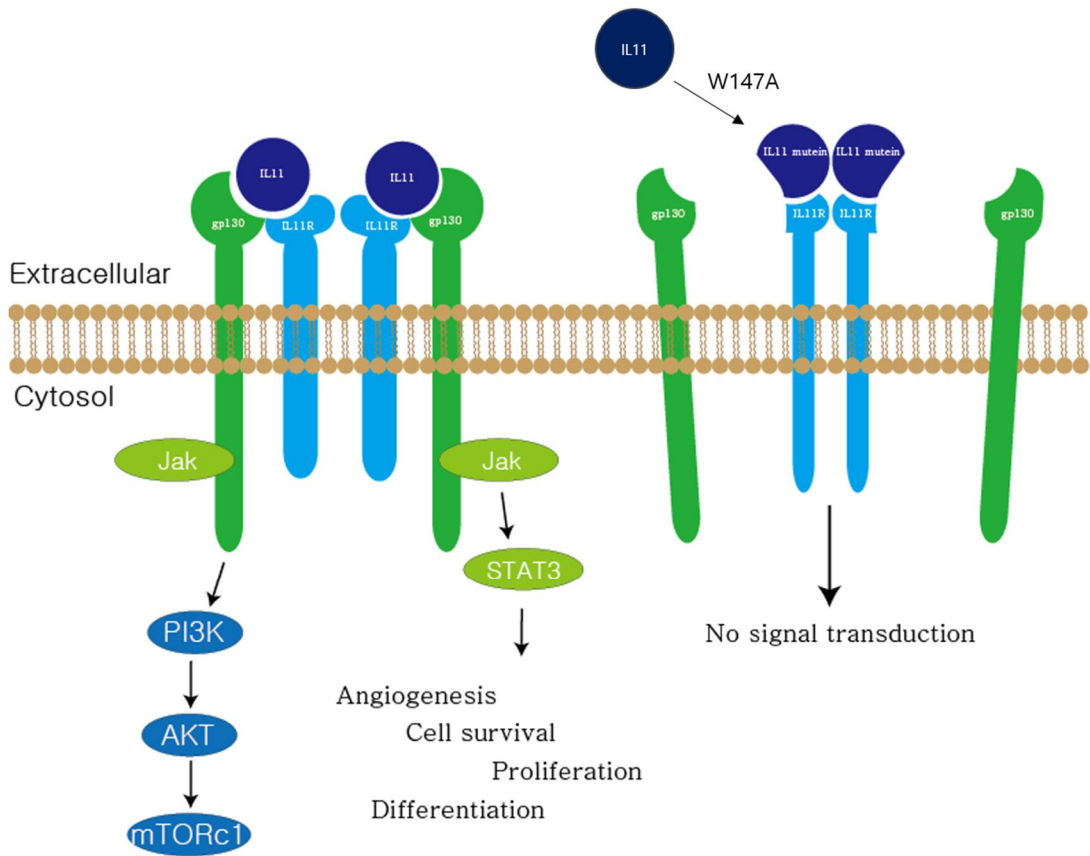


Figure 3-24. Signal of IL11 wild type and IL11 mutein. The wild type IL11 functions as a dimer and binds to both gp130 and IL11 receptors. The intracellular region of gp130 recruits Jak, and this complex transduces signals involved in angiogenesis, cell survival, proliferation, and differentiation through the stat3 and PI3K signaling pathways. However, the IL11 mutein can bind to IL11 receptors but not gp130, as it contains a mutation at residue 147 where tryptophan is replaced by alanine, which is a critical residue for gp130 binding. Therefore IL11 mutein cannot transduce a signal intracellularly and it can acts as antagonist of IL11 wild type.

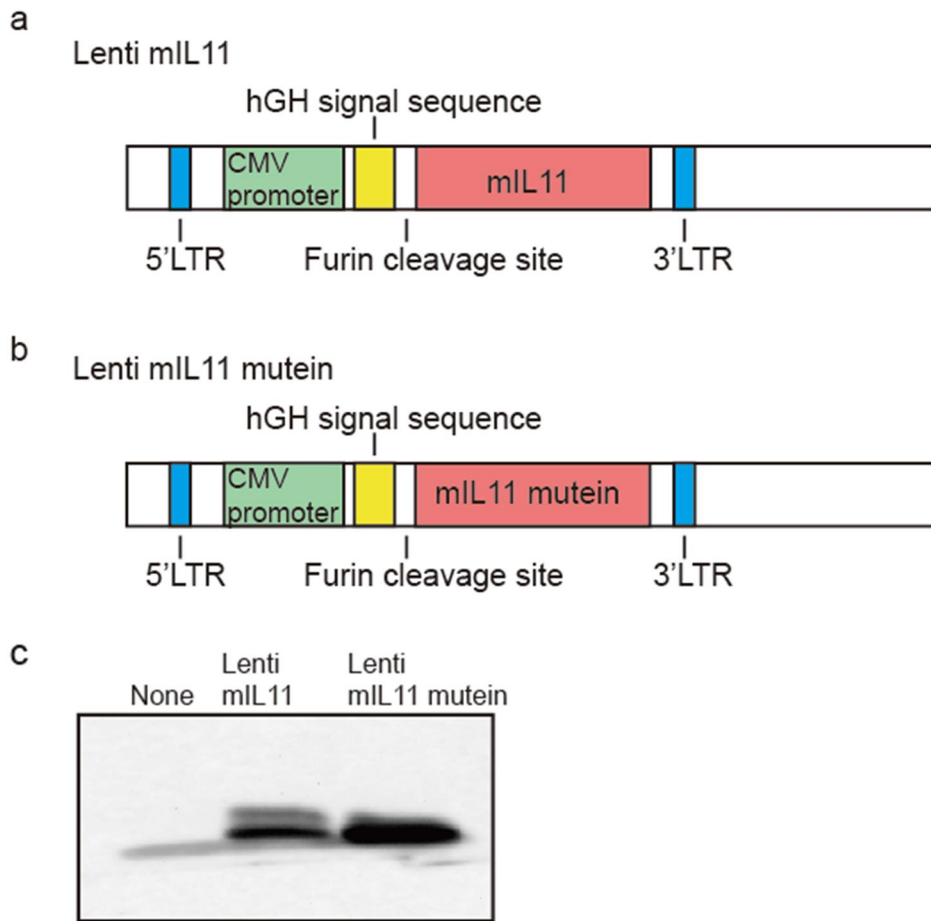


Figure 3-25. Schematic diagram of lenti mL11 and lenti mL11 mutein vector construction. The gene of mouse IL11 (a) and IL11 mutein (b) was fused with human growth hormone signal sequence for secretion and furin cleavage site for elimination of unnecessary sequence. (c) To determine the infectivity of lenti mL11 virus and lenti mL11 mutein virus, and the secretion of the proteins of mL11 and mL11 mutein in mammalian cells, 293T cells were infected with 10 μ g of lenti viruses. And secreted mL11 and mL11 mutein proteins were examined by Western blot in the conditioned medium.

To investigate whether lenti mIL11 and lenti mIL11 mutein works in the liver damaged by CCl₄ treatment in C57BL/6 mice, I injected mice with lenti mIL11 and lenti mIL11 muteins intraperitoneally at 6 weeks and intranasally (I.N.) at 7 weeks. After 1 week, C57BL/6 normal mouse were intraperitoneally injected with CCl₄ mixed with olive oil twice a week for 6 weeks (Figure 3-26). The degree of CCl₄-induced liver fibrosis in C57BL/6 mice infected with lenti mIL11 and lenti mIL11 mutein was monitored by H&E staining and Sirius red staining (Figure 3-27a). I verified no difference in the degree of liver damage in the absence of CCl₄ between mice infected with or without lenti mIL11 or the lenti mIL11 mutein (Figure 3-27a, b). The lenti mIL11 mutein but not lenti mIL11 significantly reduced collagen accumulation in the liver tissues of C57BL/6 normal mice damaged by CCl₄ treatment (Figure 3-27a). Although the accumulation of collagen stained with Sirius red was not increased in the fibrotic liver damaged by CCl₄ of lenti mIL11-infected mice more than that of CCl₄-only treated mice, the result in Figure 3-29 shows that the accumulation of α -SMA was increased in CCl₄-induced fibrotic liver of lenti mIL11-infected mice (Figure 3-29). The decreased collagen accumulation in the liver tissues were further supported by quantitative measurement of Sirius Red staining by NIH image J software (Figure 3-27b). These data indicate that mIL11 mutein acts as a competitive inhibitor against mIL11 as shown in previous report (167), and overexpression mIL11 also could act on inducing fibrotic liver tissue by accumulation of α -SMA although overexpressed mIL11 does not increase collagen accumulated area in the liver treated with CCl₄.

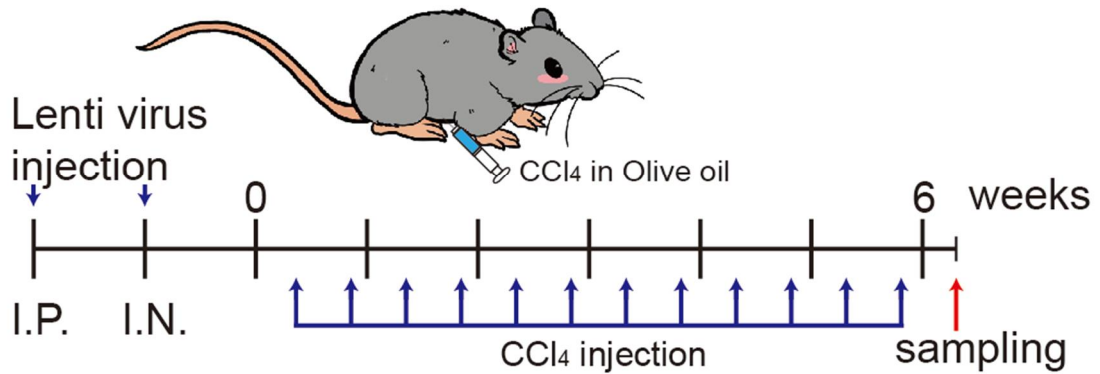
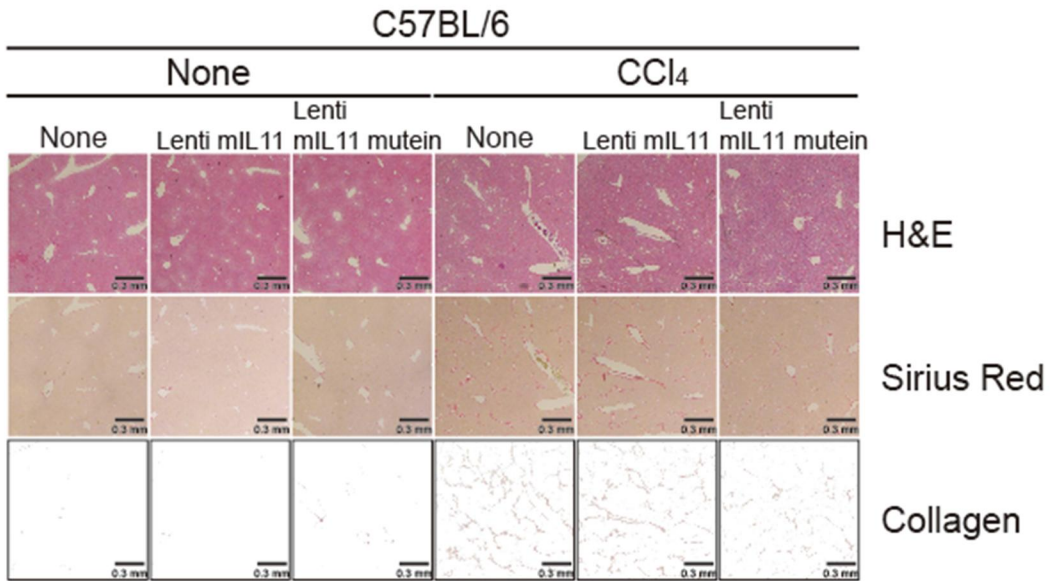


Figure 3-26. Schematic diagram of CCl₄-induced liver fibrosis model mice following injection of lenti mL11 viruses and lenti mL11 mutein for data shown in (Figure 3-21a, b). The lenti mL11 virus and lenti mL11 mutein virus were intraperitoneally (I.P.) injected into mice at 6 weeks of age. After a week, the lenti mL11 virus and lenti mL11 mutein virus were intranasally (I.N.) injected into mice at 7 weeks of age. The injection of CCl₄ was started at 8 weeks of age for 6 weeks.

a



b

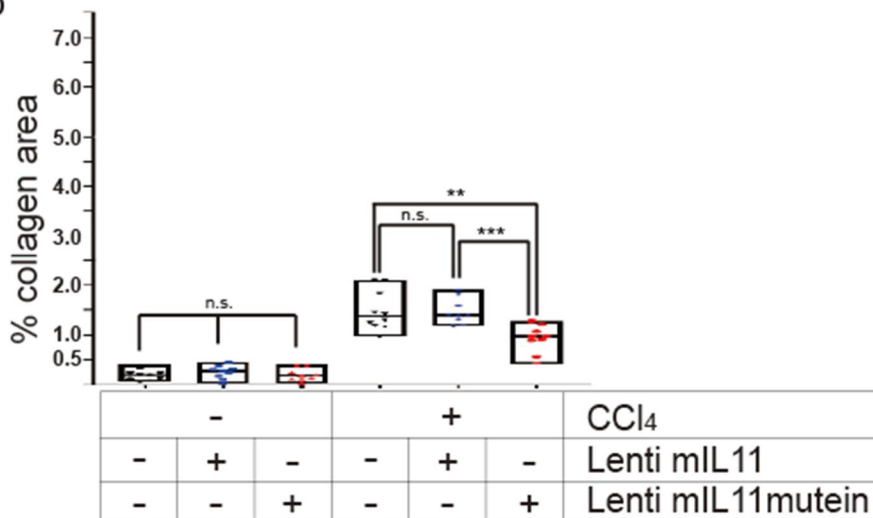


Figure 3-27. The effect of lenti mL11 and lenti mL11 mutein on CCl₄-induced liver fibrosis in C57BL/6 mouse. (a) Comparison of histological staining (hematoxylin and eosin (H&E) and picrosirius red (sirius red)) according to the presence or absence of lenti mL11 virus, lenti mL11 mutein virus, and CCl₄ in C57BL/6 mice. (b) Percentage area of collagen in picrosirius red-stained tissue sections of CCl₄ -induced fibrotic liver of C57BL/6 mice. Scale bars: 0.3 mm, * <0.05 , ** <0.01 , *** <0.001 .

3.7 mIL11 mutein is not sufficient to block the liver fibrosis in hMUDENG Tg induced by CCl₄.

To investigate whether mIL11 mediates liver fibrosis in hMUDENG Tg, i injected mice with lenti mIL11 and lenti mIL11 mutein intraperitoneally at 6 weeks and intranasally at 7 weeks; after 1 week, hMUDENG Tg mice were intraperitoneally injected with CCl₄ mixed with olive oil twice a week for 6 weeks as shown in Figure 3-26. The level of fibrotic liver induced by CCl₄ in hMUDENG Tg mice infected with with lenti mIL11 and lenti mIL11 mutein was monitored by H&E staining and Sirius red staining (Figure 3-28a). I verified no difference in levels of fibrosis in the liver in the absence of CCl₄ between mice infected with or without lenti mIL11 or the lenti mIL11 mutein (Figure 3-28a, b). However, unlike the results observed in C57BL/6 (Figure. 3-27b), when lenti mIL11 or lenti mIL11 mutein was injected into hMUDENG Tg mice treated with CCl₄, quantitative analysis of collagen accumulation and Sirius Red staining area showed no significant difference (Figure 3-28a, b). Also, the expression levels of collagen, α -SMA, and TGF- β were higher in the liver of hMUDENG Tg mice challenged with CCl₄ than that of C57BL/6 mice (Figure 3-29). These results indicate that the overexpression of hMUDENG in the liver make the liver to be more susceptible to liver damage, resulting in severe liver fibrosis by increasing the expression of fibrous proteins such as collagen and α -SMA. Taken together, these results suggest that blocking of mIL11 action in hMUDENG Tg mice is not sufficient to reduce collagen accumulation in the liver, implicating that AP5M1 causes liver damage not just through the axis of TGF- β and IL11 but also through unknown pathway.

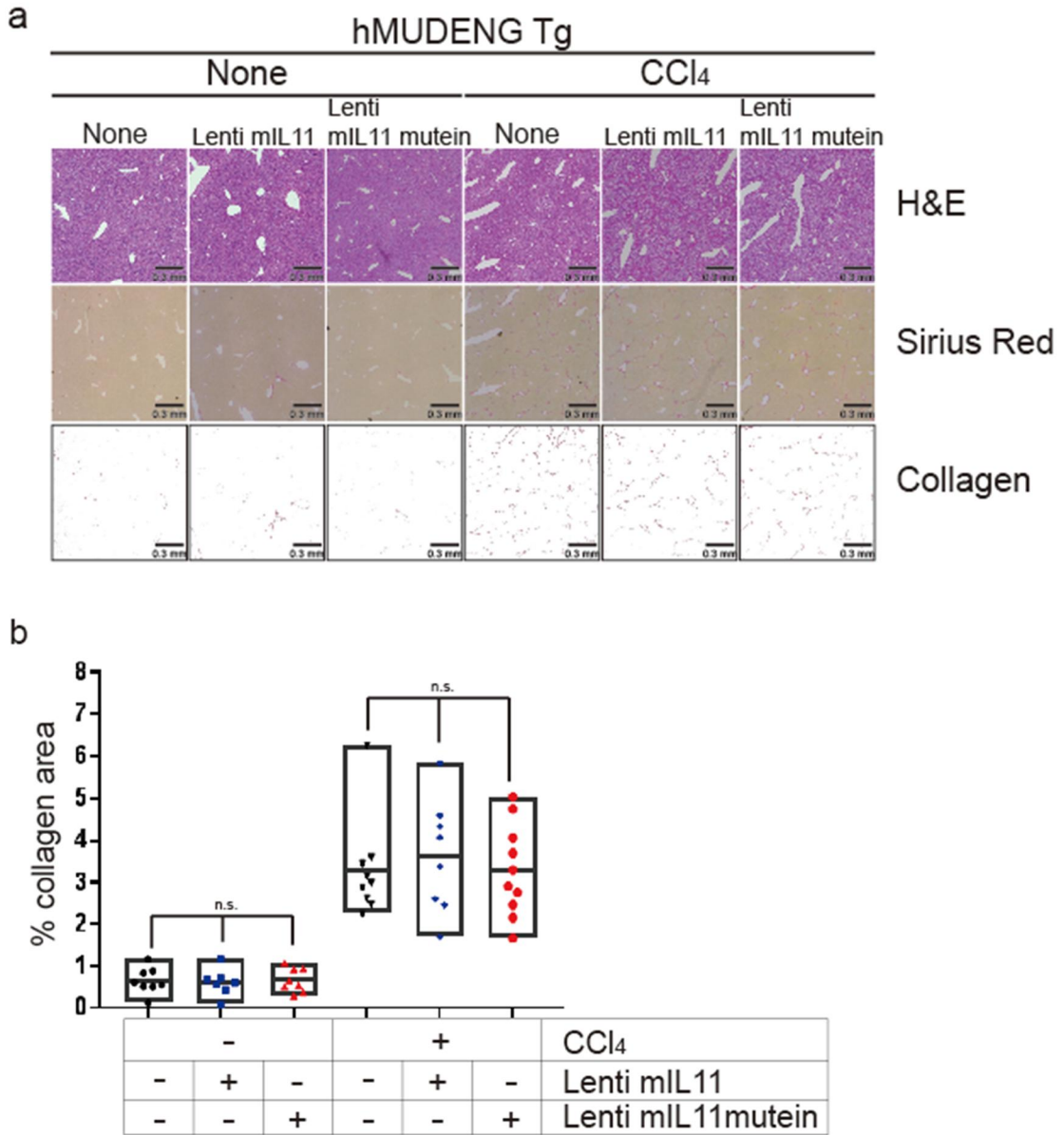


Figure 3-28. . The effect of lenti mL11 and lenti mL11 mutein on CCl₄-induced liver fibrosis in hMUDENG Tg mouse. (a) Comparison of histological staining (hematoxylin and eosin (H&E) and picosirius red (sirius red)) according to the presence or absence of lenti mL11 virus, lenti mL11 mutein virus, CCl₄ in hAP5M1-Tg mice. (b) Percentage area of collagen in picosirius red-stained tissue sections of CCl₄ -induced fibrotic liver of hAP5M1-Tg mice. Scale bars : 0.3 mm.

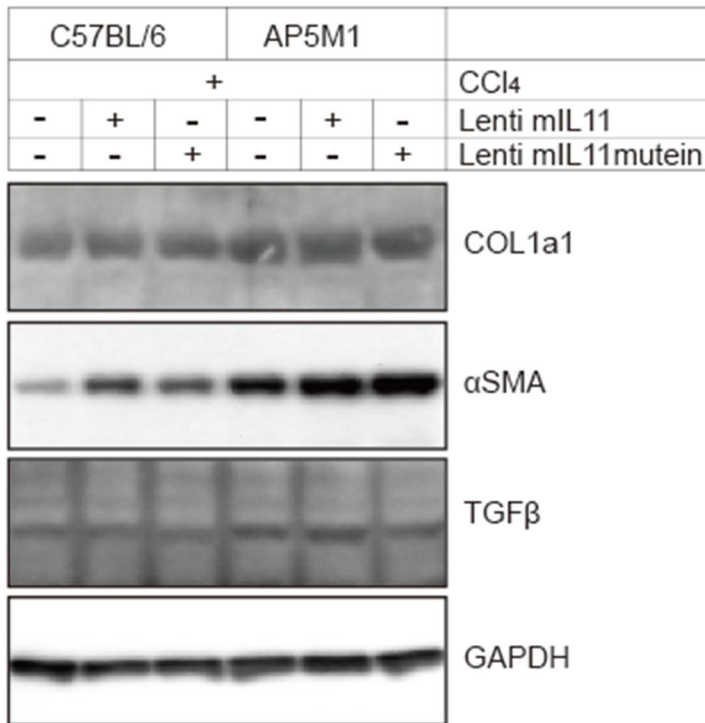


Figure 3-29. The proteins levels of collagen, α -SMA, and TGF- β in fibrotic liver induced by CCl₄ in hMUDENG Tg and C57BL/6 mouse. The fibrous proteins (collagen type1 and α -Smooth muscle actin (α -SMA)) and TGF β were examined by western blot. Although IL11 did not induce significant liver fibrosis in histological assays that stained collagen fibers in C57BL/6 mice, the expression of α -SMA was increased in the liver injected with lenti mL11 virus in C57BL/6 mice treated with CCl₄. In liver of hMUDENG-Tg mice, collagen type1, α -SMA, and TGF β were highly expressed whether IL11 and IL11 mutein were injected or not.

CHAPTER4

Conclusion

In this study, a transgenic mouse was generated to investigate how the functions of MUDENG observed in previous studies affect various tissues in mice. Although overexpression of non-tissue-specific genes can have unexpected side effects, in this study, transgenic mice were made by inserting the hMUDENG gene into the germ line to observe changes in various tissues caused by hMUDENG overexpression.

I identified that the hMUDENG mRNA could be transcribed in brain, lung, liver, skin, testis and blood cells of hMUDENG Tg mice. A prominent phenotypic change in hMUDENG Tg mice was hair loss, which appeared to affect the first hair cycle at about postnatal week 2. The exact mechanism is not yet known, but it is believed to be a result of immature liver. Immature liver is characterized by a decrease in expression of various genes related to lipid metabolism and oxidation-reduction processes. Moreover, the pronounced increase in expression of fetal liver markers in the liver of MUDENG Tg mice suggests their association with immature liver (Figure 4-1). The issue of iron homeostasis is also closely related to hair loss, further supporting the notion that hair loss in MUDENG Tg mice could be multifactorial.

No pathological changes were observed in the kidney and lung as a result of H&E staining. However, weak fibrosis and inflammatory reactions were observed in the liver tissue of hMUDENG Tg mice. RNA transcriptome analysis supported these findings, revealing upregulation of many factors related to fibrosis such as CTGF, collagen proteins, alpha smooth muscle actin, STAT3, and CYP family, and inflammatory responses such as TGF- β , IL-6, and IL-11. These results suggest that overexpression of hMUDENG may cause an inflammatory response in liver tissue, which may also lead to a fibrotic process (Figure 4-1). However, overexpression of hMUDENG alone did not strongly promote liver fibrosis.

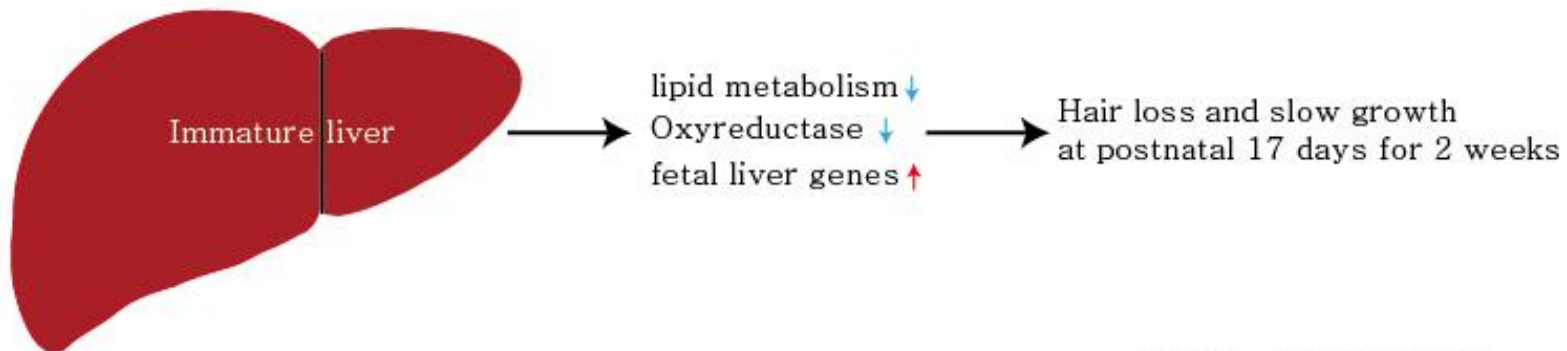
I observed that hMUDENG overexpression had an impact on CCl₄-induced liver fibrosis. Specifically, hMUDENG Tg mice exhibited a greater sensitivity to liver damage by CCl₄ compared to C57BL/6 mice, leading to a more rapid and severe progression of liver fibrosis. I thought that TGF- β and IL-11 may be important in CCl₄-induced liver fibrosis in hMUDENG Tg mice. But,

hMUDENG Tg mice did not show a significant response to additional mL11 and mL11 mutein through infection with lenti mL11 virus and lenti mL11 mutein virus (Figure 4-1).

Two hypotheses were developed to explain this. The first hypothesis was that hMUDENG Tg mice already express sufficient amounts of IL-11 and do not respond to additional IL-11. Even in the C57BL/6 mice, it was found that there was no significant difference in the fibrosis response only with the additional supply of IL-11 by infection with Lenti mL11 virus. However, when CCl₄ stimulation was added to the supply of IL-11, the response of fibrosis was intensified in C57BL/6 mice, suggesting that IL-11 could accelerate the changes caused by CCl₄ stimulation. Since liver fibrosis by CCl₄ stimulation was already sufficiently accelerated by sufficient IL-11 in hMUDENG Tg, the acceleration of fibrosis reaction was not further progressed by additional IL-11, and it is difficult to antagonistically block with IL-11 mutein already much IL-11 in hMUDENG Tg mice. The second hypothesis was that there may be additional hepatic fibrosis-inducing mechanisms independent of IL-11. This hypothesis has not yet been tested due to lack of data, and more research is needed to verify it.

MUDENG, also known as AP5M1, is a protein involved in reverse transport from the late endosome to Golgi. It has been reported that problems with late endosomes and endo-lysosomes are associated with non-alcoholic fatty liver disease (NAFLD), indicating that MUDENG may play a role in liver disease as the mu subunit of the adaptin protein 5 complex. Further studies are needed to elucidate the relationship between MUDENG and liver diseases.

At postnatal day 18 of hMUDENG Tg mice



At postnatal day 30 of hMUDENG Tg mice

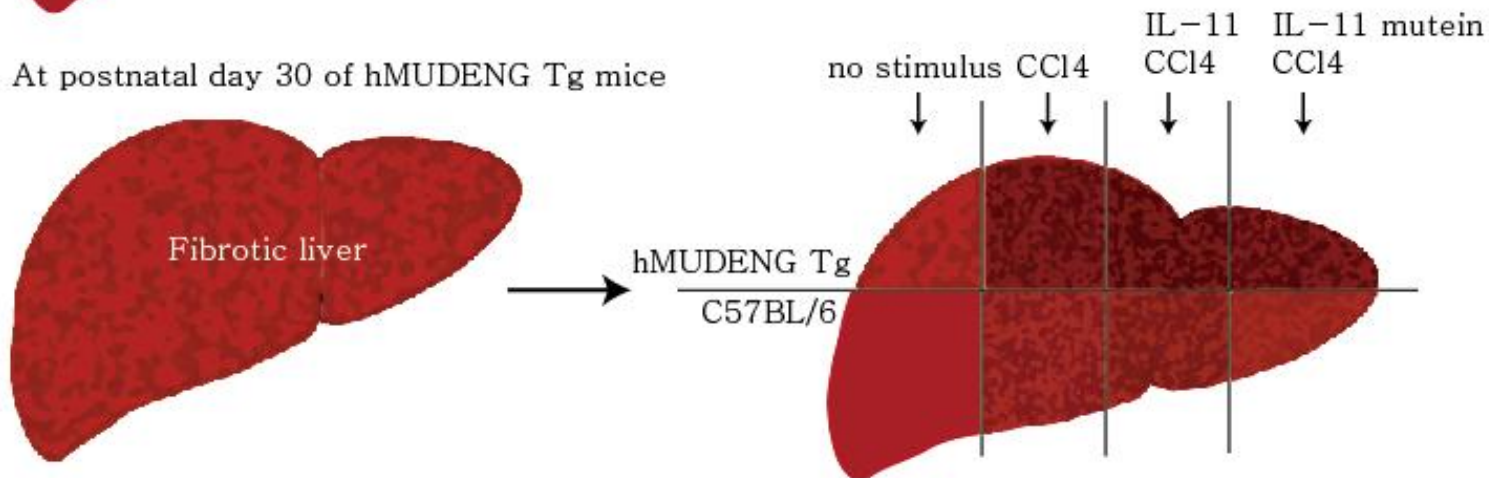


Figure 4-1. Summary figure depicting the physiological changes resulting from overexpression of hMUDENG. hMUDENG-Tg mice exhibit

immature liver at about postnatal day 18, characterized by decreased lipid metabolism, increased oxidoreductase activity, and upregulation of fetal liver genes. Additionally, immature liver in these mice can lead to early-onset hair loss during the hair cycle initiation. Moreover, hMUDENG-Tg mice show inflammatory responses and infiltration of immune cells in liver tissue, which ultimately leads to liver fibrosis. The liver tissue of hMUDENG-Tg mice demonstrates mild fibrosis progression and increased sensitivity to hepatotoxins like CCl₄, resulting in accelerated fibrotic development.

Acknowledgements

I would like to express my deep gratitude to my advisor, Professor Tae-Hyoung Kim, for his unwavering guidance, generous support, and continuous encouragement throughout my doctoral program. Professor Kim's expertise, patience, academic excellence, and dedication have played a crucial role in shaping the direction of this research and enhancing its quality. I am truly thankful for his invaluable contributions and unwavering commitment.

I would like to express my gratitude to Professor Joo-Yeon Cho for helping me in setting the direction for my graduation thesis and conducting the research. Additionally, I would like to extend my thanks to the dissertation reviewers: Prof. Seonghaeng Lee, Prof. Ilsu Bang, Prof. Jooyeon Cho, and Dr. Jaeil Park, senior researcher at KBSI. Their insightful feedback, valuable suggestions, and constructive criticism greatly contributed to the logical and coherent writing of my doctoral dissertation. Thank you for your significant contributions to the content and flow of the dissertation.

I would like to extend my sincere gratitude to Dr. Jung-hee Park and Dr. Ji-hye Han for their generous commitment of time and expertise, and their invaluable assistance in data collection, analysis, and interpretation throughout my doctoral journey. They have been a constant source of encouragement and support. Thanks to their active involvement and significant contributions, I was able to achieve high-quality research outcomes. I sincerely thank them for their generous support and encouragement.

Furthermore, I would like to express my gratitude for the financial support provided through the Doctoral Student Research Grant Program by the Korea Research Foundation. Without their generous funding, this research would not have been possible. I am grateful for their belief in the importance of this work and their contribution to its completion.

I would like to express my deep gratitude to my father (Myung Jae-kwan), mother (Park Jeong-a), and my sisters (Myung Ju-sun, Myung Ji-sun) for their unwavering support, encouragement, understanding, and constant presence as pillars of strength throughout my doctoral journey. Additionally, I would like to sincerely thank the artist Kang Eun-ae for her consistent support, understanding, and encouragement during the process of writing

my thesis, as well as for her assistance in creating the figures included in the dissertation.

I would like to extend my gratitude to my closest friends, Eunjun Park and Beomil Heo, who provided unwavering support and encouragement throughout my entire degree program. During challenging and exhausting times, they stood by my side and offered steadfast support. I am sincerely thankful to both of them for their unwavering support and friendship during my degree program.

Last but not least, I am grateful to Chosun University for providing me with the opportunity to pursue my doctoral studies. The resources, infrastructure, and scholarly environment have been instrumental in fostering my academic growth and research endeavors.

I would also like to extend my sincere thanks to all those individuals who have provided assistance and support throughout my doctoral journey, even if I haven't mentioned them. Your help and participation have been invaluable to me, and I am truly grateful for your contributions to my doctoral process.

In conclusion, this research would not have been possible without the support and contributions of all those mentioned above. While any errors or omissions remain my own, their collective efforts have played a significant role in the successful completion of this doctoral thesis.

Thank you for your unwavering support.

[Seung-Hyun Myung]

Reference

1. Lee MR, Shin JN, Moon AR, Park SY, Hong G, Lee MJ, Yun CW, et al. A novel protein, MUDENG, induces cell death in cytotoxic T cells. *Biochem Biophys Res Commun* 2008;370:504-508.
2. Kawasaki H, Taira K. A functional gene discovery in the Fas-mediated pathway to apoptosis by analysis of transiently expressed randomized hybrid-ribozyme libraries. *Nucleic Acids Res* 2002;30:3609-3614.
3. Shin JN, Han JH, Kim JY, Moon AR, Kim JE, Chang JH, Bae J, et al. MUDENG is cleaved by caspase-3 during TRAIL-induced cell death. *Biochem Biophys Res Commun* 2013;435:234-238.
4. Wagley Y, Choi JH, Wickramanayake DD, Choi GY, Kim CK, Kim TH, Oh JW. A monoclonal antibody against human MUDENG protein. *Monoclon Antib Immunodiagn Immunother* 2013;32:277-282.
5. Choi JH, Lim JB, Wickramanayake DD, Wagley Y, Kim J, Lee HC, Seo HG, et al. Characterization of MUDENG, a novel anti-apoptotic protein. *Oncogenesis* 2016;5:e221.
6. Choi JH, Min WK, Gopal J, Lee YM, Muthu M, Chun S, Oh JW. Silver nanoparticle-induced hormesis of astrogloma cells: A Mu-2-related death-inducing protein-orchestrated modus operandi. *Int J Biol Macromol* 2018;117:1147-1156.
7. Won M, Luo Y, Lee DH, Shin E, Suh DS, Kim TH, Jin H, et al. BAX is an essential key mediator of AP5M1-induced apoptosis in cervical carcinoma cells. *Biochem Biophys Res Commun* 2019;518:368-373.
8. Muthu M, Chun S, Gopal J, Park GS, Nile A, Shin J, Shin J, et al. The MUDENG Augmentation: A Genesis in Anti-Cancer Therapy? *Int J Mol Sci* 2020;21.
9. Hirst J, Barlow LD, Francisco GC, Sahlender DA, Seaman MN, Dacks JB, Robinson MS. The fifth adaptor protein complex. *PLoS Biol* 2011;9:e1001170.
10. Hirst J, Itzhak DN, Antrobus R, Borner GHH, Robinson MS. Role of the AP-5 adaptor protein complex in late endosome-to-Golgi retrieval. *PLoS Biol* 2018;16:e2004411.
11. Nilsson T, Warren G. Retention and retrieval in the endoplasmic reticulum and the Golgi apparatus. *Curr Opin Cell Biol* 1994;6:517-521.
12. Beilina A, Bonet-Ponce L, Kumaran R, Kordich JJ, Ishida M, Mamais A, Kaganovich A, et al. The Parkinson's Disease Protein LRRK2 Interacts with the GARP Complex to Promote Retrograde Transport to the trans-Golgi Network. *Cell Rep* 2020;31:107614.
13. Shin J, Choi JH, Jung S, Jeong S, Oh J, Yoon DY, Rhee MH, et al. MUDENG Expression Profiling in Cohorts and Brain Tumor Biospecimens to Evaluate Its Role in Cancer. *Front Genet* 2019;10:884.
14. Gopal J, Lee YM, Shin J, Muthu M, Jung S, Jeong S, Oh J, et al. The graviola impact on human astrogloma cells: functional significance of MUDENG. *RSC Adv* 2019;9:8935-8942.
15. Shin J, Nile A, Oh JW. Role of adaptin protein complexes in intracellular trafficking and their impact on diseases. *Bioengineered* 2021;12:8259-8278.
16. Boehm M, Bonifacino JS. Adaptins: the final recount. *Mol Biol Cell* 2001;12:2907-2920.
17. Motley A, Bright NA, Seaman MN, Robinson MS. Clathrin-mediated endocytosis in AP-2-depleted cells. *J Cell Biol* 2003;162:909-918.
18. Rappoport JZ, Benmerah A, Simon SM. Analysis of the AP-2 adaptor complex and cargo during clathrin-mediated endocytosis. *Traffic* 2005;6:539-547.
19. Han T, Yang CS, Chang KY, Zhang D, Imam FB, Rana TM. Identification of novel genes and networks governing hematopoietic stem cell development. *EMBO Rep* 2016;17:1814-1828.
20. Nakatsu F, Hase K, Ohno H. The Role of the Clathrin Adaptor AP-1: Polarized Sorting

and Beyond. *Membranes* (Basel) 2014;4:747-763.

21. Johnson KR, Gagnon LH, Chang B. A hypomorphic mutation of the gamma-1 adaptin gene (*Ap1g1*) causes inner ear, retina, thyroid, and testes abnormalities in mice. *Mamm Genome* 2016;27:200-212.
22. Usmani MA, Ahmed ZM, Magini P, Pienkowski VM, Rasmussen KJ, Hernan R, Rasheed F, et al. De novo and bi-allelic variants in *APIG1* cause neurodevelopmental disorder with developmental delay, intellectual disability, and epilepsy. *Am J Hum Genet* 2021;108:1330-1341.
23. Lewin DA, Sheff D, Ooi CE, Whitney JA, Yamamoto E, Chicione LM, Webster P, et al. Cloning, expression, and localization of a novel gamma-adaptin-like molecule. *FEBS Lett* 1998;435:263-268.
24. Zizioli D, Geumann C, Kratzke M, Mishra R, Borsani G, Finazzi D, Candiello E, et al. gamma2 and gamma1AP-1 complexes: Different essential functions and regulatory mechanisms in clathrin-dependent protein sorting. *Eur J Cell Biol* 2017;96:356-368.
25. Grant RC, Denroche RE, Borgida A, Virtanen C, Cook N, Smith AL, Connor AA, et al. Exome-Wide Association Study of Pancreatic Cancer Risk. *Gastroenterology* 2018;154:719-722 e713.
26. Kou Y, Yan X, Liu Q, Wei X, Zhang B, Li X, Pan W, et al. HBV upregulates AP-1 complex subunit mu-1 expression via the JNK pathway to promote proliferation of liver cancer cells. *Oncol Lett* 2019;18:456-464.
27. Rebendenne A, Roy P, Bonaventure B, Chaves Valadao AL, Desmarests L, Arnaud-Arnould M, Rouille Y, et al. Bidirectional genome-wide CRISPR screens reveal host factors regulating SARS-CoV-2, MERS-CoV and seasonal HCoVs. *Nat Genet* 2022;54:1090-1102.
28. Tavares LA, da Silva EM, da Silva-Januario ME, Januario YC, de Cavalho JV, Czernisz ES, Mardones GA, et al. CD4 downregulation by the HIV-1 protein Nef reveals distinct roles for the gamma1 and gamma2 subunits of the AP-1 complex in protein trafficking. *J Cell Sci* 2017;130:429-443.
29. Jiao J, Jiang L, Luo Y. N6-Methyladenosine-Related RNA Signature Predicting the Prognosis of Ovarian Cancer. *Recent Pat Anticancer Drug Discov* 2021;16:407-416.
30. Okabayashi Y, Sugimoto Y, Totty NF, Hsuan J, Kido Y, Sakaguchi K, Gout I, et al. Interaction of Shc with adaptor protein adaptins. *J Biol Chem* 1996;271:5265-5269.
31. Saafan H, Foerster S, Parra-Guillen ZP, Hammer E, Michaelis M, Cinatl J, Jr., Volker U, et al. Utilising the EGFR interactome to identify mechanisms of drug resistance in non-small cell lung cancer - Proof of concept towards a systems pharmacology approach. *Eur J Pharm Sci* 2016;94:20-32.
32. Montgomery MK, Bayliss J, Keenan S, Rhost S, Ting SB, Watt MJ. The role of Ap2a2 in PPAR α -mediated regulation of lipolysis in adipose tissue. *The FASEB Journal* 2019;33:13267-13279.
33. Raj T, Li YI, Wong G, Humphrey J, Wang M, Ramdhani S, Wang YC, et al. Integrative transcriptome analyses of the aging brain implicate altered splicing in Alzheimer's disease susceptibility. *Nat Genet* 2018;50:1584-1592.
34. Nelson PT, Fardo DW, Katsumata Y. The MUC6/AP2A2 Locus and Its Relevance to Alzheimer's Disease: A Review. *J Neuropathol Exp Neurol* 2020;79:568-584.
35. Wu CC, Li H, Xiao Y, Deng WW, Sun ZJ. Expression levels of SIX1, ME2, and AP2M1 in adenoid cystic carcinoma and mucoepidermoid carcinoma. *Oral Dis* 2020;26:1687-1695.
36. Shi C, Lan W, Wang Z, Yang D, Wei J, Liu Z, Teng Y, et al. Alantolactone inhibits cell autophagy and promotes apoptosis via AP2M1 in acute lymphoblastic leukemia. *Cancer Cell Int* 2020;20:442.
37. Sapsutthipas S, Kitagawa Y, Tokunaga K, Ikuta K, Kameoka M. Viral factors involved in

- adapter-related protein complex 2 alpha 1 subunit-mediated regulation of human immunodeficiency virus type 1 replication. *Southeast Asian J Trop Med Public Health* 2011;42:311-319.
38. Johnson A, Vert G. Single Event Resolution of Plant Plasma Membrane Protein Endocytosis by TIRF Microscopy. *Front Plant Sci* 2017;8:612.
 39. Ting SB, Deneault E, Hope K, Cellot S, Chagraoui J, Mayotte N, Dorn JF, et al. Asymmetric segregation and self-renewal of hematopoietic stem and progenitor cells with endocytic Ap2a2. *Blood* 2012;119:2510-2522.
 40. Chen C, Nguyen BN, Mitchell G, Margolis SR, Ma D, Portnoy DA. The Listeriolysin O PEST-like Sequence Co-opts AP-2-Mediated Endocytosis to Prevent Plasma Membrane Damage during Listeria Infection. *Cell Host Microbe* 2018;23:786-795 e785.
 41. Neveu G, Ziv-Av A, Barouch-Bentov R, Berkerman E, Mulholland J, Einav S. AP-2-associated protein kinase 1 and cyclin G-associated kinase regulate hepatitis C virus entry and are potential drug targets. *J Virol* 2015;89:4387-4404.
 42. Yuan S, Chu H, Huang J, Zhao X, Ye ZW, Lai PM, Wen L, et al. Viruses harness YxxO motif to interact with host AP2M1 for replication: A vulnerable broad-spectrum antiviral target. *Sci Adv* 2020;6:eaba7910.
 43. Faundez V, Horng JT, Kelly RB. A function for the AP3 coat complex in synaptic vesicle formation from endosomes. *Cell* 1998;93:423-432.
 44. Odorizzi G, Cowles CR, Emr SD. The AP-3 complex: a coat of many colours. *Trends Cell Biol* 1998;8:282-288.
 45. Wilkin M, Tongngok P, Gensch N, Clemence S, Motoki M, Yamada K, Hori K, et al. Drosophila HOPS and AP-3 complex genes are required for a Deltex-regulated activation of notch in the endosomal trafficking pathway. *Dev Cell* 2008;15:762-772.
 46. Huizing M, Sarangarajan R, Strovel E, Zhao Y, Gahl WA, Boissy RE. AP-3 mediates tyrosinase but not TRP-1 trafficking in human melanocytes. *Mol Biol Cell* 2001;12:2075-2085.
 47. Ueda K, Ogawa S, Matsuda K, Hasegawa Y, Nishi E, Yanagi K, Kaname T, et al. Blended phenotype of combination of HERC2 and AP3B2 deficiency and Angelman syndrome caused by paternal isodisomy of chromosome 15. *Am J Med Genet A* 2021;185:3092-3098.
 48. Zhu M, Jia L, Li F, Jia J. Identification of KIAA0513 and Other Hub Genes Associated With Alzheimer Disease Using Weighted Gene Coexpression Network Analysis. *Front Genet* 2020;11:981.
 49. Van Damme N, Guatelli J. HIV-1 Vpu inhibits accumulation of the envelope glycoprotein within clathrin-coated, Gag-containing endosomes. *Cell Microbiol* 2008;10:1040-1057.
 50. Corredor AP, Gonzalez J, Baquero LA, Curtidor H, Olaya-Galan NN, Patarroyo MA, Gutierrez MF. In silico and in vitro analysis of boAP3d1 protein interaction with bovine leukaemia virus gp51. *PLoS One* 2018;13:e0199397.
 51. Garcia E, Nikolic DS, Piguet V. HIV-1 replication in dendritic cells occurs through a tetraspanin-containing compartment enriched in AP-3. *Traffic* 2008;9:200-214.
 52. Gao L, Zhu L, Huang L, Zhou J. Synergistic defects of UNC13D and AP3B1 leading to adult hemophagocytic lymphohistiocytosis. *Int J Hematol* 2015;102:488-492.
 53. Li SY, Yoshida Y, Kobayashi E, Kubota M, Matsutani T, Mine S, Machida T, et al. Serum anti-AP3D1 antibodies are risk factors for acute ischemic stroke related with atherosclerosis. *Sci Rep* 2021;11:13450.
 54. Selcuklu SD, Donoghue MT, Rehmet K, de Souza Gomes M, Fort A, Kovvuru P, Muniyappa MK, et al. MicroRNA-9 inhibition of cell proliferation and identification of novel miR-9 targets by transcriptome profiling in breast cancer cells. *J Biol Chem* 2012;287:29516-29528.
 55. Mantripragada KK, Diaz de Stahl T, Patridge C, Menzel U, Andersson R, Chuzhanova N,

- Kluwe L, et al. Genome-wide high-resolution analysis of DNA copy number alterations in NF1-associated malignant peripheral nerve sheath tumors using 32K BAC array. *Genes Chromosomes Cancer* 2009;48:897-907.
56. Dell'Angelica EC, Mullins C, Bonifacino JS. AP-4, a novel protein complex related to clathrin adaptors. *J Biol Chem* 1999;274:7278-7285.
 57. Hirst J, Bright NA, Rous B, Robinson MS. Characterization of a fourth adaptor-related protein complex. *Mol Biol Cell* 1999;10:2787-2802.
 58. Hirst J, Irving C, Borner GH. Adaptor protein complexes AP-4 and AP-5: new players in endosomal trafficking and progressive spastic paraplegia. *Traffic* 2013;14:153-164.
 59. Jordan C, Geisel G, Alecu JE, Zhang B, Sahin M, Ebrahimi-Fakhari D. Disease Severity and Motor Impairment Correlate With Health-Related Quality of Life in AP-4-Associated Hereditary Spastic Paraplegia. *Neurol Genet* 2021;7:e605.
 60. Abou Jamra R, Philippe O, Raas-Rothschild A, Eck SH, Graf E, Buchert R, Borck G, et al. Adaptor protein complex 4 deficiency causes severe autosomal-recessive intellectual disability, progressive spastic paraplegia, shy character, and short stature. *Am J Hum Genet* 2011;88:788-795.
 61. Novikova G, Kapoor M, Tew J, Abud EM, Efthymiou AG, Chen SX, Cheng H, et al. Integration of Alzheimer's disease genetics and myeloid genomics identifies disease risk regulatory elements and genes. *Nat Commun* 2021;12:1610.
 62. Aguilar RC, Boehm M, Gorshkova I, Crouch RJ, Tomita K, Saito T, Ohno H, et al. Signal-binding specificity of the mu4 subunit of the adaptor protein complex AP-4. *J Biol Chem* 2001;276:13145-13152.
 63. Burgos PV, Mardones GA, Rojas AL, daSilva LL, Prabhu Y, Hurley JH, Bonifacino JS. Sorting of the Alzheimer's disease amyloid precursor protein mediated by the AP-4 complex. *Dev Cell* 2010;18:425-436.
 64. Simmen T, Honing S, Icking A, Tikkanen R, Hunziker W. AP-4 binds basolateral signals and participates in basolateral sorting in epithelial MDCK cells. *Nat Cell Biol* 2002;4:154-159.
 65. Boehm M, Aguilar RC, Bonifacino JS. Functional and physical interactions of the adaptor protein complex AP-4 with ADP-ribosylation factors (ARFs). *EMBO J* 2001;20:6265-6276.
 66. Borner GH, Antrobus R, Hirst J, Bhumbra GS, Kozik P, Jackson LP, Sahlender DA, et al. Multivariate proteomic profiling identifies novel accessory proteins of coated vesicles. *J Cell Biol* 2012;197:141-160.
 67. Seaman MNJ. Back From the Brink: Retrieval of Membrane Proteins From Terminal Compartments: Unexpected Pathways for Membrane Protein Retrieval From Vacuoles and Endolysosomes. *Bioessays* 2019;41:e1800146.
 68. Breza M, Hirst J, Chelban V, Banneau G, Tissier L, Kol B, Bourinaris T, et al. Expanding the Spectrum of AP5Z1-Related Hereditary Spastic Paraplegia (HSP-SPG48): A Multicenter Study on a Rare Disease. *Mov Disord* 2021;36:1034-1038.
 69. Maruta K, Ando M, Otomo T, Takashima H. [A case of spastic paraplegia 48 with a novel mutation in the AP5Z1 gene]. *Rinsho Shinkeigaku* 2020;60:543-548.
 70. Schlipf NA, Schule R, Klimpe S, Karle KN, Synofzik M, Wolf J, Riess O, et al. AP5Z1/SPG48 frequency in autosomal recessive and sporadic spastic paraplegia. *Mol Genet Genomic Med* 2014;2:379-382.
 71. Denton K, Mou Y, Xu CC, Shah D, Chang J, Blackstone C, Li XJ. Impaired mitochondrial dynamics underlie axonal defects in hereditary spastic paraplegias. *Hum Mol Genet* 2018;27:2517-2530.
 72. Marenholz I, Esparza-Gordillo J, Ruschendorf F, Bauerfeind A, Strachan DP, Spycher BD, Baurecht H, et al. Meta-analysis identifies seven susceptibility loci involved in the atopic march. *Nat Commun* 2015;6:8804.

73. Peng C, Van Meel ER, Cardenas A, Rifas-Shiman SL, Sonawane AR, Glass KR, Gold DR, et al. Epigenome-wide association study reveals methylation pathways associated with childhood allergic sensitization. *Epigenetics* 2019;14:445-466.
74. Calender A, Rollat Farnier PA, Buisson A, Pinson S, Bentaher A, Lebecque S, Corvol H, et al. Whole exome sequencing in three families segregating a pediatric case of sarcoidosis. *BMC Med Genomics* 2018;11:23.
75. Zuo X, Sun L, Yin X, Gao J, Sheng Y, Xu J, Zhang J, et al. Whole-exome SNP array identifies 15 new susceptibility loci for psoriasis. *Nat Commun* 2015;6:6793.
76. Du J, Ji Y, Qiao L, Liu Y, Lin J. Cellular endo-lysosomal dysfunction in the pathogenesis of non-alcoholic fatty liver disease. *Liver Int* 2020;40:271-280.
77. Trefts E, Gannon M, Wasserman DH. The liver. *Curr Biol* 2017;27:R1147-R1151.
78. Guglielmi A, Ruzzenente A, Conci S, Valdegamberi A, Iacono C. How much remnant is enough in liver resection? *Dig Surg* 2012;29:6-17.
79. Kim HJ, Kim CY, Hur YH, Koh YS, Kim JC, Cho CK, Kim HJ. Comparison of remnant to total functional liver volume ratio and remnant to standard liver volume ratio as a predictor of postoperative liver function after liver resection. *Korean J Hepatobiliary Pancreat Surg* 2013;17:143-151.
80. Rajamani AS, Rammohan A, Sai VVR, Rela M. Current techniques and future trends in the diagnosis of hepatic steatosis in liver donors: A review. *Journal of Liver Transplantation* 2022;7:100091.
81. Macpherson I, Abeysekera KWM, Harris R, Mansour D, McPherson S, Rowe I, Rosenberg W, et al. Identification of liver disease: why and how. *Frontline Gastroenterol* 2022;13:367-373.
82. Khan RA, Luo Y, Wu F-X. Machine learning based liver disease diagnosis: A systematic review. *Neurocomputing* 2022;468:492-509.
83. Kasarala G, Tillmann HL. Standard liver tests. *Clin Liver Dis (Hoboken)* 2016;8:13-18.
84. Giannini EG, Testa R, Savarino V. Liver enzyme alteration: a guide for clinicians. *CMAJ* 2005;172:367-379.
85. Koyama Y, Brenner DA. Liver inflammation and fibrosis. *J Clin Invest* 2017;127:55-64.
86. Robinson MW, Harmon C, O'Farrelly C. Liver immunology and its role in inflammation and homeostasis. *Cell Mol Immunol* 2016;13:267-276.
87. Friedman SL. Hepatic stellate cells: protean, multifunctional, and enigmatic cells of the liver. *Physiol Rev* 2008;88:125-172.
88. Bataller R, Brenner DA. Liver fibrosis. *J Clin Invest* 2005;115:209-218.
89. Berumen J, Baglieri J, Kisseleva T, Mekeel K. Liver fibrosis: Pathophysiology and clinical implications. *WIREs Mech Dis* 2021;13:e1499.
90. Kisseleva T, Brenner D. Molecular and cellular mechanisms of liver fibrosis and its regression. *Nat Rev Gastroenterol Hepatol* 2021;18:151-166.
91. Acharya P, Chouhan K, Weiskirchen S, Weiskirchen R. Cellular Mechanisms of Liver Fibrosis. *Front Pharmacol* 2021;12:671640.
92. Sang C, Yan H, Chan WK, Zhu X, Sun T, Chang X, Xia M, et al. Diagnosis of Fibrosis Using Blood Markers and Logistic Regression in Southeast Asian Patients With Non-alcoholic Fatty Liver Disease. *Front Med (Lausanne)* 2021;8:637652.
93. Hassan S, Syed S, Kehar SI. Review of diagnostic techniques of hepatic fibrosis. *J Pak Med Assoc* 2014;64:941-945.
94. Petitsclerc L, Gilbert G, Nguyen BN, Tang A. Liver Fibrosis Quantification by Magnetic Resonance Imaging. *Top Magn Reson Imaging* 2017;26:229-241.
95. Zhang YN, Fowler KJ, Ozturk A, Potu CK, Louie AL, Montes V, Henderson WC, et al.

Liver fibrosis imaging: A clinical review of ultrasound and magnetic resonance elastography. *J Magn Reson Imaging* 2020;51:25-42.

96. Mannan R, Misra V, Misra SP, Singh PA, Dwivedi M. A comparative evaluation of scoring systems for assessing necro-inflammatory activity and fibrosis in liver biopsies of patients with chronic viral hepatitis. *J Clin Diagn Res* 2014;8:FC08-12.

97. Krishna M. Histological Grading and Staging of Chronic Hepatitis. *Clin Liver Dis (Hoboken)* 2021;17:222-226.

98. Kisseleva T. The origin of fibrogenic myofibroblasts in fibrotic liver. *Hepatology* 2017;65:1039-1043.

99. Brenner DA, Kisseleva T, Scholten D, Paik YH, Iwaisako K, Inokuchi S, Schnabl B, et al. Origin of myofibroblasts in liver fibrosis. *Fibrogenesis Tissue Repair* 2012;5:S17.

100. Mederacke I, Hsu CC, Troeger JS, Huebener P, Mu X, Dapito DH, Pradere JP, et al. Fate tracing reveals hepatic stellate cells as dominant contributors to liver fibrosis independent of its aetiology. *Nat Commun* 2013;4:2823.

101. Hellerbrand C, Stefanovic B, Giordano F, Burchardt ER, Brenner DA. The role of TGFbeta1 in initiating hepatic stellate cell activation in vivo. *J Hepatol* 1999;30:77-87.

102. Dewidar B, Meyer C, Dooley S, Meindl-Beinker AN. TGF-beta in Hepatic Stellate Cell Activation and Liver Fibrogenesis-Updated 2019. *Cells* 2019;8.

103. Saxena NK, Ikeda K, Rockey DC, Friedman SL, Anania FA. Leptin in hepatic fibrosis: evidence for increased collagen production in stellate cells and lean littermates of ob/ob mice. *Hepatology* 2002;35:762-771.

104. Liu Y, Meyer C, Muller A, Herweck F, Li Q, Mullenbach R, Mertens PR, et al. IL-13 induces connective tissue growth factor in rat hepatic stellate cells via TGF-beta-independent Smad signaling. *J Immunol* 2011;187:2814-2823.

105. Widjaja AA, Singh BK, Adami E, Viswanathan S, Dong J, D'Agostino GA, Ng B, et al. Inhibiting Interleukin 11 Signaling Reduces Hepatocyte Death and Liver Fibrosis, Inflammation, and Steatosis in Mouse Models of Nonalcoholic Steatohepatitis. *Gastroenterology* 2019;157:777-792 e714.

106. Pellicoro A, Ramachandran P, Iredale JP, Fallowfield JA. Liver fibrosis and repair: immune regulation of wound healing in a solid organ. *Nat Rev Immunol* 2014;14:181-194.

107. Jeulin H, Velay A, Murray J, Schvoerer E. Clinical impact of hepatitis B and C virus envelope glycoproteins. *World J Gastroenterol* 2013;19:654-664.

108. Saeed U, Waheed Y, Ashraf M. Hepatitis B and hepatitis C viruses: a review of viral genomes, viral induced host immune responses, genotypic distributions and worldwide epidemiology: *Asian Pac J Trop Dis.* 2014 Apr;4(2):88-96. doi: 10.1016/S2222-1808(14)60322-4.

109. Fattovich G, Stroffolini T, Zagni I, Donato F. Hepatocellular carcinoma in cirrhosis: Incidence and risk factors. *Gastroenterology* 2004;127:S35-S50.

110. Clouston AD, Powell EE, Walsh MJ, Richardson MM, Demetris AJ, Jonsson JR. Fibrosis correlates with a ductular reaction in hepatitis C: roles of impaired replication, progenitor cells and steatosis. *Hepatology* 2005;41:809-818.

111. Leung TM, Nieto N. CYP2E1 and oxidant stress in alcoholic and non-alcoholic fatty liver disease. *J Hepatol* 2013;58:395-398.

112. Osná NA, Donohue TM, Jr., Kharbanda KK. Alcoholic Liver Disease: Pathogenesis and Current Management. *Alcohol Res* 2017;38:147-161.

113. Wang Z, Li B, Jiang H, Ma Y, Bao Y, Zhu X, Xia H, et al. IL-8 exacerbates alcohol-induced fatty liver disease via the Akt/HIF-1alpha pathway in human IL-8-expressing mice. *Cytokine* 2021;138:155402.

114. You M, Arteel GE. Effect of ethanol on lipid metabolism. *J Hepatol* 2019;70:237-248.

115. You M, Fischer M, Deeg MA, Crabb DW. Ethanol induces fatty acid synthesis pathways by activation of sterol regulatory element-binding protein (SREBP). *J Biol Chem* 2002;277:29342-29347.
116. Henkel AS. Genetic Disorders of Bile Acid Transport. *Clin Liver Dis (Hoboken)* 2021;18:237-242.
117. Marchioni Beery RM, Vaziri H, Forouhar F. Primary Biliary Cirrhosis and Primary Sclerosing Cholangitis: a Review Featuring a Women's Health Perspective. *J Clin Transl Hepatol* 2014;2:266-284.
118. Woolbright BL, Jaeschke H. Novel insight into mechanisms of cholestatic liver injury. *World J Gastroenterol* 2012;18:4985-4993.
119. Cotter TG, Rinella M. Nonalcoholic Fatty Liver Disease 2020: The State of the Disease. *Gastroenterology* 2020;158:1851-1864.
120. Im HJ, Ahn YC, Wang JH, Lee MM, Son CG. Systematic review on the prevalence of nonalcoholic fatty liver disease in South Korea. *Clin Res Hepatol Gastroenterol* 2021;45:101526.
121. Brunt EM, Tiniakos DG. Pathological features of NASH. *Front Biosci* 2005;10:1475-1484.
122. Lian CY, Zhai ZZ, Li ZF, Wang L. High fat diet-triggered non-alcoholic fatty liver disease: A review of proposed mechanisms. *Chem Biol Interact* 2020;330:109199.
123. Tariq Z, Green CJ, Hodson L. Are oxidative stress mechanisms the common denominator in the progression from hepatic steatosis towards non-alcoholic steatohepatitis (NASH)? *Liver Int* 2014;34:e180-190.
124. Brandl K, Schnabl B. Intestinal microbiota and nonalcoholic steatohepatitis. *Curr Opin Gastroenterol* 2017;33:128-133.
125. Yanguas SC, Cogliati B, Willebrords J, Maes M, Colle I, van den Bossche B, de Oliveira C, et al. Experimental models of liver fibrosis. *Arch Toxicol* 2016;90:1025-1048.
126. Leo MA, Lieber CS. Hepatic fibrosis after long-term administration of ethanol and moderate vitamin A supplementation in the rat. *Hepatology* 1983;3:1-11.
127. Basu S. Carbon tetrachloride-induced lipid peroxidation: eicosanoid formation and their regulation by antioxidant nutrients. *Toxicology* 2003;189:113-127.
128. Weber LW, Boll M, Stampfl A. Hepatotoxicity and mechanism of action of haloalkanes: carbon tetrachloride as a toxicological model. *Crit Rev Toxicol* 2003;33:105-136.
129. Low TY, Leow CK, Salto-Tellez M, Chung MC. A proteomic analysis of thioacetamide-induced hepatotoxicity and cirrhosis in rat livers. *Proteomics* 2004;4:3960-3974.
130. Bao YL, Wang L, Pan HT, Zhang TR, Chen YH, Xu SJ, Mao XL, et al. Animal and Organoid Models of Liver Fibrosis. *Front Physiol* 2021;12:666138.
131. Tolba R, Kraus T, Liedtke C, Schwarz M, Weiskirchen R. Diethylnitrosamine (DEN)-induced carcinogenic liver injury in mice. *Lab Anim* 2015;49:59-69.
132. Jha P, Knopf A, Koefeler H, Mueller M, Lackner C, Hoefler G, Claudel T, et al. Role of adipose tissue in methionine-choline-deficient model of non-alcoholic steatohepatitis (NASH). *Biochim Biophys Acta* 2014;1842:959-970.
133. Ito M, Suzuki J, Tsujioka S, Sasaki M, Gomori A, Shirakura T, Hirose H, et al. Longitudinal analysis of murine steatohepatitis model induced by chronic exposure to high-fat diet. *Hepatol Res* 2007;37:50-57.
134. Ichimura M, Kawase M, Masuzumi M, Sakaki M, Nagata Y, Tanaka K, Suruga K, et al. High-fat and high-cholesterol diet rapidly induces non-alcoholic steatohepatitis with advanced fibrosis in Sprague-Dawley rats. *Hepatol Res* 2015;45:458-469.
135. Tag CG, Sauer-Lehnen S, Weiskirchen S, Borkham-Kamphorst E, Tolba RH, Tacke F, Weiskirchen R. Bile duct ligation in mice: induction of inflammatory liver injury and fibrosis by

obstructive cholestasis. *J Vis Exp* 2015.

136. Chang ML, Yeh CT, Chang PY, Chen JC. Comparison of murine cirrhosis models induced by hepatotoxin administration and common bile duct ligation. *World J Gastroenterol* 2005;11:4167-4172.
137. Park KC, Park JH, Jeon JY, Kim SY, Kim JM, Lim CY, Lee TH, et al. A new histone deacetylase inhibitor improves liver fibrosis in BDL rats through suppression of hepatic stellate cells. *Br J Pharmacol* 2014;171:4820-4830.
138. Morita SY, Tsuda T, Horikami M, Teraoka R, Kitagawa S, Terada T. Bile salt-stimulated phospholipid efflux mediated by ABCB4 localized in nonraft membranes. *J Lipid Res* 2013;54:1221-1230.
139. Arsov T, Larter CZ, Nolan CJ, Petrovsky N, Goodnow CC, Teoh NC, Yeh MM, et al. Adaptive failure to high-fat diet characterizes steatohepatitis in *Alms1* mutant mice. *Biochem Biophys Res Commun* 2006;342:1152-1159.
140. Chisari FV, Filippi P, McLachlan A, Milich DR, Riggs M, Lee S, Palmiter RD, et al. Expression of hepatitis B virus large envelope polypeptide inhibits hepatitis B surface antigen secretion in transgenic mice. *J Virol* 1986;60:880-887.
141. Kim CW, Addy C, Kusunoki J, Anderson NN, Deja S, Fu X, Burgess SC, et al. Acetyl CoA Carboxylase Inhibition Reduces Hepatic Steatosis but Elevates Plasma Triglycerides in Mice and Humans: A Bedside to Bench Investigation. *Cell Metab* 2017;26:394-406 e396.
142. Sonoda J, Chen MZ, Baruch A. FGF21-receptor agonists: an emerging therapeutic class for obesity-related diseases. *Horm Mol Biol Clin Investig* 2017;30.
143. Wheeler PE. The loss of functional body hair in man: the influence of thermal environment, body form and bipedality. *Journal of Human Evolution* 1985;14:23-28.
144. Montagna W. The evolution of human skin(?). *Journal of Human Evolution* 1985;14:3-22.
145. Jablonski NG, Chaplin G. Colloquium paper: human skin pigmentation as an adaptation to UV radiation. *Proc Natl Acad Sci U S A* 2010;107 Suppl 2:8962-8968.
146. Dry FW. The coat of the mouse (*Mus musculus*). *Journal of Genetics* 1926;16:287-340.
147. Muller-Rover S, Handjiski B, van der Veen C, Eichmuller S, Foitzik K, McKay IA, Stenn KS, et al. A comprehensive guide for the accurate classification of murine hair follicles in distinct hair cycle stages. *J Invest Dermatol* 2001;117:3-15.
148. Datta K, Singh AT, Mukherjee A, Bhat B, Ramesh B, Burman AC. *Eclipta alba* extract with potential for hair growth promoting activity. *J Ethnopharmacol* 2009;124:450-456.
149. Burg D, Yamamoto M, Namekata M, Haklani J, Koike K, Halasz M. Promotion of anagen, increased hair density and reduction of hair fall in a clinical setting following identification of FGF5-inhibiting compounds via a novel 2-stage process. *Clin Cosmet Investig Dermatol* 2017;10:71-85.
150. Suzuki T, Kikuguchi C, Nishijima S, Yamamoto T. Insufficient liver maturation affects murine early postnatal hair cycle. *Biochem Biophys Res Commun* 2020;521:172-177.
151. Suzuki T, Kikuguchi C, Nishijima S, Nagashima T, Takahashi A, Okada M, Yamamoto T. Postnatal liver functional maturation requires Cnot complex-mediated decay of mRNAs encoding cell cycle and immature liver genes. *Development* 2019;146.
152. Park SY, Na SY, Kim JH, Cho S, Lee JH. Iron plays a certain role in patterned hair loss. *J Korean Med Sci* 2013;28:934-938.
153. Trost LB, Bergfeld WF, Calogeras E. The diagnosis and treatment of iron deficiency and its potential relationship to hair loss. *J Am Acad Dermatol* 2006;54:824-844.
154. Almohanna HM, Ahmed AA, Tsatalis JP, Tosti A. The Role of Vitamins and Minerals in Hair Loss: A Review. *Dermatol Ther (Heidelb)* 2019;9:51-70.

155. Adil A, Godwin M. The effectiveness of treatments for androgenetic alopecia: A systematic review and meta-analysis. *J Am Acad Dermatol* 2017;77:136-141 e135.
156. Michelet JF, Commo S, Billoni N, Mahe YF, Bernard BA. Activation of cytoprotective prostaglandin synthase-1 by minoxidil as a possible explanation for its hair growth-stimulating effect. *J Invest Dermatol* 1997;108:205-209.
157. Gaffar A, Scherl D, Afflitto J, Coleman EJ. The effect of triclosan on mediators of gingival inflammation. *J Clin Periodontol* 1995;22:480-484.
158. Kurbel S, Kurbel B, Zanic-Matanic D. Minoxidil and male-pattern alopecia: a potential role for a local regulator of sebum secretion with vasoconstrictive effects? *Med Hypotheses* 1999;53:402-406.
159. McClellan KJ, Markham A. Finasteride. *Drugs* 1999;57:111-126.
160. Hulin-Curtis SL, Petit D, Figg WD, Hsing AW, Reichardt JK. Finasteride metabolism and pharmacogenetics: new approaches to personalized prevention of prostate cancer. *Future Oncol* 2010;6:1897-1913.
161. Zhang J, Qi F, Dong J, Tan Y, Gao L, Liu F. Application of Baricitinib in Dermatology. *J Inflamm Res* 2022;15:1935-1941.
162. Jabbari A, Dai Z, Xing L, Cerise JE, Ramot Y, Berkun Y, Sanchez GA, et al. Reversal of Alopecia Areata Following Treatment With the JAK1/2 Inhibitor Baricitinib. *EBioMedicine* 2015;2:351-355.
163. Ali E, Owais R, Sheikh A, Shaikh A. Olumniant (Baricitinib) oral tablets: An insight into FDA-approved systemic treatment for Alopecia Areata. *Annals of Medicine and Surgery* 2022;80:104157.
164. VanBuren CA, Everts HB. Vitamin A in Skin and Hair: An Update. *Nutrients* 2022;14.
165. Guo EL, Katta R. Diet and hair loss: effects of nutrient deficiency and supplement use. *Dermatol Pract Concept* 2017;7:1-10.
166. Truksa J, Gelbart T, Peng H, Beutler E, Beutler B, Lee P. Suppression of the hepcidin-encoding gene *Hamp* permits iron overload in mice lacking both hemojuvelin and matriptase-2/TMPRSS6. *Br J Haematol* 2009;147:571-581.
167. Underhill-Day N, McGovern LA, Karpovich N, Mardon HJ, Barton VA, Heath JK. Functional characterization of W147A: a high-affinity interleukin-11 antagonist. *Endocrinology* 2003;144:3406-3414.
168. Shah R, John S. Cholestatic Jaundice. [Updated 2022 Jul 12]. In: StatPearls [Internet]. Treasure Island (FL): StatPearls Publishing; 2023 Jan-. Available from: <https://www.ncbi.nlm.nih.gov/books/NBK482279/>